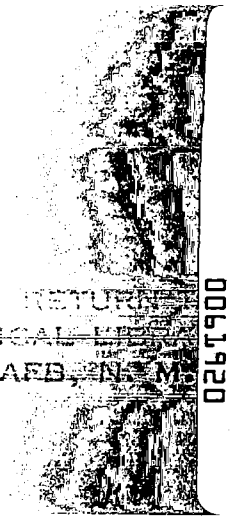

NASA Contractor Report 3178

Correlation of Data Related to Shock-Induced Trailing-Edge Separation and Extrapolation to Flight Reynolds Number

J. F. Cahill and P. C. Connor

CONTRACT NAS2-9331
SEPTEMBER 1979

NASA

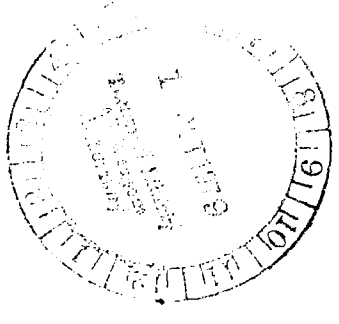

NASA Contractor Report 3178

Correlation of Data Related to Shock-Induced Trailing-Edge Separation and Extrapolation to Flight Reynolds Number

J. F. Cahill and P. C. Connor
Lockheed-Georgia Company
Marietta, Georgia

Prepared for
Ames Research Center
under Contract NAS2-9331

National Aeronautics
and Space Administration

Scientific and Technical
Information Branch

1979

CORRELATION OF DATA RELATING TO SHOCK-INDUCED TRAILING-EDGE SEPARATION AND EXTRAPOLATION TO FLIGHT REYNOLDS NUMBER

BY

J. F. CAHILL AND P. C. CONNOR

SUMMARY

Analyses have been conducted of pressure distribution data from a number of previous wind tunnel and flight investigations of high speed transport type wings. These analyses have produced a correlation of the development of trailing-edge separation resulting from increases in Mach number and/or angle of attack and have shown that scale effects on this correlated separation development and the resulting shock location changes fall into a regular and apparently universal pattern. Based on these results a procedure has been developed for extrapolation of low Reynolds number wind tunnel data to flight conditions. Further studies appear warranted to refine the correlation through a detailed consideration of boundary layer characteristics, and to evaluate scale effects on supercritical wings.

INTRODUCTION

Serious problems have become apparent in recent years with regard to accurate wind tunnel simulation of trailing-edge separation on aircraft wings at transonic speeds. References 1 and 2 present a number of papers which discuss the general characteristics of this problem and paper number 11 in Reference 1, by Pearcey, Haines, and Osborne explains in some detail the combination of aerodynamic phenomena which are significant in determining separation development. The magnitude of potential differences between wind tunnel predictions and actual flight experience is perhaps best documented in the case of the C-141 airplane where shock locations measured in flight were in some cases farther aft than the wind tunnel indication by 20% chord. This difference in shock location of course results in a large discrepancy in lift and pitching moment acting on the wing. The significance of these discrepancies can be appreciated by a consideration of the fact that the potential for such differences is greatest at high Mach number, high lift, high dynamic pressure flight conditions for which airloads define the critical conditions for structural design of the wing.

During 1975, tests were made on a semispan model of the C-141 airplane in the high Reynolds number Compressible Flow Facility at the Lockheed-Georgia Company. These tests covered the Reynolds number range between previously available wind tunnel tests and those encountered in flight. The results of those tests, presented in Reference 3, confirm the fact that previously noted discrepancies can be attributed entirely to Reynolds number differences when the effective angle of attack of each spanwise station is properly taken into account. Unfortunately those data also disclosed that the shape of the scale effect curves on trailing-edge separation is highly variable and no simple curve-extension extrapolation will produce a proper prediction of the high Reynolds number result.

Following completion of the semispan tests discussed above, efforts were initiated at Lockheed to develop a means to generalize the available results on shock induced trailing edge separation in a manner which would enable a reliable prediction of flight-scale separation based on the results of wind tunnel measurements at lower Reynolds numbers. After promising indications had been obtained that such generalizations were possible, the current study was undertaken to demonstrate a technique for Reynolds number extrapolation of wing pressure distribution data involving such separated flows.

Programs are now underway for the design and construction of high Reynolds number transonic wind tunnels which will enable a proper simulation of full scale aerodynamic characteristics. The extrapolation procedure which is the objective of the study reported herein will be useful for prediction of flight characteristics in the interim period until those wind tunnels become operational, and in fact for any instance when tests are conducted at less than the flight Reynolds number.

SYMBOLS

A	curve-fit constant in correlation parameter
B1/2	correlation parameter, $\dfrac{P_O/P_P \sqrt{M} - A}{\sqrt{1 - XCSH}}$
B1/2*	key value at arbitrarily selected point on correlation curves
Δ B1/2*	increment in key value from its value at a Reynolds number of 10×10^6
C_P	pressure coefficient $P - P_O / q$

$C_{P_{.3}}$	pressure coefficient at 30% chord
CPTE	trailing-edge pressure coefficient
CPTEO	base value of trailing-edge pressure coefficient
Δ CPTEO	increment in base value of CPTEO from its value at a Reynolds number of 10×10^6
CPSH	peak negative value of pressure coefficient immediately forward of shock
H	boundary layer shape factor, δ^*/θ
M	free-stream Mach number
MLN	local Mach number normal to wing element lines
P	local static pressure
P_P	static pressure corresponding to CPSH
P_O	free-stream static pressure
PML	tentative correlation parameter, MLN $\sqrt{M}$
PXX	general trial correlation parameter $P_O/P_P \, M^{X.X}$ ($P05 = P_O/P_P \, \sqrt{M}$)
R_{MAC}	Reynolds number based on mean aerodynamic chord
RN	Reynolds number based on local chord
W.T.	wind tunnel
XCSH	chordwise location of terminal shock
$dC_P/d\frac{X}{C}$	slope of pressure rise through shock
α	angle of attack
α CFF	effective angle of attack
η	spanwise station, fraction of semispan

BACKGROUND

A typical set of scale effect variations from the tests of Reference 3 are shown in Figure 1. These data illustrate quite effectively the influence of Reynolds number changes on trailing-edge separation and shock location through the range from existing wind tunnel capabilities to those encountered by large transport aircraft in flight. Data are included from a complete C-141 model in the AEDC 16 foot transonic wind tunnel, a semispan model in the Lockheed-Georgia 20 x 28 inch Compressible Flow Facility, and from flight tests. These data generally indicate a good match of data from these various sources, although some discrepancies are noted which can probably be attributed to a lack of precision in techniques used for fixing transition. For conditions in which the boundary layer is turbulent over essentially the full wing chord, a continuous improvement in trailing-edge pressure recovery occurs as Reynolds number is increased, and is accompanied by a continuous aft movement in shock location. Data measured with natural transition at low Reynolds number show a trailing-edge pressure recovery considerably greater than those with the transition fixed near the leading edge, and in fact similar to those encountered at the very much higher flight Reynolds number. This fact has been used to advantage in some cases (along with boundary layer trips just forward of the shock) to simulate higher Reynolds numbers, but the current study is concerned only with those data having essentially full-chord turbulent boundary layers.

The good match of wind tunnel and flight data shown in Figure 1 requires a proper consideration of local angles of attack at each spanwise station. Differences in effective angle of attack among the various wind tunnel conditions or between wind tunnel and flight conditions can be encountered because of aeroelastic distortions of the wing or because of tunnel-wall induced distortions of the airstream. Data in Figure 1 are compared at a constant local angle of attack defined in accordance with the concept illustrated in Figure 2. Data such as these from the semispan model at high dynamic pressure were used as a base and effective angles of attack from the other tests were defined by reading α_{CFF} at their corresponding values of $C_{P.3°}$. This procedure rests of course on the assumption of validity of a simple "strip theory" for variations of pressure distribution with angle of attack for each spanwise station, and as illustrated by the results in Figure 1, this assumption is acceptable within the range of distortions encountered. A complete accounting for differences between wind tunnel and flight results can therefore be accomplished by a consideration of Reynolds number effects on airfoil aerodynamic characteristics, plus a consideration of differences in aeroelastic characteristics.

Shock locations shown in Figure 1, and throughout this report, are defined at the intersection of the steep pressure rise through the shock with the locus of pressure coefficient values representing a local sonic velocity normal to element lines of the wing planform. This definition is illustrated in the top sketch of Figure 3. In cases for which local separation bubbles cause the local velocities at the base of the shock to exceed $M_{LN} = 1$, the abrupt pressure rise through the shock is extended linearly to define the shock location.

For several of the sources of data used in this analysis, pressure-measuring orifices were located with sufficiently small spacing that several pressure measurements were available in the steep pressure rise through the shock. The slope of the shock pressure rise for these cases was examined and found to vary (to an acceptable accuracy) with Reynolds number as shown in the bottom sketch of Figure 3. Slopes taken from this figure were used as an aid in fairing chordwise pressure distributions in those cases where orifice spacing was greater. By using this procedure, shock locations could be established with little question for orifice spacings as large as 5% chord. With wider spacing than 5%, it is doubtful that acceptable definition of shock location is possible.

This report describes the evolution of an empirical correlation of the development of trailing-edge separation on swept wings at transonic speeds, and utilization of that correlation in a procedure for extrapolation of wind tunnel data to flight Reynolds number. This study has been accomplished using pressure distribution data from several previous test programs in several wind tunnels and in flight. These data sources are outlined briefly below and described in somewhat greater detail as they are encountered in the discussion which follows.

C-141

Full span model, AEDC 16T, Reference 4
Semispan model, Gelac CFF, Reference 3
Flight, Reference 5

C-5A

Full span model, AEDC 16T, Reference 6
Flight, Reference 7

RAE Model 864[1]

Semispan model, NASA Ames 11 Foot Tunnel

F-8 SCW

Flight, Reference 8

[1] Unpublished NASA-Ames data.

CORRELATION OF TRAILING EDGE SEPARATION

While the possible modes of separation on a wing at transonic speeds include various combinations of separation at the shock and at the trailing edge, as discussed by Pearcey, Haines, and Osborne (Reference 1), large scale effect differences in wing loads have only been observed as a result of the trailing edge separation. Figure 4, from Paper 20 of Reference 2, illustrates the dependence of shock location on downstream pressure distribution which, in turn, is controlled by trailing-edge pressure recovery. The plot on the left of Figure 4 shows data from tests of a C-141 model with and without vortex generators at 70 percent chord, with a transition-fixing grit strip near the leading edge. In tests without the vortex generators, a separation is present which seems to originate somewhat aft of 80% chord. Adding the vortex generators (which are aft of the shock for both model conditions) eliminates the trailing-edge separation. Because of this change in the downstream boundary condition, the entire subsonic velocity distribution downstream of the shock must change. This change then imposes a requirement for a change in shock location since the shock must produce a pressure rise which is compatible with both the upstream local supersonic Mach number and the downstream subsonic Mach number. The shock will move to the chordwise location where a shock at the local Mach number produces the required pressure rise. The plot on the right of Figure 4 shows another example where shock location changes in response to a change in the pressure distribution downstream of the shock, which in this case is caused by changes in aileron deflection. These data, from tests of a C-5A model, show large changes in shock location resulting from the same requirement for establishing compatibility between upstream and downstream pressures. Good agreement is shown between measured pressure distributions downstream of the shock and those obtained from low speed measurements and converted to the higher Mach number by the Karman-Tsien compressibility factor.

Significant differences due to Reynolds number changes should therefore be best correlated by consideration of the scale effects on that pressure recovery. In fact Pearcey in 1961 (Reference 9) defined significant separation as the first appearance of a deterioration in trailing-edge recovery resulting from a shock pressure rise. For the airfoils being studied at that time trailing-edge separation resulted from the rearward spread of a separation bubble originating at the shock and "significant separation" was found to occur when the local Mach number just forward of the shock reached a value between 1.2 and 1.4, depending on curvature changes in the airfoil forward upper surface. The local Mach number is an important factor in this case of course because of its influence in defining the strength of the shock pressure rise.

Initial Correlation

Initial attempts in this study to correlate the occurance of trailing edge separation were conducted using portions of the available wind tunnel and flight test results on the C-141 and C-5 airplanes. Since, on a swept wing, the intensity of the shock pressure rise is dependent upon the local Mach number normal to the shock, the variation of trailing-edge pressure recovery with that local Mach number in a manner following that of Pearcey and Osborne (Reference 9) was first examined. As shown in Figure 5, a consistent family of curves is formed by data measured over a matrix of values of Mach number and angle of attack. Since the shape of these curves showed a consistent variation as the free stream Mach number was varied, correlation parameters including Mach number were next investigated. The same set of test data are shown in Figure 6 plotted as a function of the parameter PML, equal to MLN $\sqrt{M}$. As can be seen in Figure 6, the initial separation occurs at a single value of the parameter PML and furthermore the deterioration of trailing edge pressure recovery as Mach number and/or angle of attack are increased collapses into a single curve. This correlation of indicated separation was therefore investigated for a number of different test conditions. A series of data sets correlated in this way is shown in Figures 7 through 11. The development of trailing-edge separation is shown to collapse in a satisfactory manner to a single curve which has a characteristic shape for each spanwise station tested. Increases in Reynolds number shift this curve bodily to higher values of PML and CPTE, but do not change the shape of the correlating curve.

This result was, of course, much more than had been anticipated at the beginning of this effort, since the deterioration of pressure recovery into drastically separated conditions is shown to be accounted for by a relatively simple parameter involving terms which can readily be measured in wind tunnel or flight tests. Furthermore, since the shape of the correlation curves remains unchanged by variation in Reynolds number, scale effect variations can be shown quite simply by considering only the magnitude of the change in location of those curves on the coordinate grid. However, since most basic studies on shock-boundary layer interaction show that separation characteristics in a number of cases can be predicted in terms of the shock pressure rise, the results of the present study can best be related to those basic results if the correlation parameter were converted to terms involving the pressure rise directly, rather than through local Mach number. The evolution of a suitable correlation parameter involving the pressure rise as its principle component was accomplished by a simple search for a combination of the pertinent terms which would collapse the indicated separation in a manner similar to that already shown. This search was aided by a recognition of the fact that in the initial correlation, no consideration was needed of the portion of the pressure rise which occurred through the shock or in the subsonic flow downstream of the shock. The data sets of Figure 6, converted to the correlating parameter $\frac{P_O}{P_P} M^{3/2} = P15$ are shown in Figure 12. This correlation was evolved, as was the initial correlation, from a purely pragmatic determination that the separation development collapsed into a single curve when plotted as a function of the parameter P15. As shown in Figure 13 however, an intimate relationship exists between the two parameters, so that equal success of the two correlations is not surprising.

Shock Location Effects

Correlations of trailing-edge pressure recovery shown in the preceding section would imply a fairly conclusive demonstration that separation development can be described as a function of the single parameter PML, or P15. The aerodynamic environment in which that separation development was established was however rather limited in scope since the C-141 and the C-5 wings are geometrically fairly similar, and data included in that portion of the study covered a Mach number range only between 0.8 and 0.85. The next phase of the study was undertaken with the objective of determining the range of applicability of this correlation concept by including data from tests of other configurations and over wider ranges of test conditions.

Suitable pressure distribution data were available from NASA tests of a model called the RAE Model 864 in the Ames 11 foot transonic tunnel over a wide range of test conditions. General geometric characteristics of the model and test values of Mach number and Reynolds number are shown in Figure 14. Typical upper surface pressure distributions are shown in Figure 15. Airfoil sections for this model have been characterized as "moderately supercritical" with high aft loading and high negative leading-edge pressure coefficients. The variation of trailing-edge pressure recovery for the three spanwise stations for which data were considered on this wing are shown plotted against the correlation parameter P15 in Figure 16. A strong variation of separation development with Mach number is obvious in these data. Attempts to improve the correlation by simple variations to improve the Mach number accountability of the correlating parameter were unsuccessful.

In reviewing the characteristics of the pressure distributions for which successful correlation had been accomplished (C-141 and C-5) and those for the RAE Model 864, it became readily apparent that shock locations for the latter case were not only much more variable than in the cases considered previously, but that the variation in separation development with Mach number bore a strong resemblance to the variation in shock location. This fact is illustrated by the data plotted in Figure 17. This variation is further detailed in Figure 18 where the values of several candidate correlation parameters (PXX) at a constant value of trailing edge pressure recovery are plotted against $\sqrt{(1-XCSH)}$. PXX is a designation for a family of correlating parameters in which the pressure rise P_O/P_P is multiplied by free stream Mach number raised to varying powers. Thus P15 is $P_O/P_P\, M^{1.5}$, P05 is $P_O/P_P\, M^{0.5}$. The linear variation shown for P05 implies that a parameter of the form $\dfrac{\frac{P_O}{P_P}\sqrt{M - A}}{\sqrt{1-XCSH}}$ should collapse the variation of CPTE for various Mach numbers, at least for values of CPTE near that used to prepare

the plot of Figure 18. This parameter is given the designation B1/2. Several variations of the rationale just described were attempted before the combination of terms in the resulting parameter were evolved. Data showing trailing-edge pressure recovery as a function of the parameter B1/2 are presented in Figure 19 and show that, with few exceptions, these data points collapse into a single curve as well as the previous correlation which did not require a recognition of shock location.

Similar plots showing the development of trailing-edge separation for each of the three spanwise stations on this model for several Reynolds numbers are shown in Figures 20 through 22. Data for spanwise stations η = .595 and .793 correlate quite well with only a few scattered points in each case. Data for the third station, η = .434 show considerably more scatter.

Values of the curve-fit constant "A" are shown on the figures for each spanwise station. Initial selections of the values for this constant were made from plots similar to Figure 18, but due to the rather large extrapolation required, these selections frequently required change. Final values were selected after an iterative trial of several values near the initial selection.

Since the curves which fit the variation of trailing-edge separation remain unchanged as Reynolds number is varied, and only change location on the coordinate grid, composite plots including data for all Reynolds numbers can be assembled by plotting the differences (CPTE - CPTEO) versus (B1/2 - B1/2*) where CPTEO is the base (or maximum) value of pressure recovery for each individual curve and B1/2* is an arbitrarily selected point on the steeply rising portion of the curve. Plots of this type are shown in Figures 23 through 25 for the three spanwise stations. For η = .793, the composite correlation shown in Figure 23 is excellent with the exception of a few points measured at high angles of attack and low Mach number at each Reynolds number. Figure 24, for η = .595 shows that the data correlated quite well for (CPTE - CPTEO) to approximately -.3, after which a considerable spread occurs. Figure 25, for η = .434 shows a sizeable spread but with a fairly good grouping of data in the region of the break in pressure recovery.

Generality of Correlation

The correlating parameter B1/2 was next evaluated for application to the C-141 and C-5 data which had previously been shown only for a limited range of test conditions. Figure 26 shows a planform sketch of the C-141 wing and the spanwise stations at which pressure distribution data were available from a variety of sources. Tests had been made at a number of angles of attack, at Mach numbers from 0.75 through 0.9,

and over a Reynolds number range from 3 million to 75 million. Typical chordwise pressure distributions (Figure 27) show this wing to be a conventional "pre-supercritical" configuration with rather flat velocity gradients forward of the shock. At the most inboard station, a relatively weak compression occurs on the forward portion of the wing. For these cases, as well as all others, correlations were based on the peak negative pressure coefficient immediately forward of the terminal shock and the existence of the higher velocities near the leading edge had no obvious influence on the correlation.

The variation of trailing-edge pressure recovery with the parameter $B1/2$ is shown in Figures 28 through 30 for the three spanwise stations tested on this wing. The correlation is generally quite good, although the data at wing station $\eta = .389$ show more scatter than the other two stations. The flight data also generally seem to scatter more than the wind tunnel results, and except for station $\eta = .193$, do not contain enough points for a good definition of curve shape in the separated conditions. Composite plots are shown in Figures 31 through 33. These plots show fairly good collapsing of the data from the various sources considered. A number of "stray" points (possibly 15% in Figure 32) deviate from the mean curves by a magnitude large enough to be of concern. The possibility of accounting for these deviations is discussed in a later section.

A sketch of the C-5A wing planform and the range of variables covered by available test data are shown in Figure 34. Typical pressure distributions in Figure 35 are seen to be quite similar to those for the C-141 wing. Individual plots showing the variation of pressure recovery (Figures 36 and 37) indicate quite good correlation, although with evidence of a few scattered points similar to those shown for the C-141 configuration. In this case, sufficient flight test points are available to define the development of separation and to confirm the mean curve shapes. Composite plots are shown in Figures 38 and 39.

Applicability to Supercritical Wings

As indicated previously, the pressure distributions for the RAE 864 wing exhibit some of the characteristics incorporated in modern supercritical wings. Those characteristics are, in that case, much less prominent than in wings designed for recent evaluations of the supercritical wing design concept. Data from the F-8 SCW configuration reported in Reference 8 provide an example of the latter type of configuration. Figure 40 shows a sketch of the wing for the F-8 SCW and summarizes test conditions for which pressure distribution data are available.

While these data are available only at flight Reynolds number (and do not therefore offer the opportunity for scale effect evaluation) they are valuable for determining the applicability of the correlation parameter to this distinctly different wing design. Pressure distribution data in Figure 41 show that the terminal shock on this wing occurs very far aft on the chord, and is preceeded by a significantly higher peak negative pressure near the leading edge, a rather strong compression, and re-acceleration to supercritical local Mach numbers. The initial compression varies in steepness from some cases which appear to be discrete strong shocks to rather diffuse decelerations spread over the major portion of the wing chord.

The variation of trailing-edge pressure coefficient with the parameter B1/2, based on the peak negative pressure coefficient just preceeding the terminal shock, is shown in Figures 42 and 43. Data in Figure 42 for spanwise station η = .306, show an excellent collapsing of the separation development. Data in Figure 43 for η = .653 are also quite good, but with somewhat greater scatter than the inboard station.

A comparison of data in Figures 42 and 43 shows that significant differences are encountered in values of the parameter B1/2 and in the intensity of separation. Values of peak negative pressure coefficients for these two spanwise stations at the leading edge and at the terminal shock are shown in Figure 44 to illustrate the source of these differences. At η = .306, each of these peak pressure values falls in rather a narrow band, with the leading-edge values significantly more negative than those at the shock. At the outboard station, values of the two peak pressures are roughly equal to those at η = .306 for the lowest Mach number shown (M = .9), but for higher Mach numbers, the leading-edge peaks decrease and the shock peaks increase so that they are nearly equal to each other. The higher values of peak negative pressure coefficients at the shock, CPSH, result in an earlier and more intense separation at the outboard station. These data, combined with the differences in trailing-edge pressure recovery shown in Figures 42 and 43, tend to substantiate the significance of the terminal shock pressure rise as the determinant of trailing-edge separation.

SCALE EFFECT ON CORRELATED SEPARATION DEVELOPMENT

Since the development of trailing-edge separation, as shown in preceeding sections, follows a single curve for each spanwise station, the displacement of those curves as a function of Reynolds number provides a very simple means for examining scale effects on the separation phenomenon. The scale effect on the correlated data are shown for several cases in Figure 45. These scale effects are shown in terms of the two parameters CPTEO and B1/2* defined previously.

Increasing Reynolds number causes a regular and gradual improvement in the maximum trailing-edge pressure recovery, CPTEO and shifts the break in the recovery curve to higher values of B1/2. The slope of these variations with Reynolds number was found to be the same for each set of data examined (each spanwise station). Figure 46 shows a composite of all of the scale effect data plotted as increments (Δ CPTEO and Δ B1/2*) from the values of these factors at a Reynolds number of 10 million. The consistency of data shown by this figure is quite good, and it would appear that the generality of the scale effects when presented in this manner can be accepted with reasonable confidence. This statement is based of course on results from the C-141, the C-5A, and the RAE Model 864. Wind tunnel data on the F-8 SCW configuration would be very valuable to determine applicability to that kind of supercritical design.

The scale effects on shock induced trailing-edge separation, which, as illustrated in Figure 1 are highly variable and rather complex, have now been reduced to a relatively simple and predictable variation. The source of the variability in Reynolds number effects can be readily appreciated by a consideration of the variations shown in Figure 47. Here the correlation curves for an example case are shown for a number of Reynolds numbers, and values of the correlation parameter B1/2 for several angles of attack are superimposed. At low angles of attack, where no strong separation exists, the variation of pressure recovery, and therefore of shock location will be small and regular. At intermediate angles of attack, the variation can cover cases with severe separation at low Reynolds number and no separation at the flight values. The variations with Reynolds number will therefore be quite steep initially, but flatten out for full scale conditions. At higher angles of attack, where some separation exists for all Reynolds numbers considered, the variations will again be less steep.

FACTORS INFLUENCING CORRELATION

Data discussed in previous sections have shown a rather satisfactory collapsing of separation development resulting from increases in Mach number and/or angle of attack, and an indication of generality in the effects of Reynolds number changes on those correlated data. A disappointing number of individual points scatter from the correlation curves, however, and might be brought into agreement with the general mass of the data through consideration of more detailed characteristics of the flow. Some reservation must also be expressed concerning complete generality of the relationships presented since the basic phenomena leading to successful correlation of these data are not completely understood. Brief explorations of several factors have been conducted in an attempt to shed further light on these two points.

Favorable Influence of Forward Velocity Gradients

Significant variations in key values (CPTEO and B1/2*) from the correlated separation development curves have been shown to result from Reynolds number changes. When these results are viewed in the light of similar variations produced at constant Reynolds number by varying the chordwise location of transition strips forward of the shock (see Reference 10 and paper 21 in Reference 1, for instance) it must be concluded that the Reynolds number effect results largely from its influence on the condition of the boundary layer approaching and transiting the shock. This boundary layer condition can also be modified at constant Reynolds number by variations in velocity gradients experienced by the boundary layer between the stagnation point and the shock. The possibility that such influences might be responsible for the few "stray" points which deviate from the correlation curves has been examined in a very coarse way as illustrated in Figure 48. This figure contains the same information as Figure 36, but with test points identified by the value of the peak negative pressure coefficient just forward of the shock, CPSH. This value is a rough indicator of the average favorable velocity gradient on the forward portion of the chord. As shown in Figure 48, the points which deviate from the correlation curve show a fairly consistent variation with the value of CPSH. Correlation curves are drawn through these points in Figure 48 indicating that an effective Reynolds number might be defined if an influence of favorable gradients on boundary layer properties for those cases can be substantiated as being comparable to the influence of a rather large Reynolds number change. The concept of showing such effects as a function of boundary layer properties rather than of Reynolds number is in fact a much preferable procedure. This concept should be investigated further.

As a further evaluation of the possibility that correlations could be refined by a consideration of boundary layer properties, the rather considerable scatter shown by the flight data for station η = .389 of the C-141 wing were examined in relation to measured boundary layer data from Reference 5. Values of B1/2 which did not fall on the plotted correlation plots were taken as indications of alternate possibilities for the location of the "break" in the variation of trailing-edge pressure recovery as illustrated in Figure 48. These indicated "break" values are shown in Figure 49 plotted against the associated values of the shape factor, H, for the boundary layer profiles. While far from conclusive, these data present the possibility of a significant correlation, and therefore add credence to the possibility of refining correlations.

Relationship to Shock-Boundary Layer Interaction Phenomena

The correlations which have been shown previously have been developed without the necessity for consideration of whether local separations are present in the immediate vicinity of the shock. A visual examination of the pressure distributions which are the

source data for this study would indicate that separation bubbles followed by re-attachment are present in some cases but no systematic classification of the data in this regard has been attempted. It is instructive therefore to review these data in relation to shock-boundary layer interaction separation criteria in an attempt to identify cause-and-effect relationships. Figure 50 shows a comparison of shock pressure rise from one of the data sets of this study with the separation criteria of Erdos and Pallone (Reference 11) and of Reshotko-Tucker (Reference 12). The shock pressure rise is shown as the ratio of the static pressure at a local Mach number of one to the peak minimum pressure forward of the shock, P_1/P_p. Intersections of the curve of shock pressure rise with the separation criteria curves should indicate the probability of separations at the shock. Plots similar to that shown in Figure 50 were prepared for each of the data sets used in this study. Generally, for the data presented in this manner, the intersection indicated by the Reshotko-Tucker criterion tends to match the intersection for the Erdos and Pallone incipient separation criterion at low Reynolds numbers and to move progressively toward agreement with the plateau pressure criterion as the Reynolds number is increased. No correlation has been observed between the trailing-edge separation development and these predictions of separation at the shock Figure 51 shows a plot against Reynolds number of the value of B1/2 for which the value of P_1/P_p matches the various separation criteria, and the value at which the trailing-edge pressure recovery first departs from its base value. In the case of each of the separation criteria curves, the pressure rise through the shocks, P1, exceeds the pertinent separation pressure rise for values of B1/2 greater than the value plotted as illustrated. Data shown in Figure 51, indicate that the trailing-edge separation occurs at values of B1/2 less than that for which a shock separation would be predicted at low Reynolds numbers, but at higher values for the highest Reynolds numbers. This fact seems generally to be true except for the outboard station on the C-5 wing where the trailing-edge separation seems always to be delayed to values of B1/2 greater than that where shock separation is predicted.

REYNOLDS NUMBER EXTRAPOLATION PROCEDURE

The fact that a single curve, Figure 46, represents the variation with Reynolds number of values of key points on the separation development correlation curves for a number of significantly different configurations (and the fact that the correlation curves do not change shape as Reynolds number changes) provides the basis for a procedure which should enable reasonably accurate extrapolations of small scale wind tunnel data to flight Reynolds numbers. This section describes such an extrapolation procedure and illustrates the manner in which it can be implemented.

Extrapolation Concept

This concept for extrapolating low scale wind tunnel data to flight Reynolds numbers relies on the following assumptions which are substantiated in earlier sections of this report or in previous papers:

(1) The slopes of the scale effect curves of Figure 46 are generally applicable.

(2) The shapes of the curves showing the correlated separation development (CPTE VS B1/2) do not vary as Reynolds number changes.

(3) As trailing-edge separation develops, the shock location will move forward following a curve which is independent of Reynolds number, transition strip location, or use of vortex generators. (This curve will change with Mach number and may change with angle of attack).

The procedure for utilizing these assumptions in extrapolating to higher Reynolds numbers is summarized in Figure 52. Pressure distribution data measured in the wind tunnel will properly define the shape of the pressure distribution on the wing back to the shock location. At the test Reynolds number, trailing-edge separation may be present and the shock location will occur farther forward than to be anticipated at full scale. By performing tests over the widest possible Reynolds number range, with several locations of transition strips, and with vortex generators, if necessary, the effect of trailing edge separation on shock location can be defined Also at each test Reynolds number (but with full chord turbulent flow) the development of trailing-edge separation can be correlated in terms of the parameter B1/2, and the values of CPTEO and B1/2* are therefore established. Typical examples of each of these test results are shown as circle symbols in the sketches on Figure 52, progressing from right to left.

Extrapolation to full scale is now accomplished by utilizing the slope of the general scale effect curves from Figure 46 and displacing the separation development curve to pass through the values of CPTEO and B1/2* at the appropriate flight Reynolds number. A curve defining the full scale relationship among shock location, B1/2, and trailing-edge pressure coefficient can now be derived for each Mach number which will define, for any angle of attack, the pressure coefficient and chordwise location of points at the beginning of shock, the foot of the shock, and the trailing edge. This will be illustrated in the example to follow. This procedure will therefore provide, with sufficient accuracy for engineering purposes, a prediction of the upper surface pressure distribution to be expected in flight. This procedure, as outlined here considers

one spanwise station and a fixed value of the effective angle of attack defined earlier. The complete spanwise load distribution on the wing can now be assembled by repeating this process for a number of spanwise stations and by a consideration of the aeroelastic distortion of both the wind tunnel model and the full scale wing.

Wind Tunnel Data Requirements

Proper implementation of the scale extrapolation concept discussed here can be accomplished using data which would normally be obtained during the development of a new aircraft design. Emphasis on certain details of instrumentation arrangement and model configurations to be tested will aid in establishing the required correlations.

Orifice spacing must be quite close in the portion of the chord where shocks will be encountered. In assembling the data used in this study, no useful information could be obtained if orifices were located with a spacing greater than 5% chord. Closer spacing was found to be valuable in eliminating the necessity for extrapolations to define the value of CPSH. A spacing of 2 1/2 to 3% chord would be recommended.

Trailing-edge pressure coefficients have been used to define the occurance and development of separation in this study. Orifices for measurement of trailing-edge pressures require special care in model fabrication and handling since they are easily damaged. In the case of some supercritical airfoils, with very high aft loadings and cusped trailing edges, the pressure variation around the trailing edge is quite large so that the pressure distribution plot becomes a smooth curve with an infinite slope at the trailing edge. In those cases, an upper surface pressure measurement near to, but forward of, the trailing edge should provide a better indicator of separation.

Pressure distribution measurements must be made at a number of Mach number and angle of attack points during the development of the separation in order to provide an adequate definition of the correlation curves. This may require smaller increments in both Mach number and angle of attack than normally tested.

A proper definition of the variation in shock location with trailing-edge pressure recovery requires wind tunnel measurements for a number of test conditions which change the onset of trailing-edge separation. Previous testing to investigate the nature of these phenomena has indicated that adequate variations can be established by testing through the maximum available range of Reynolds number, by testing at low Reynolds numbers with transition-fixing strips at the most forward and the most rearward chordwise locations which will assure a turbulent boundary layer at the shock, and by testing with vortex generators to suppress the trailing-edge separation. Figure 53 is an example of this variation for station η = .193 of the C-141 wing obtained from wind tunnel data with and without vortex generators at two Reynolds numbers. These data are shown for a Mach number of 0.85 and show no variation with angle of attack. In other cases, an angle of attack accountability may be required. The basic wind tunnel data which establishes the base for extrapolation must represent a full-chord

turbulent condition since it must be presumed that this condition will exist in the flight case. Tests at wind tunnel Reynolds numbers high enough to assure natural transition very near the leading edge are very valuable for this purpose since they eliminate the uncertainties which result from the lack of precision in transition fixing techniques. The other model conditions discussed above are needed only for the purpose of defining the effect of trailing-edge separation on shock location.

Comparison of Extrapolation With Flight Data

An example of the extrapolation procedure is presented in this section to clarify details of its implementation and to illustrate the comparison of extrapolated data with high Reynolds number test data. Figure 54 summarizes data at $\mathcal{M} = .193$ from low Reynolds number tests of the C-141 airplane. These data are typical of those which might be obtained from tests in existing wind tunnels for a new aircraft design and include a pressure distribution at -2^{o} angle of attack and a Reynolds number of 6×10^{6} and the correlated separation development at the same Reynolds number showing the key values CPTEO and B1/2*. These key values, plus similar values obtained from data measured at Reynolds numbers up to 10 million (which are achievable in several existing wind tunnels) are shown plotted against Reynolds number. The variation of shock location against trailing-edge pressure recovery are the data shown previously in Figure 53.

The first step in the extrapolation procedure, illustrated in Figure 55, simply involves fitting the general scale effect curves to the low Reynolds number measured values of B1/2* and CPTEO, and moving the separation development curves to values indicated for the higher Reynolds numbers. Such curves are shown for Reynolds numbers of 25 and 72 million.

The procedure for defining high Reynolds number values of CPTE, CPSH and shock location is illustrated in Figure 56. For an assumed series of values of B1/2, values of CPTE, and XCSH can be read from the two curves as illustrated. XCSH defines the shock location which can be located, by definition, on the locus of MLN = 1. The corresponding value of CPSH can be calculated from B1/2 and its location defined by using the appropriate slope of the shock pressure rise from Figure 3. Since $B1/2 = \frac{\frac{P_O}{P_P}\sqrt{M}-A}{\sqrt{1 - XCSH}}$, and CPSH is the pressure coefficient corresponding to P_P, CPSH can be calculated from:

$$CPSH = \frac{1}{.7M^2}\left[\frac{\sqrt{M}}{(B1/2)\sqrt{1 - XCSH} + A} - 1\right]$$

A curve describing the locus of values of CPSH (at which the shock pressure rise begins) can now be placed on the pressure distribution plot as shown on Figure 57. The predicted high Reynolds number pressure distribution is now completed by extrapolating the wind tunnel pressure distribution to its intersection with the CPSH locus, and completing the pressure rise curves through the shock and from the foot of the shock to the trailing edge value CPTE. Guidance in extrapolating the pressure distribution can be obtained either from the measured data which result in aft shock locations (far aft transition locations or with vortex generators) or from analytical determinations. The pressure rise from the foot of the shock to the trailing edge can be assumed to be linear without incurring serious error.

Figure 58 compares two pressure distributions measured in flight at a Reynolds number of 72 million with predictions accomplished as just described. The correlation between the extrapolated data (dashed lines) and the flight-measured points is shown to be reasonably good, and certainly within the accuracy required for an engineering determination of wing load distributions. Because of the scatter present in the basic information used in this correlation and extrapolation process, and the simplifying assumptions which are inherent in the generalizations applied, random discrepancies between extrapolated and measured data must be anticipated. The discrepancy shown in Figure 58 is quite small in comparison with the differences shown in Figure 57 where a change in shock location of 10% chord is predicted between wind tunnel and flight conditions. In extreme cases, wind tunnel data have been shown to result in shock locations which differ from flight measurements by 20 to 30 percent chord.

A comparison is shown in Figure 59 of data for the same station on the C-141 wing extrapolated to the highest Reynolds number tested in the semispan model tests of Reference 3. In this instance, the agreement is quite good at 4° angle of attack but the agreement deteriorates somewhat for lower angles of attack. The data for this spanwise station is one of the cases where the experimental results do not agree well with the generalized scale effect plot of Figure 46.

Figure 60 presents a comparison of flight data at the outboard station of the C-5A wing with the predicted extrapolation. In this case again, the agreement is quite good.

CONCLUSIONS AND RECOMMENDATIONS

1. The development of trailing-edge separation as Mach number and angle of attack increase has been found to collapse into a single curve when correlated against the parameter $B\sqrt{1/2}$. This correlation has been successful for a number of high speed transport type wings having significantly different airfoil section characteristics.

2. An extrapolation procedure has been developed which will enable engineering estimates of full scale wing load distributions from low Reynolds number wind tunnel measurements.

3. Refinement of the correlation process through a consideration of boundary layer properties appears to be possible.

4. Additional studies of scale effects on supercritical wings would be desirable.

REFERENCES

1. AGARD C.P. No. 35 "Transonic Aerodynamics", September 1968.

2. AGARD C.P. No. 83 "Facilities and Techniques for Aerodynamic Testing at Transonic Speeds and High Reynolds Number", April 1971.

3. NASA CR-2604 "High Reynolds Number Tests of a C-141A Aircraft Semispan Model to Investigate Shock-Induced Separation", W. T. Blackerby and J. F. Cahill, October 1975.

4. Lockheed-Georgia Company Report LG1T6-1-16 "Development of Testing Technique Required to Duplicate Full Scale Wing Shock Location on a Wind Tunnel Model", J. M. Wright, May 1966.

5. AFFDL-TR-68-84 "Flight Test Investigation of Transonic Shock-Boundary Layer Phenomena", J. F. Cahill and B. L. Cooper, July 1968.

6. Lockheed-Georgia Company Report LG1T6-1-43 "Investigation of Static Pressure Distribution at High Mach and Reynolds Numbers of a 0.040-Scale Model in the AEDC 16-Foot Transonic Wind Tunnel", G. C. Bolen, April 1968.

7. ARL TR 74-0117 "Wing Pressure Distribution and Boundary Layer Data Obtained from C-5A Flight Testing", J. F. Cahill and W. A. Stevens, October 1974.

8. NASA TM-X 3544 "F-8 Supercritical Wing Flight Pressure, Boundary Layer, and Wake Measurements and Comparison with Wind Tunnel Data", L. C. Montoya and Richard D. Banner, July 1977.

9. "Boundary Layer and Flow Control" edited by G. V. Lachmann, Pergamon Press 1961, P. 1197FF by H. H. Pearcey.

10. NASA TN D-3580 "Wind Tunnel-Flight Correlation of Shock-Induced Separated Flow", D. L. Loving, 1966.

11. "Shock-Boundary Layer Interaction and Flow Separation" Heat Transfer and Fluid Mechanics Institute Procs., Stanford University Press., J. Erdos and A. Pallone, 1962.

12. NACA TN 3454 "Effect of a Discontinuity on Turbulent Boundary Layer Thickness Parameters with Application to Shock Induced Separation", E. Reshotko and M. Tucker, 1955.

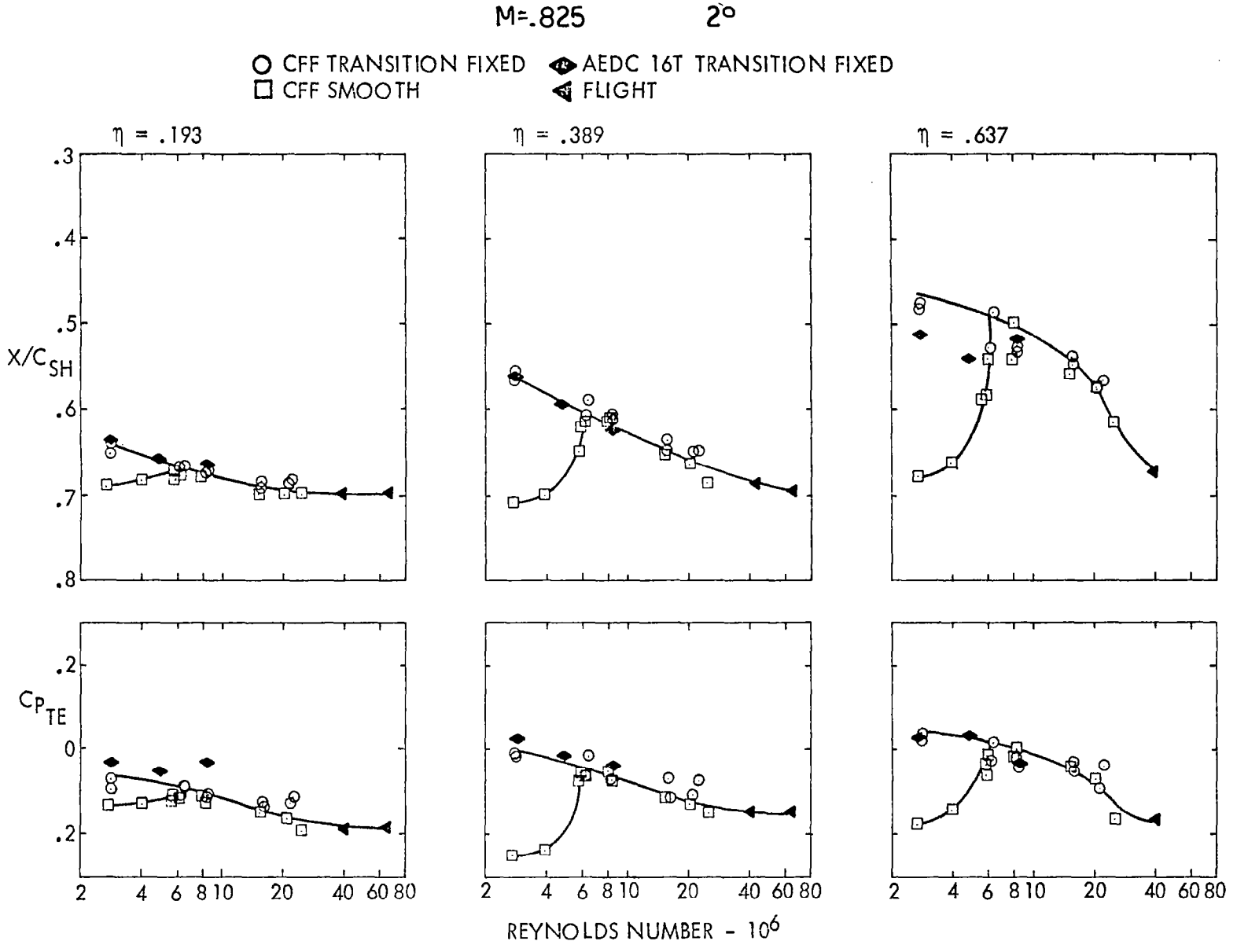

FIGURE 1. - SCALE EFFECT ON TRAILING-EDGE PRESSURE AND SHOCK LOCATION. C-141, FROM REFERENCE 3

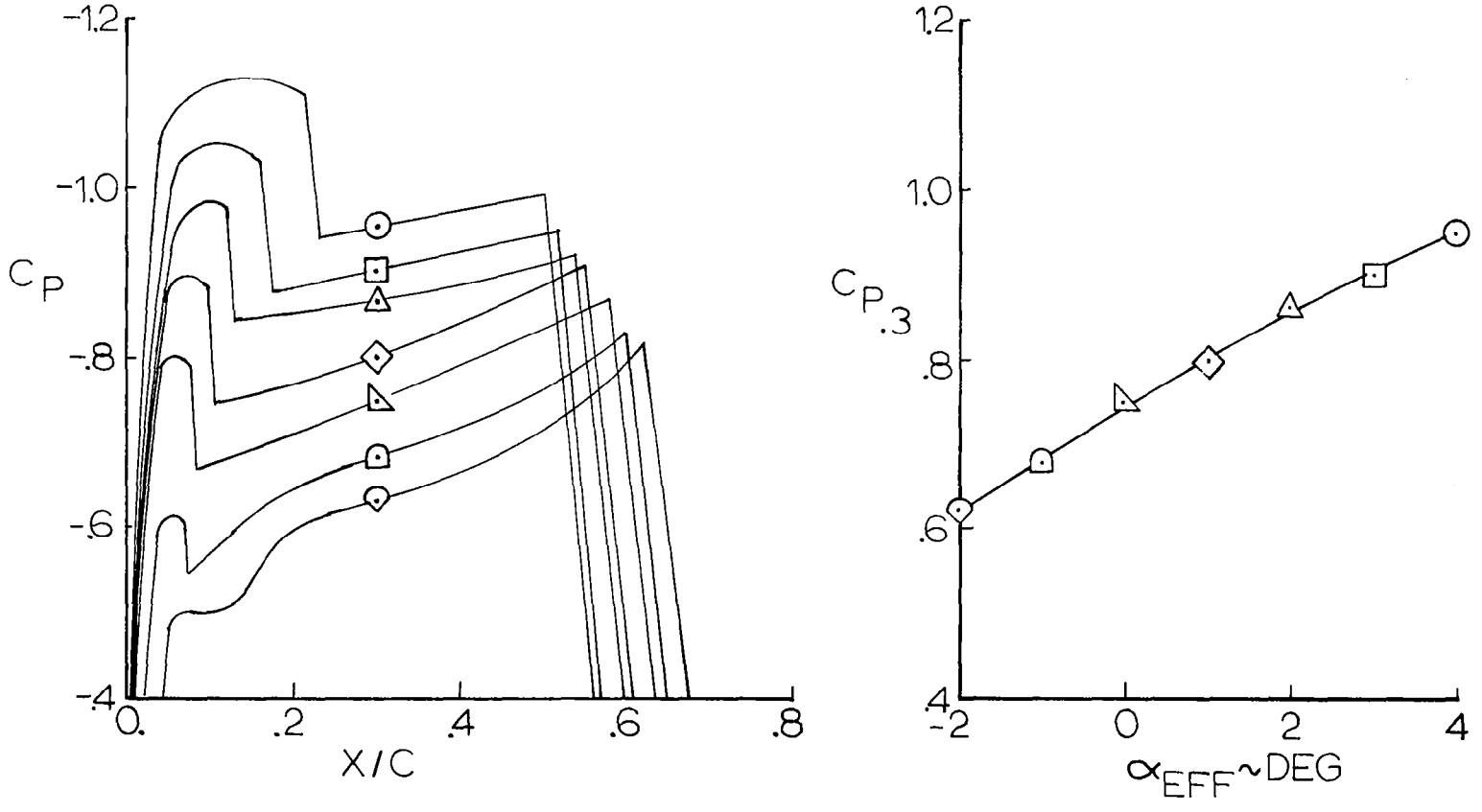

FIGURE 2. - DEFINITION OF EFFECTIVE ANGLE OF ATTACK

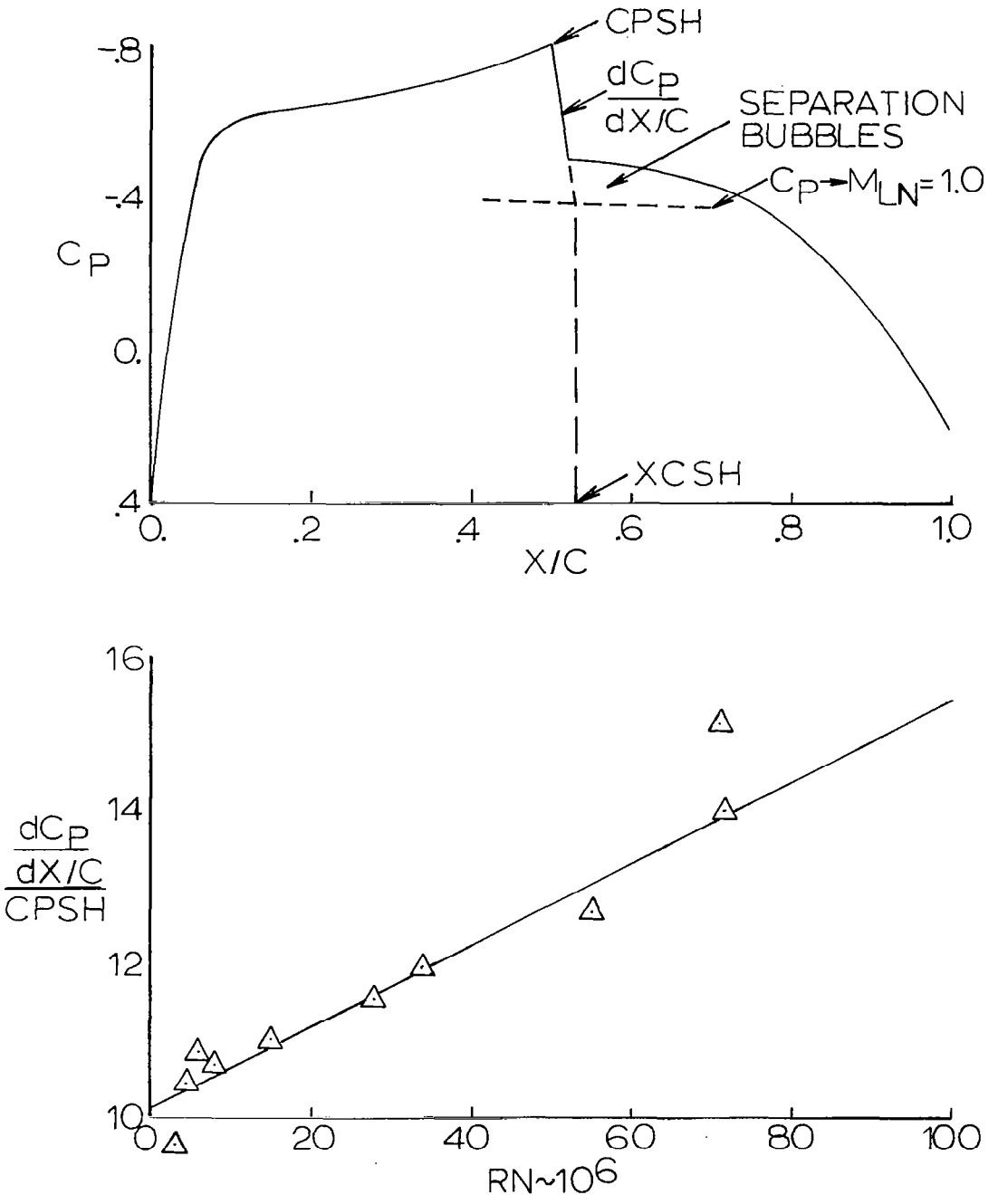

FIGURE 3. - SLOPE OF PRESSURE RISE THROUGH SHOCK

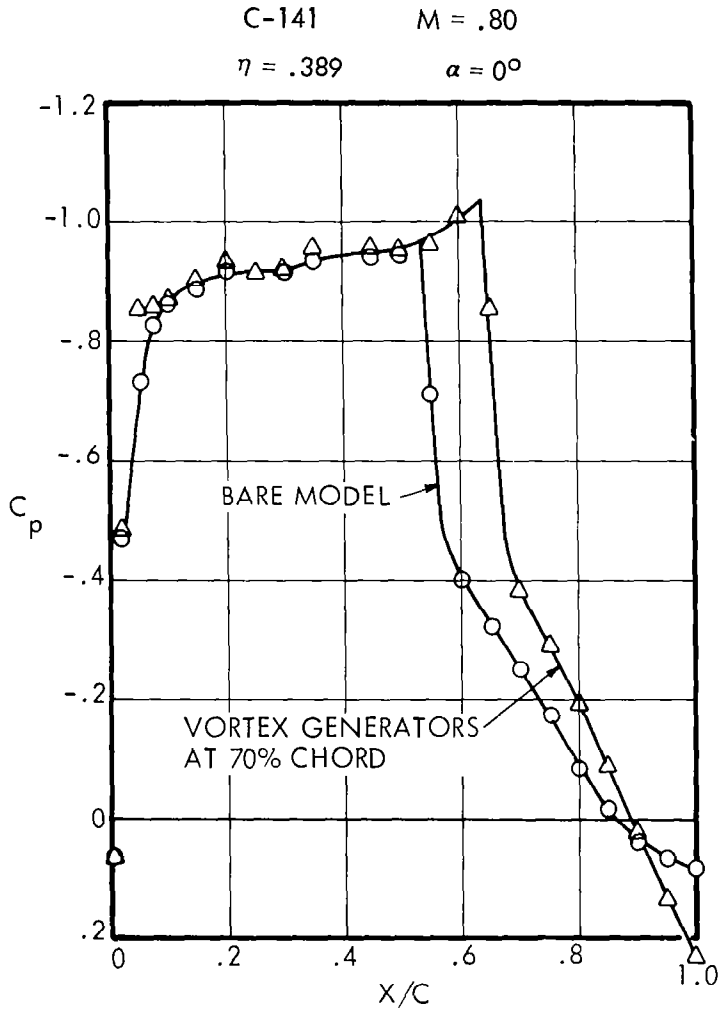

EFFECT OF VORTEX GENERATORS BEHIND SHOCK

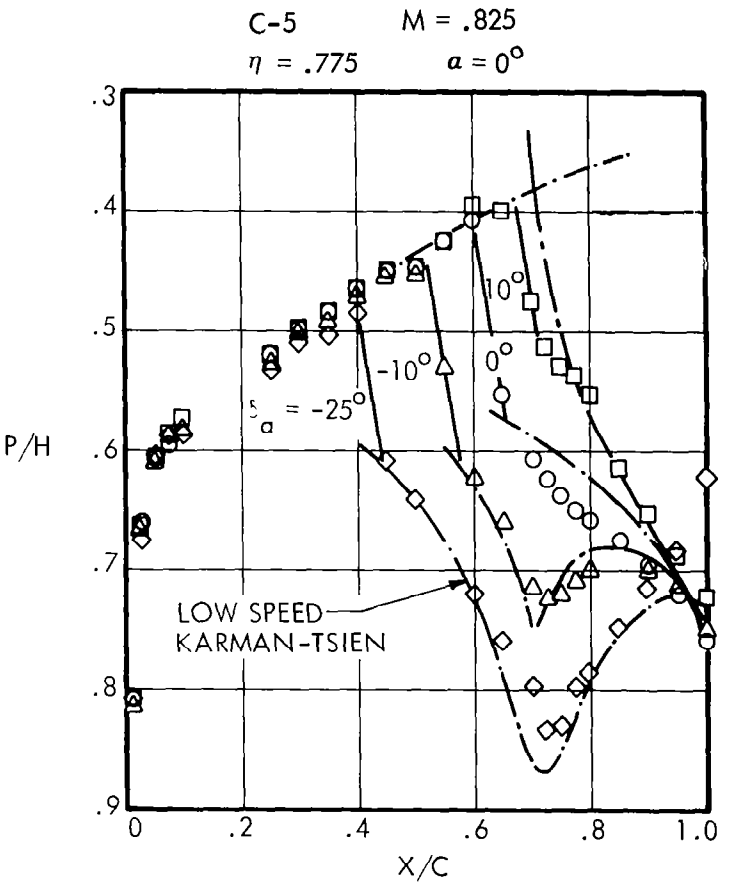

EFFECT OF AILERON DEFLECTION ON SHOCK LOCATION

FIGURE 4. - DOWNSTREAM PRESSURE CONTROLS SHOCK LOCATION

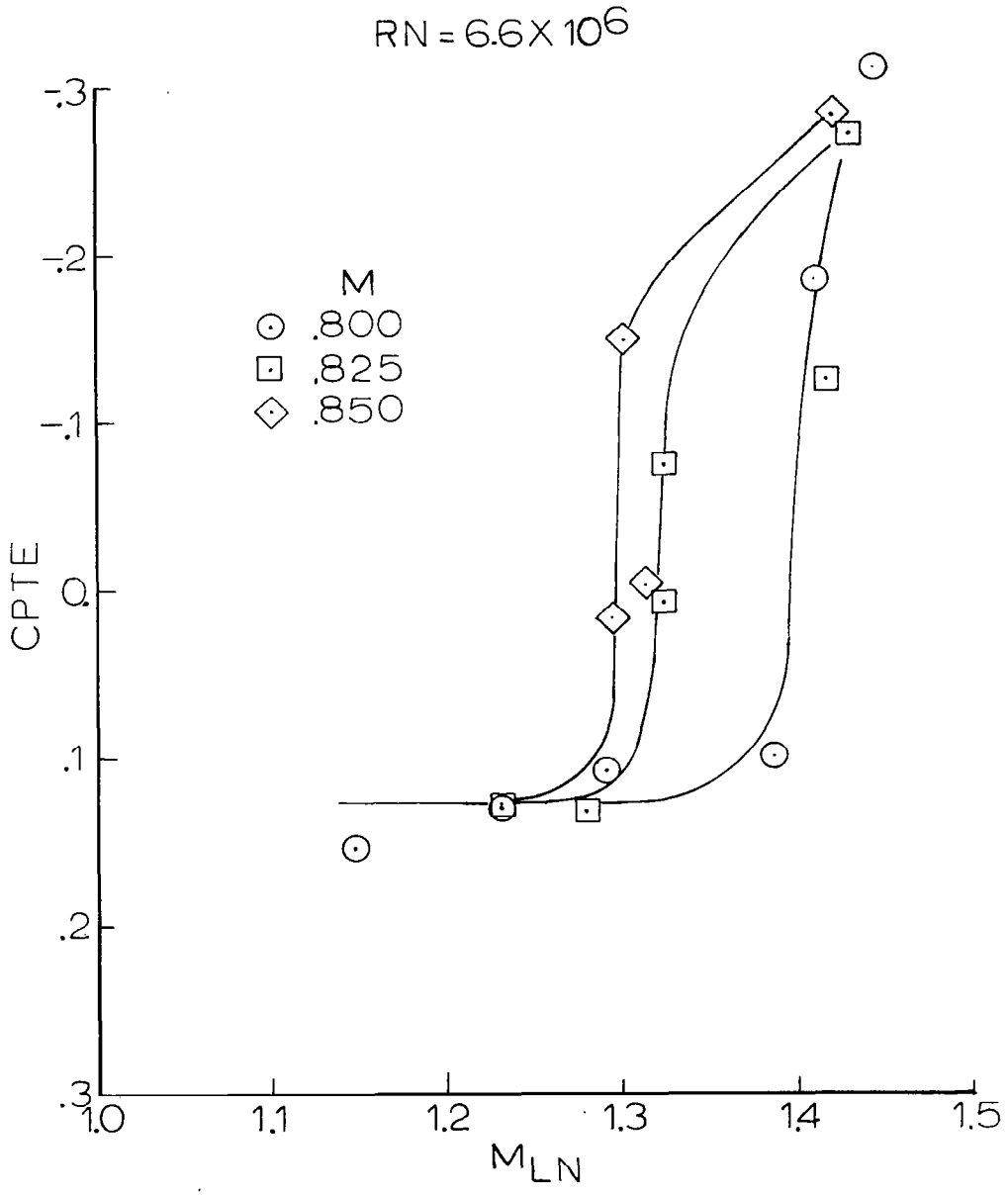

FIGURE 5. - TRAILING-EDGE PRESSURE COEFFICIENT VERSUS PEAK LOCAL MACH NUMBER. C-5, $\mathcal{R}$ = .45

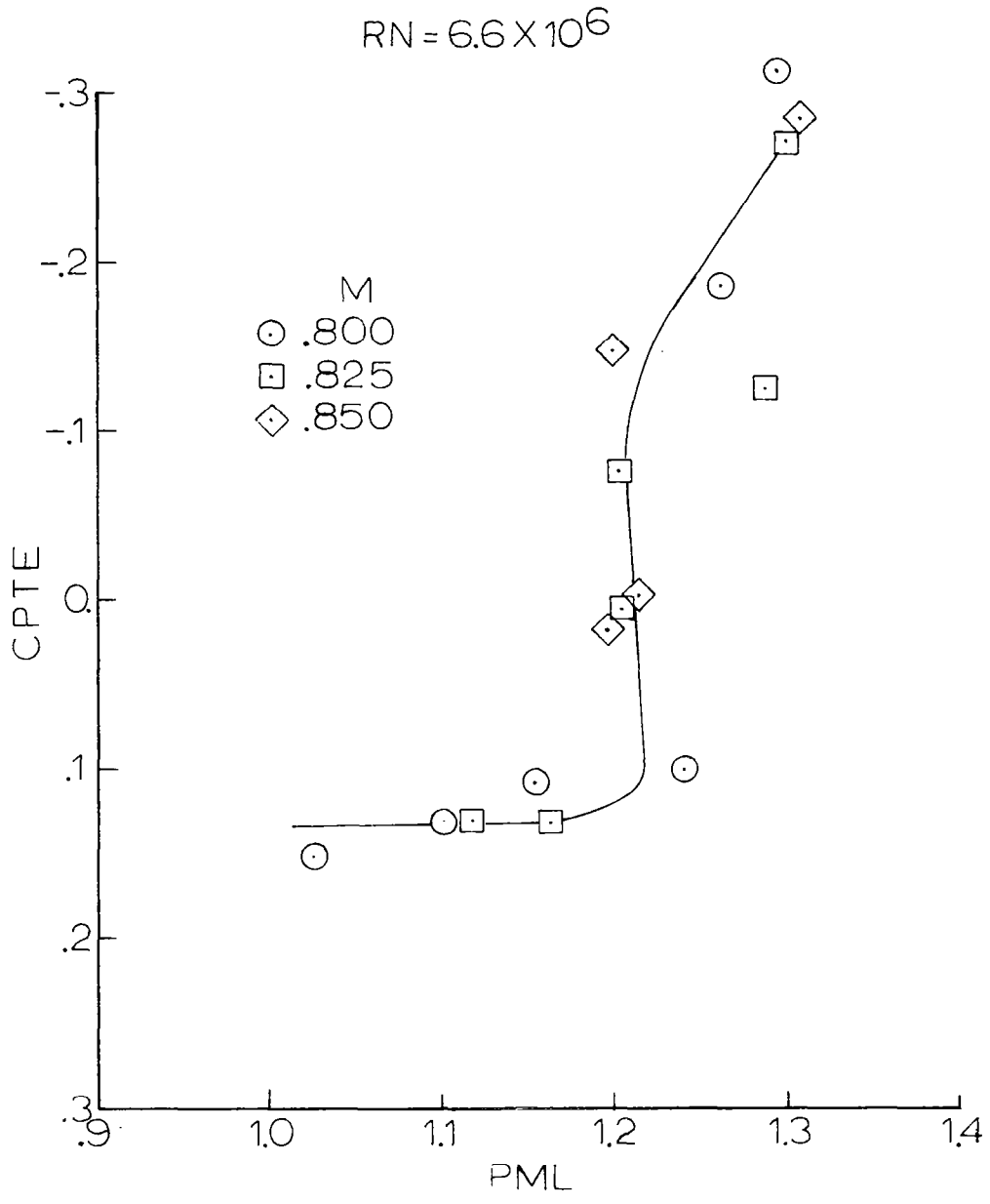

FIGURE 6. - INITIAL CORRELATION OF TRAILING-EDGE SEPARATION. C-5, $\mathcal{R}$ = .45

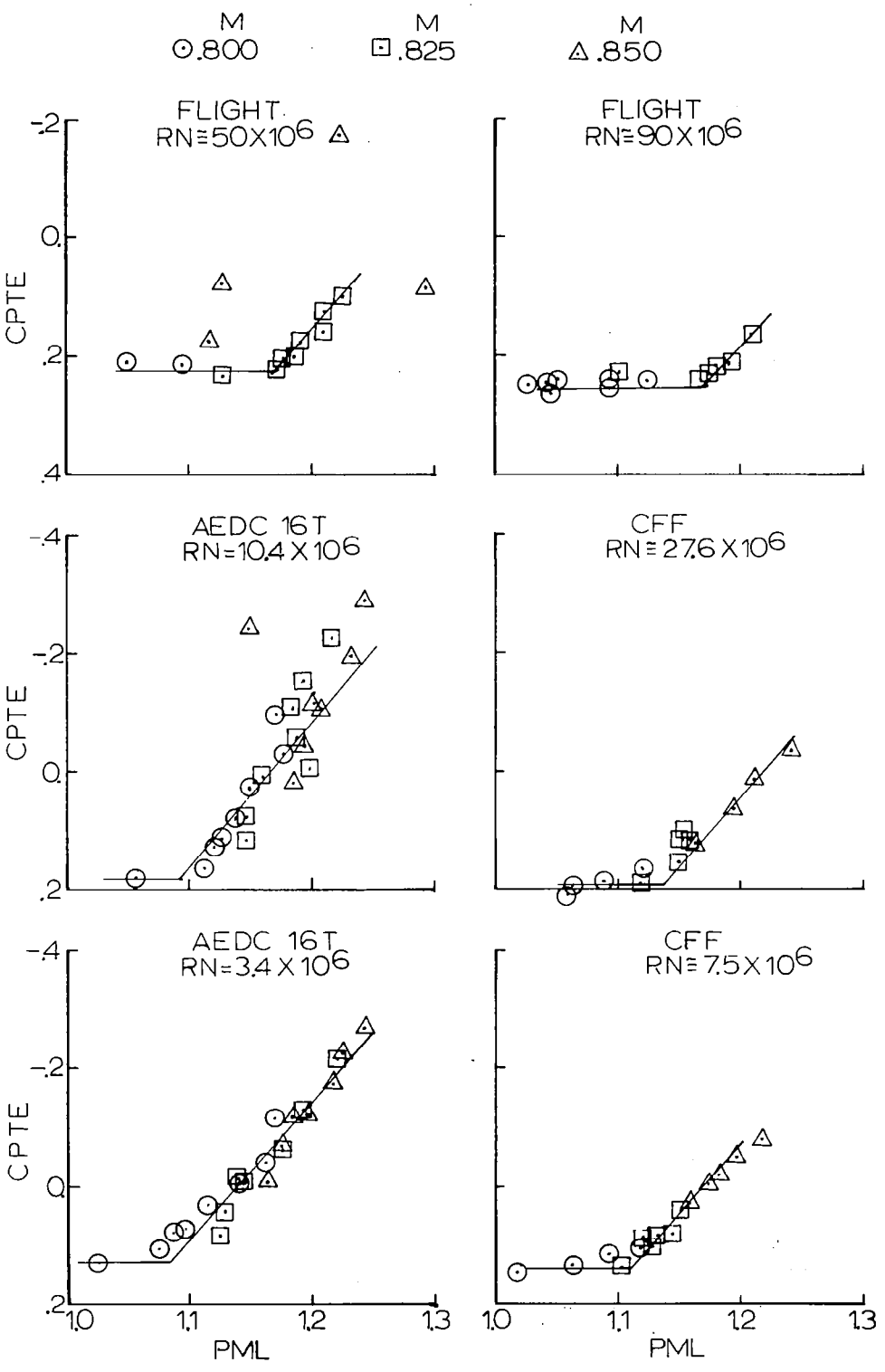

FIGURE 7. - INITIAL CORRELATION. C-141, $\mathcal{R}$ = .193

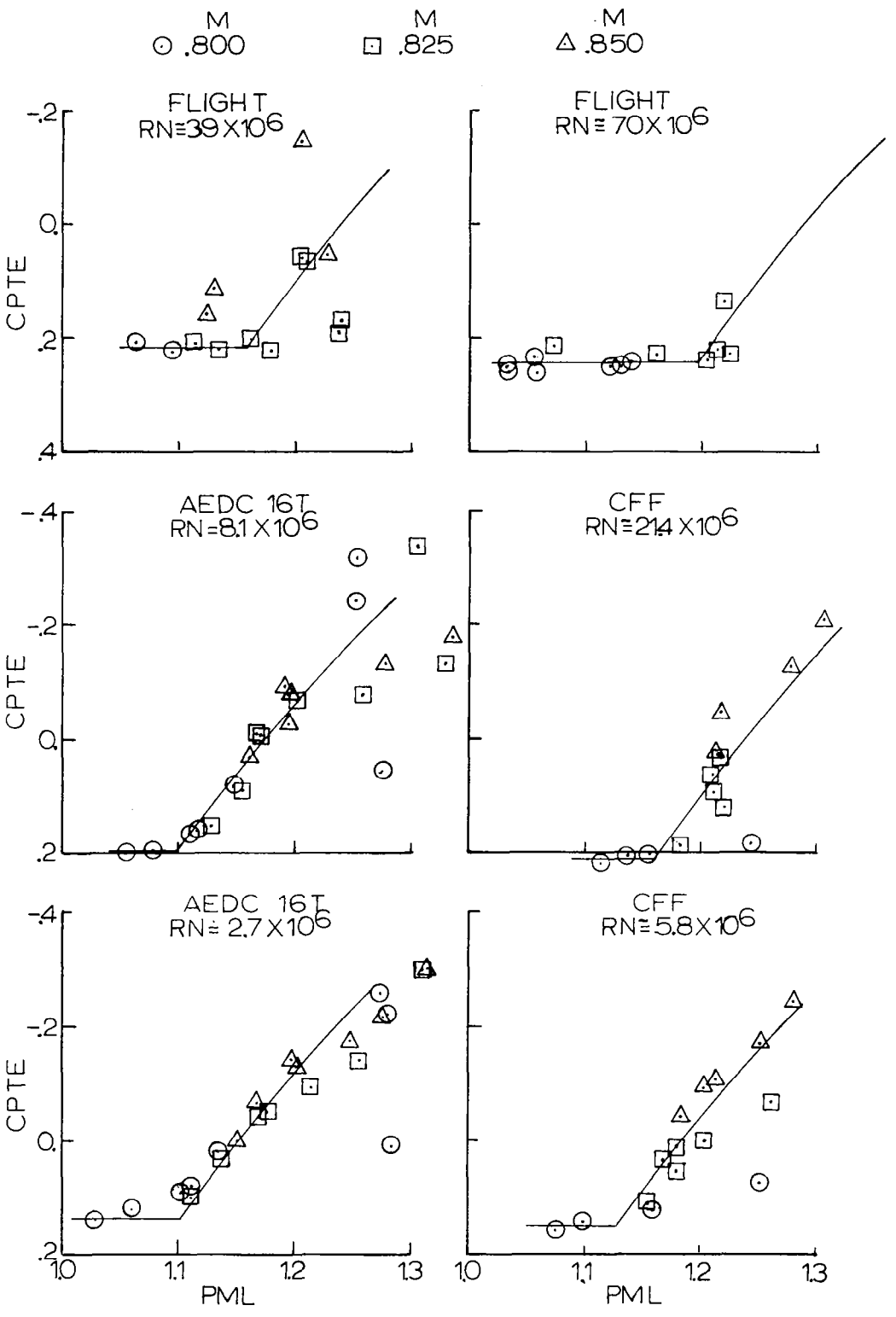

FIGURE 8. - INITIAL CORRELATION. C-141, n = .389

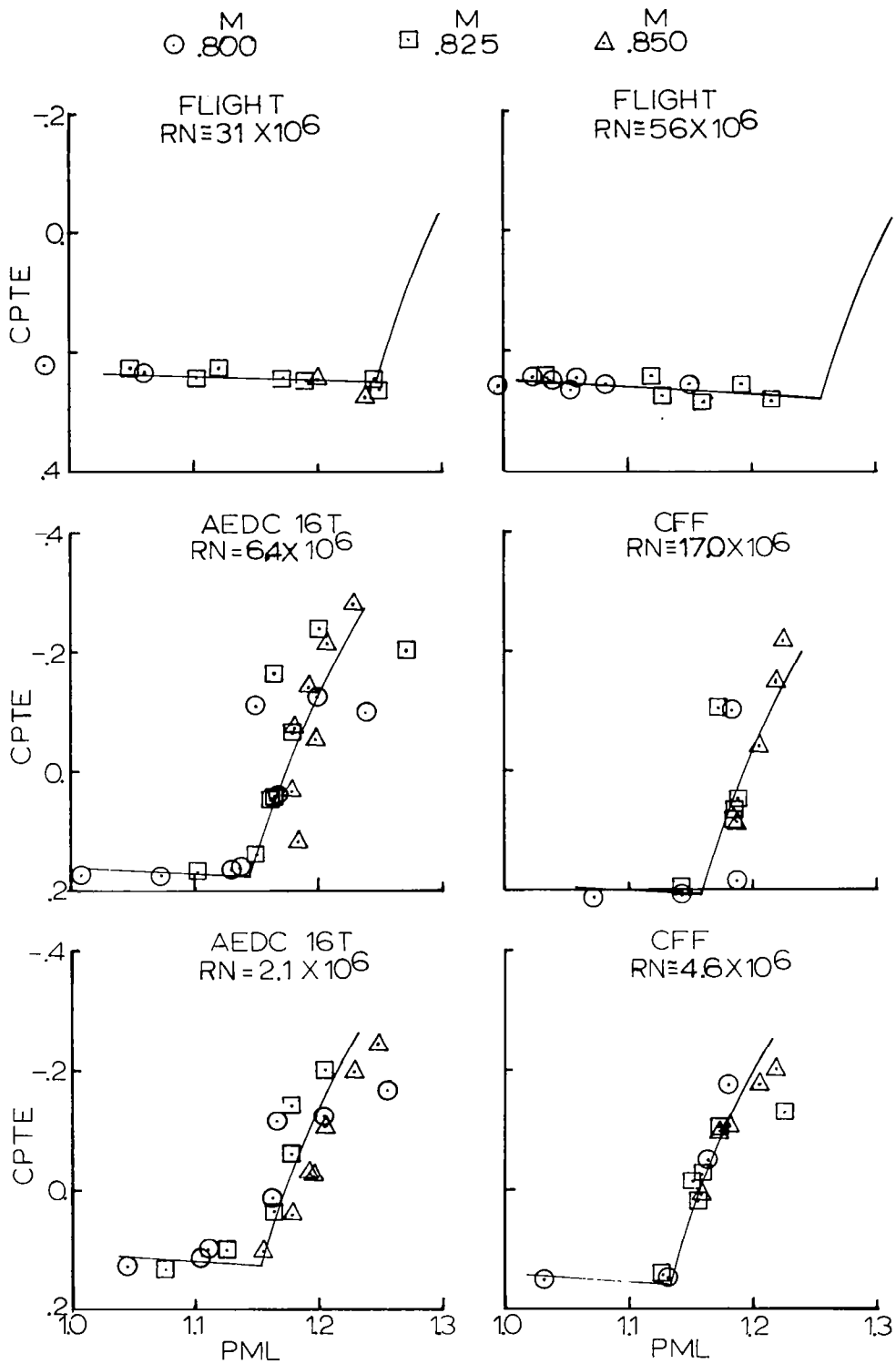

FIGURE 9. - INITIAL CORRELATION. C-141, $\mathcal{R}$ = .637

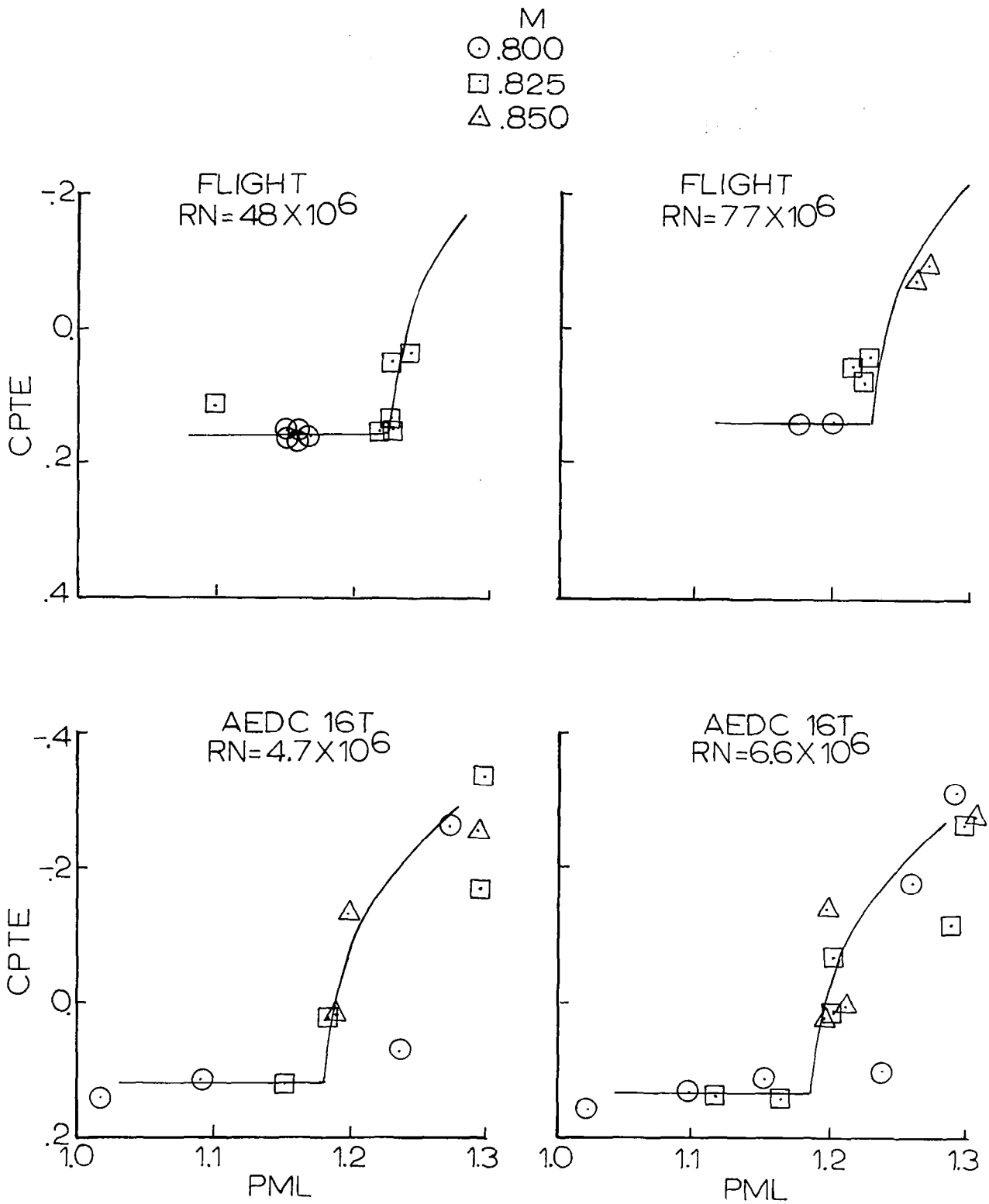

FIGURE 10. - INITIAL CORRELATION. C-5, $\mathcal{N}$ = .45

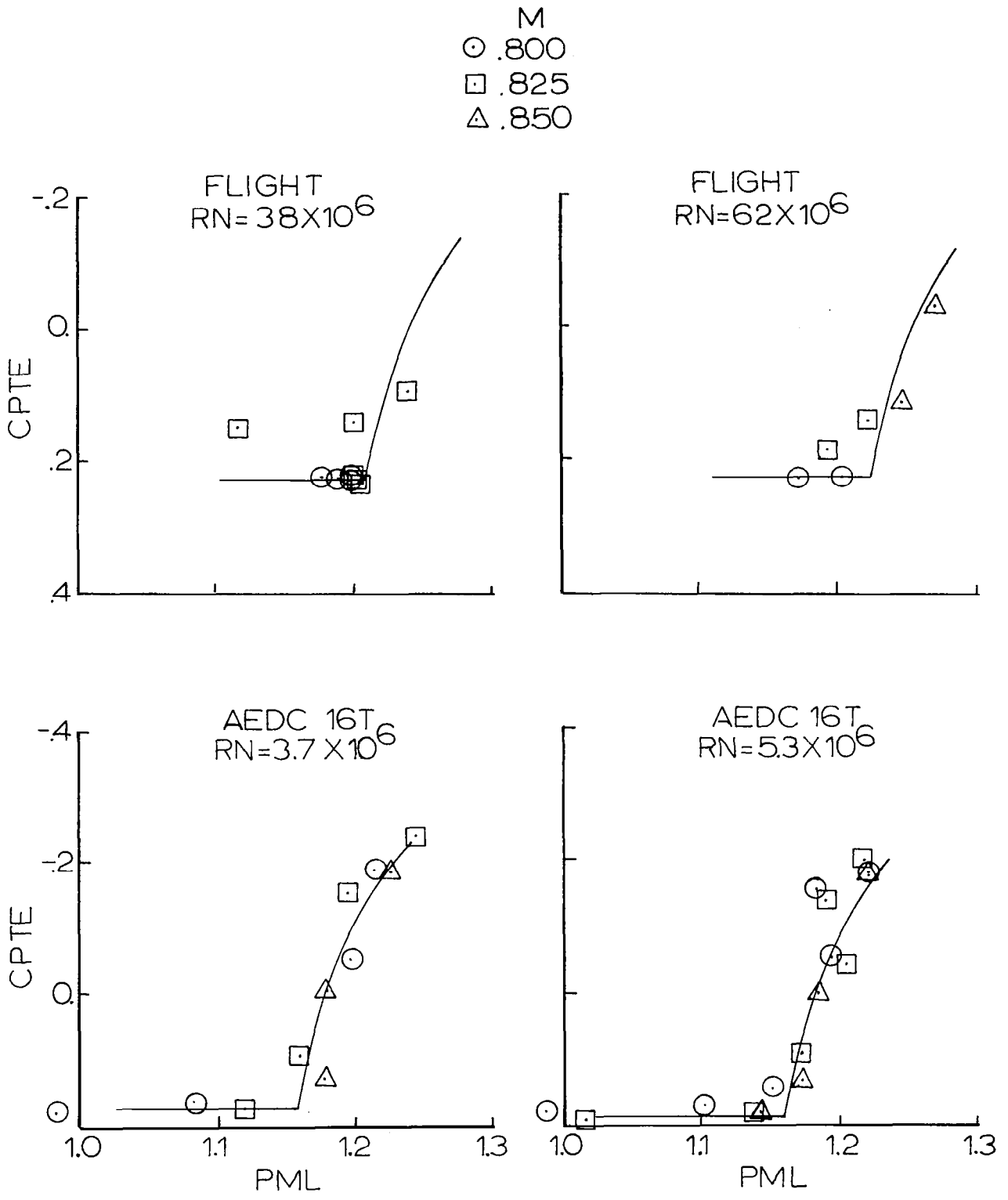

FIGURE 11. - INITIAL CORRELATION. C-5, $\mathcal{R}$ = .70

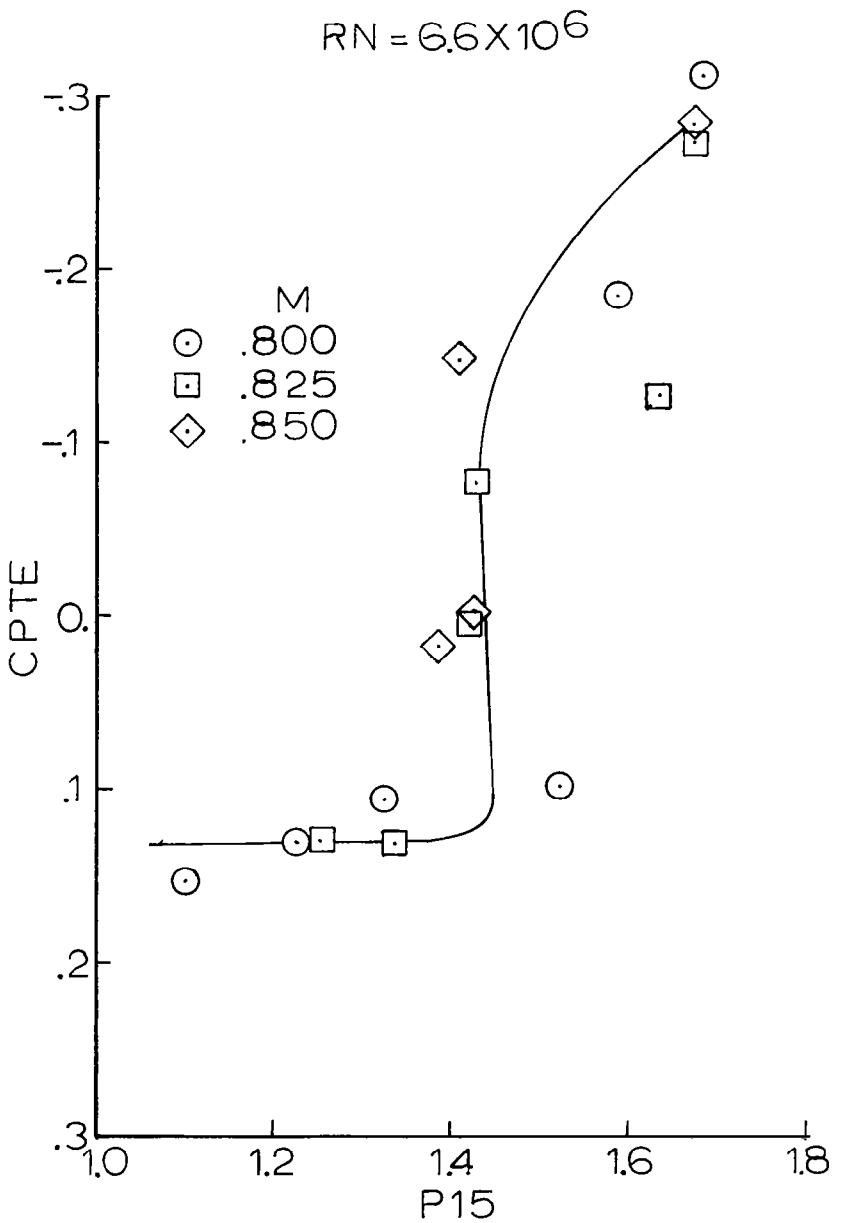

FIGURE 12. - CORRELATING PARAMETER P15

C-5 η = .45

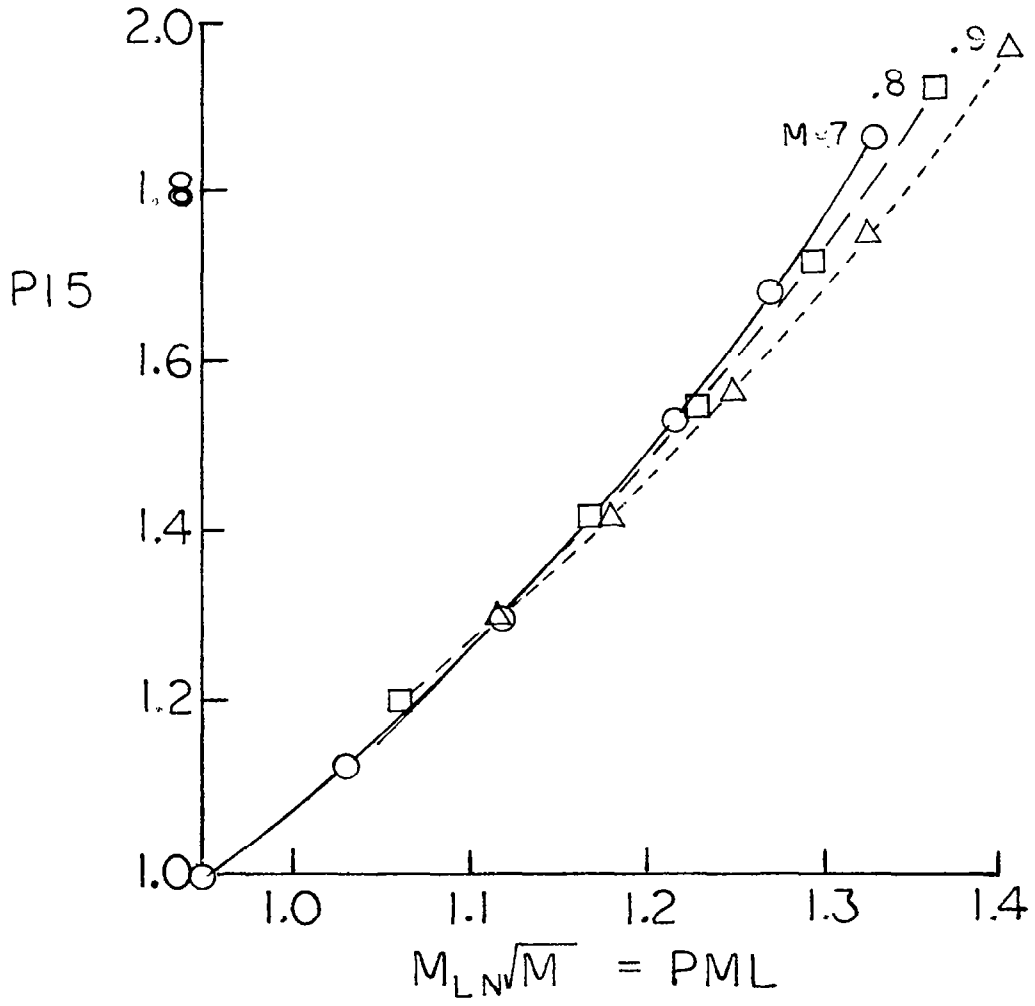

FIGURE 13. - RELATIONSHIP BETWEEN CORRELATING PARAMETERS

RAE 864

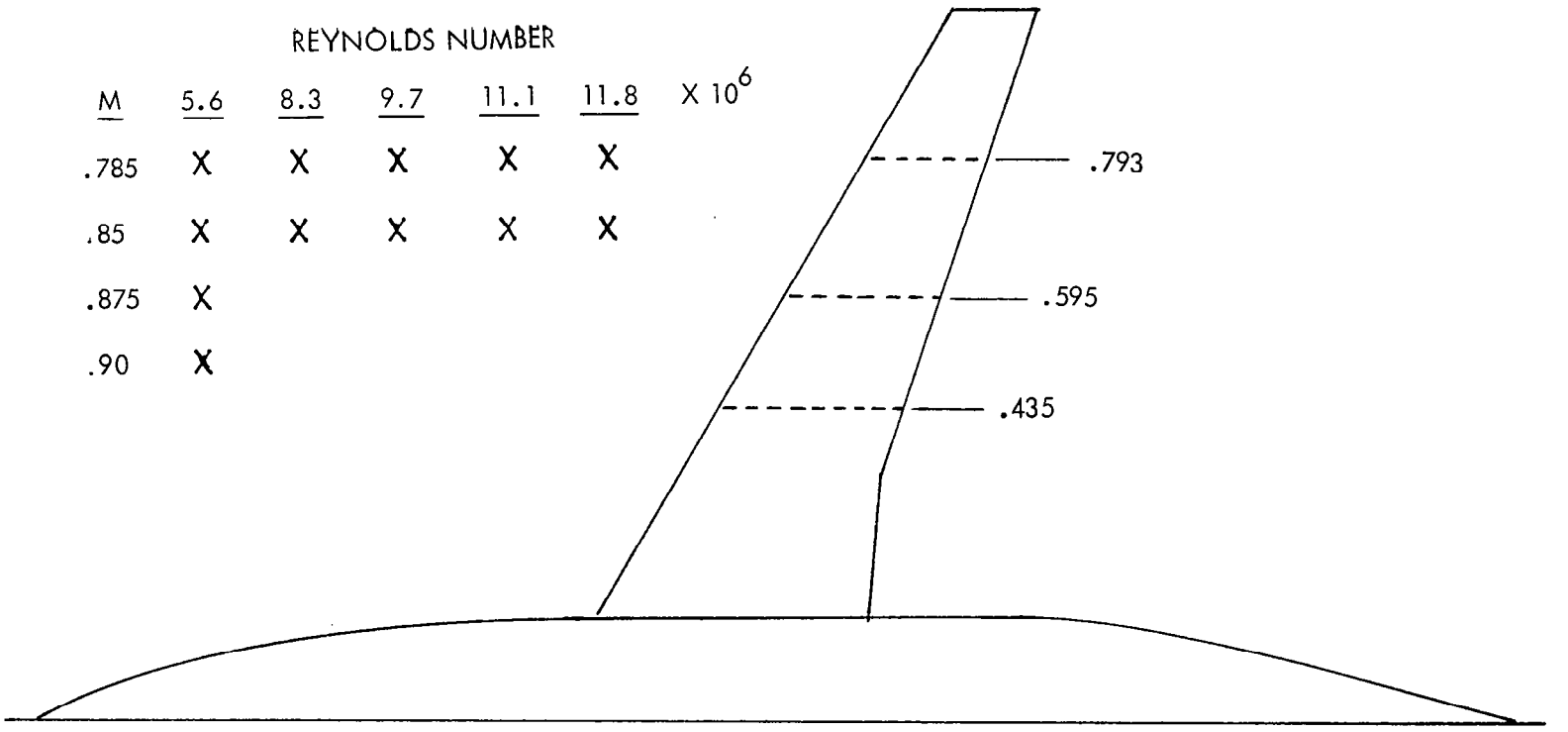

FIGURE 14. - RAE MODEL 864 CONFIGURATION AND DATA

RAE 864

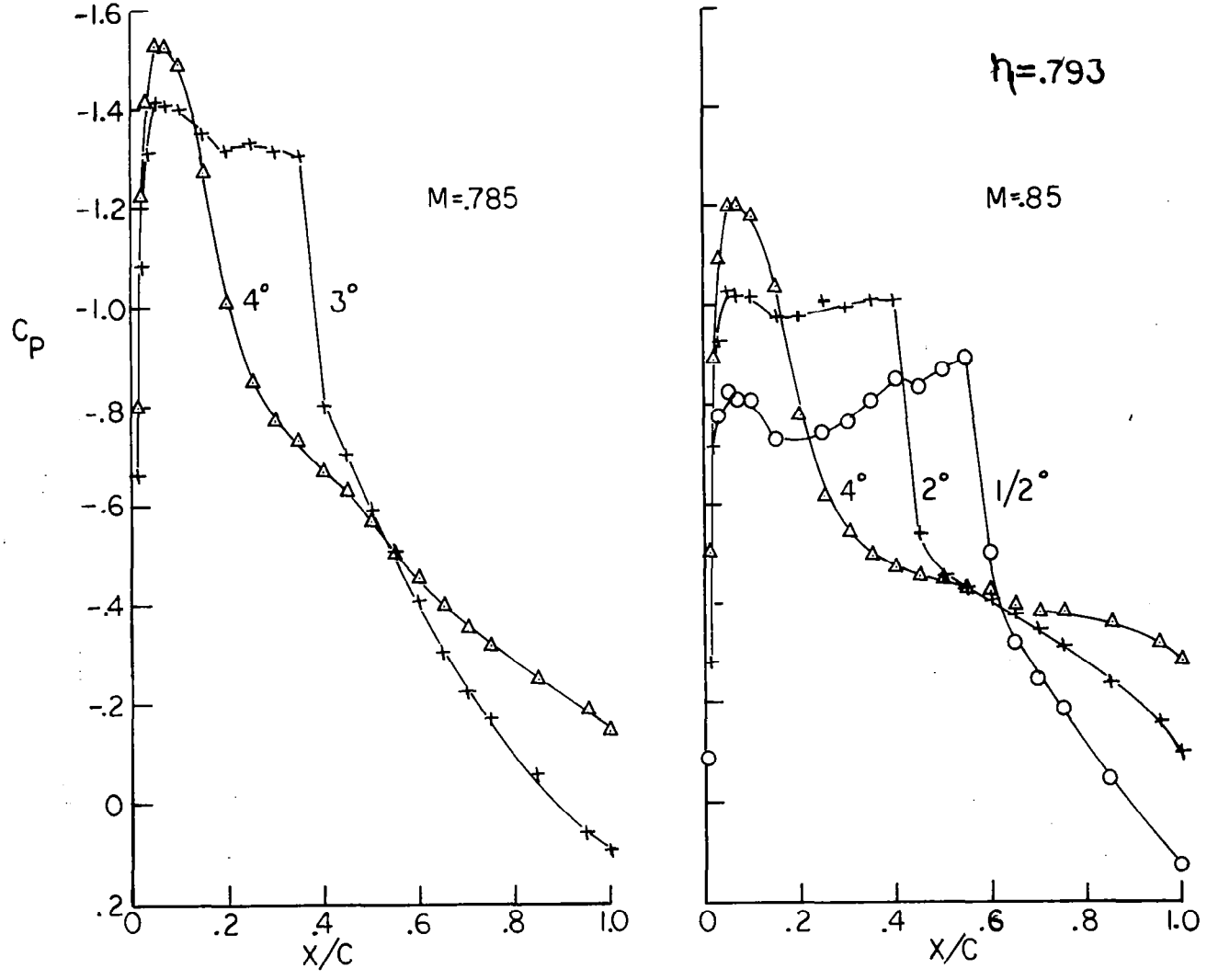

FIGURE 15. - TYPICAL PRESSURE DISTRIBUTIONS, RAE MODEL 864

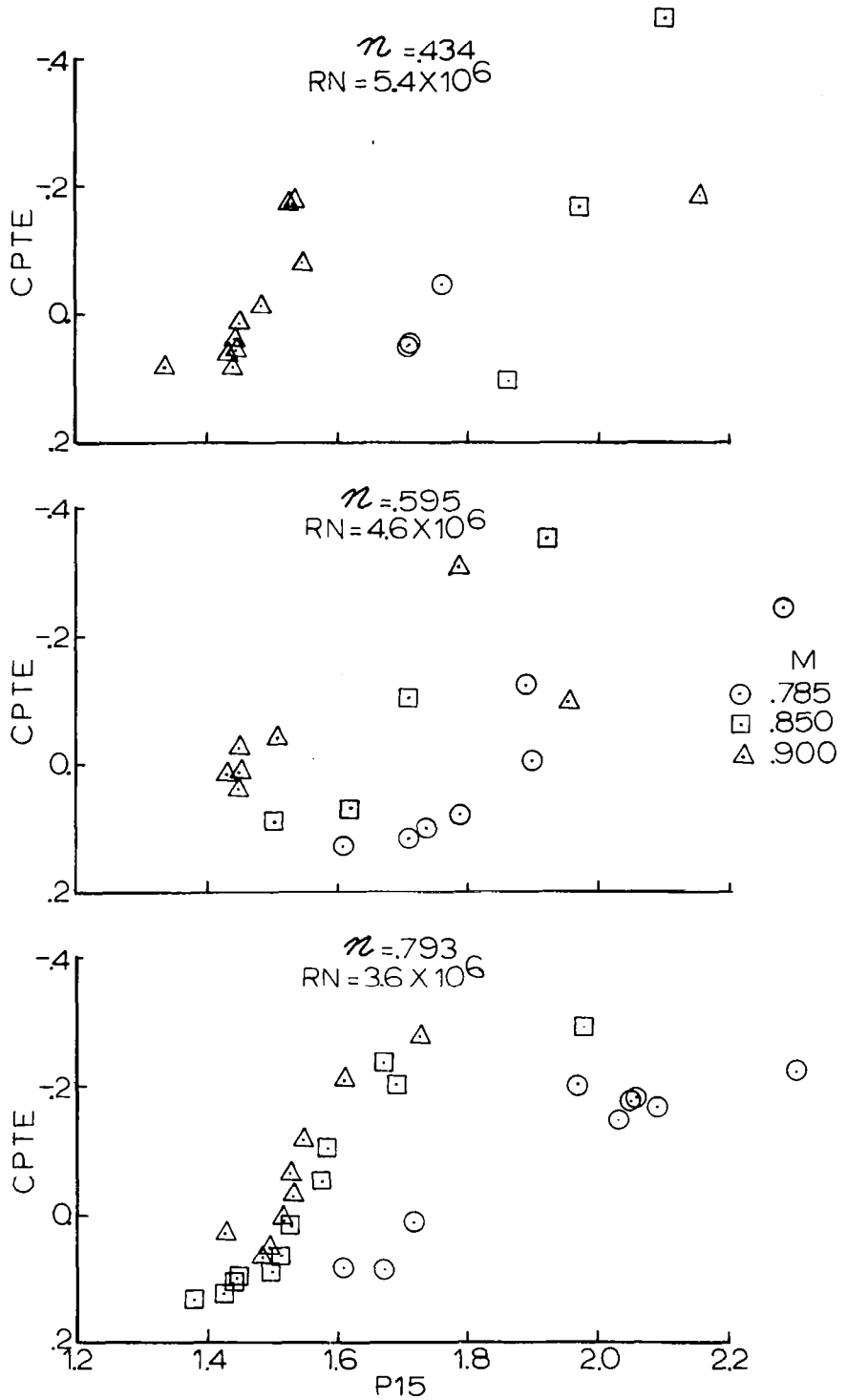

FIGURE 16. - CPTE VERSUS P15. RAE MODEL 864

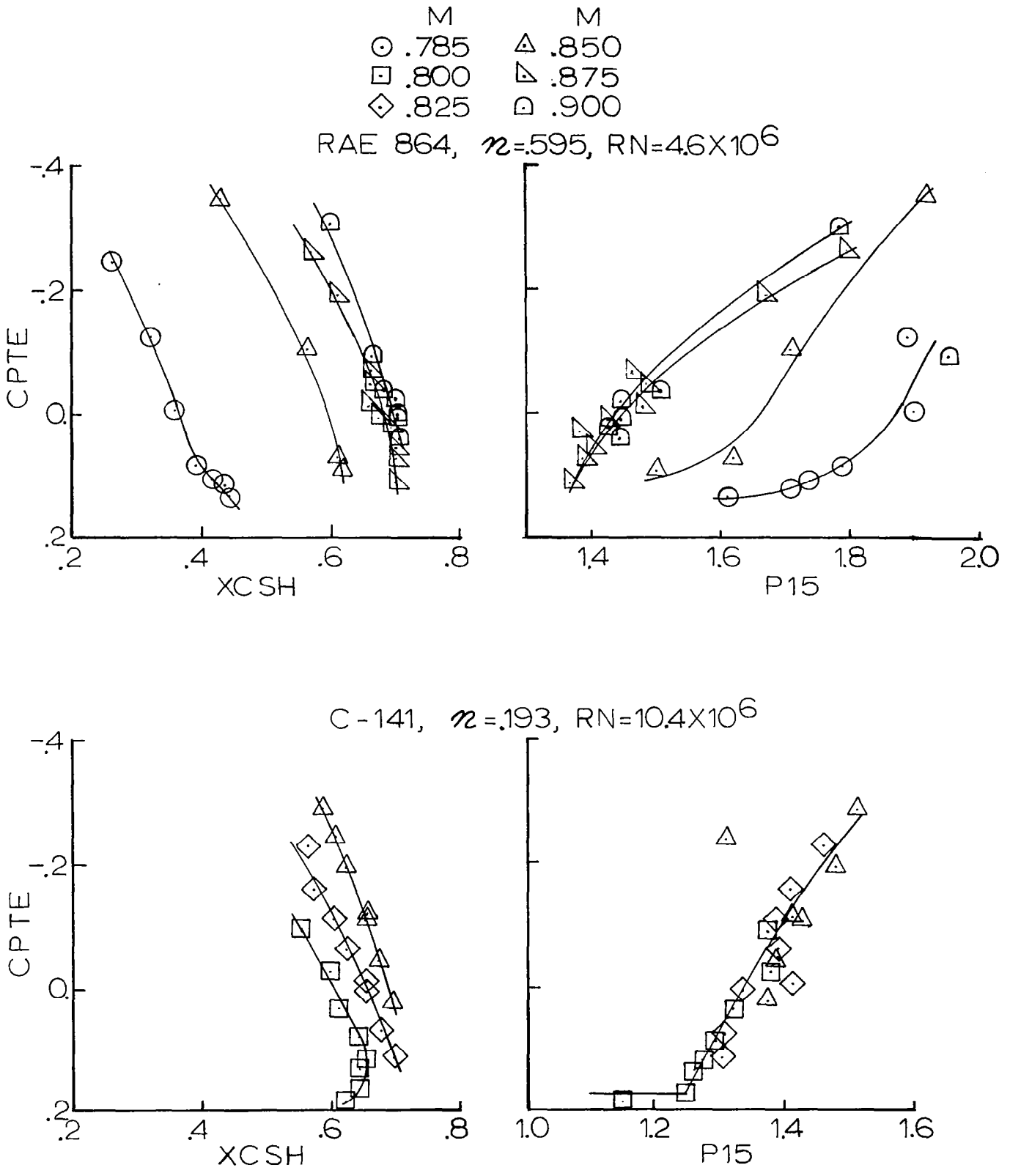

FIGURE 17. - VARIATION OF CPTE WITH P15 AND SHOCK LOCATION

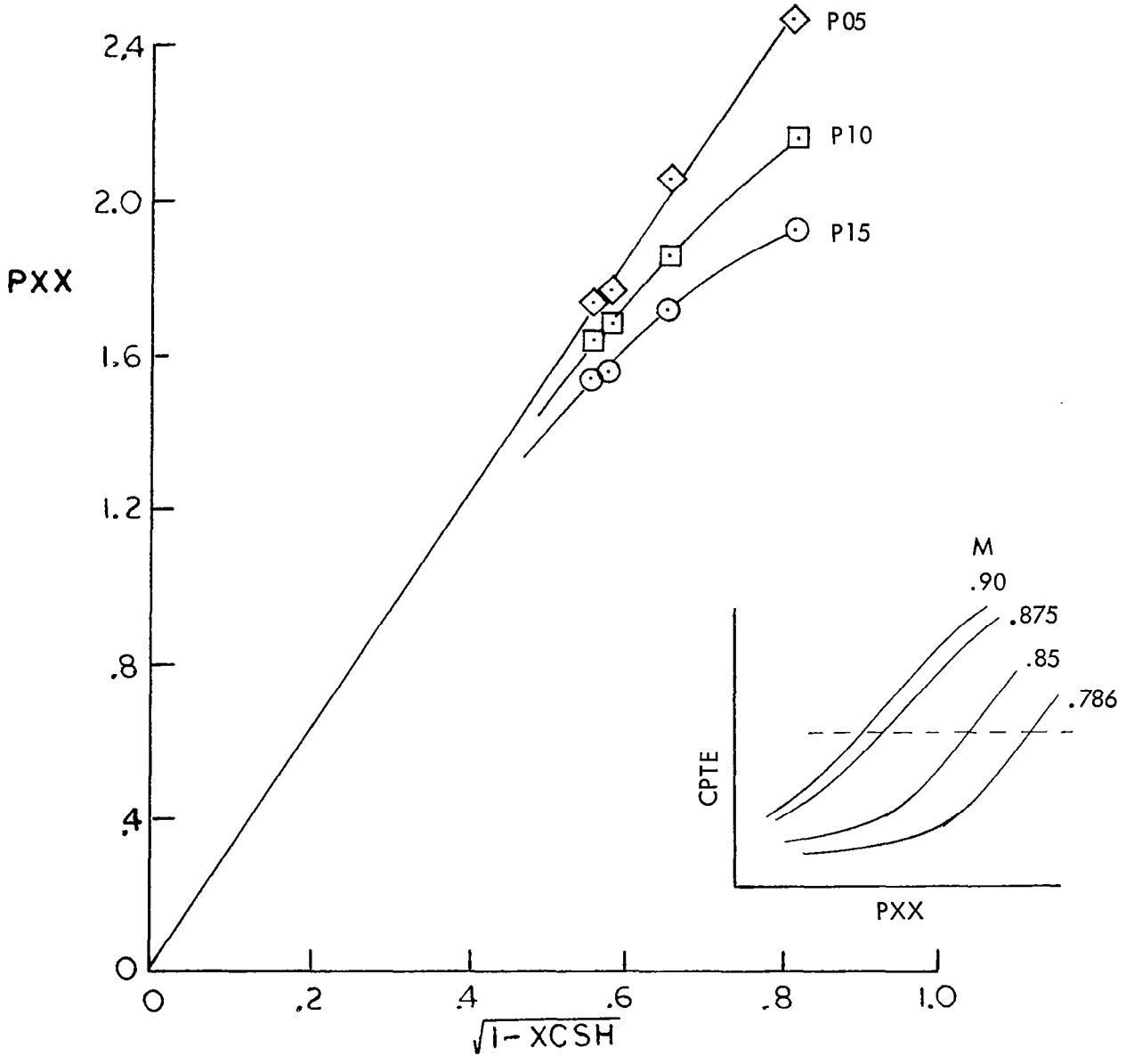

FIGURE 18. - EVOLUTION OF CORRELATING PARAMETER B 1/2.

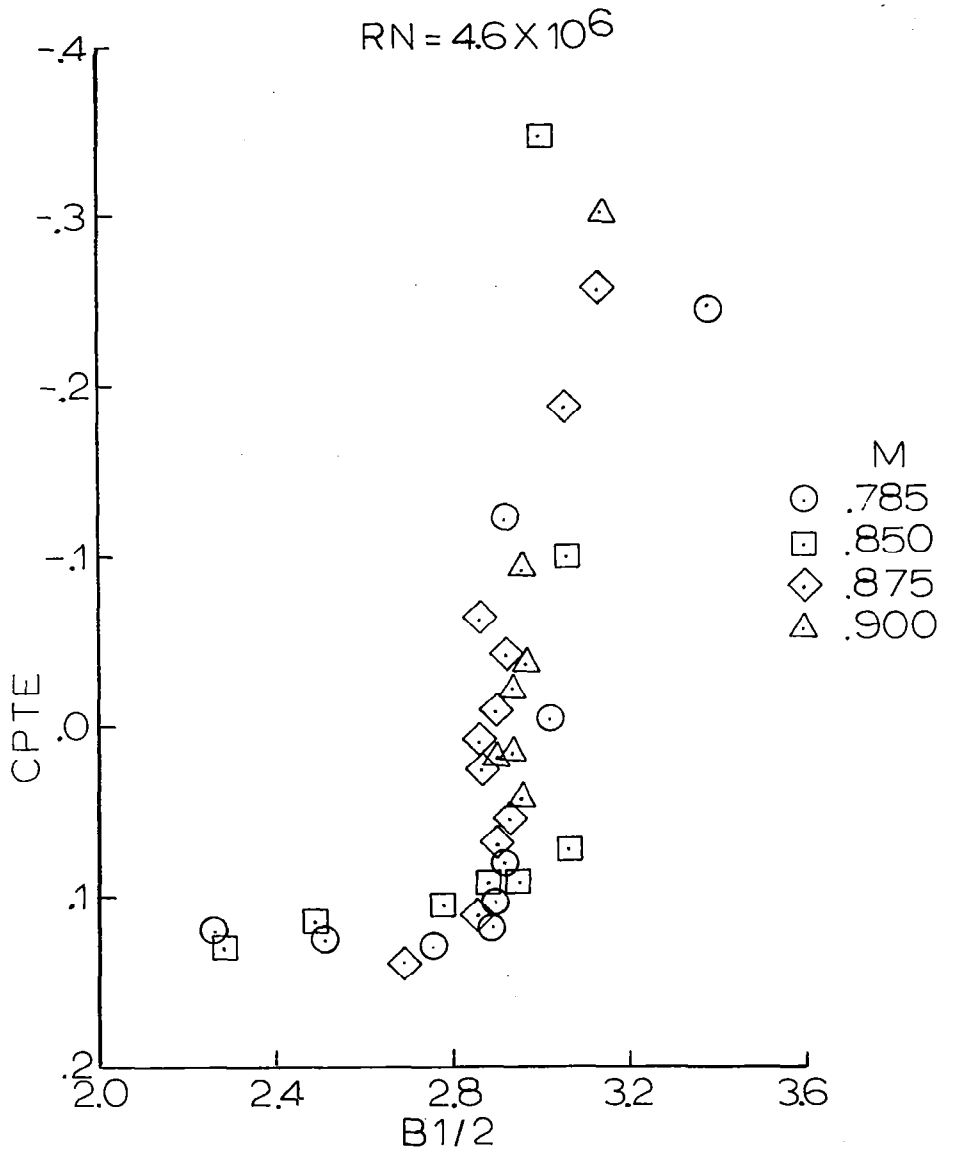

FIGURE 19. - CORRELATION OF SEPARATION DEVELOPMENT WITH SHOCK LOCATION ACCOUNTABILITY. RAE MODEL 864, $\mathcal{R}$ = .595

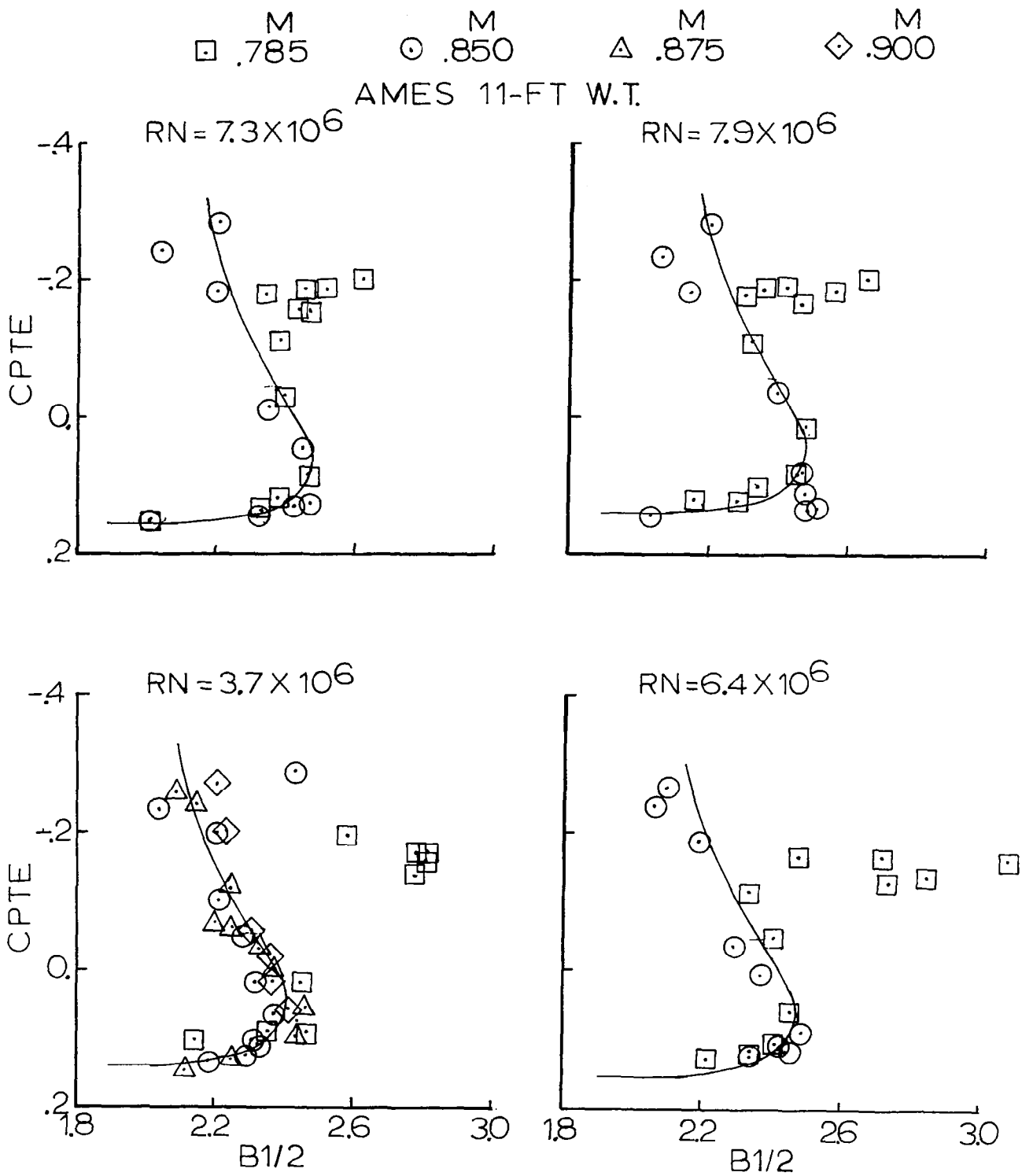

FIGURE 20. - FINAL CORRELATION. RAE MODEL 864, $\mathcal{M}$ = .793, A = .250

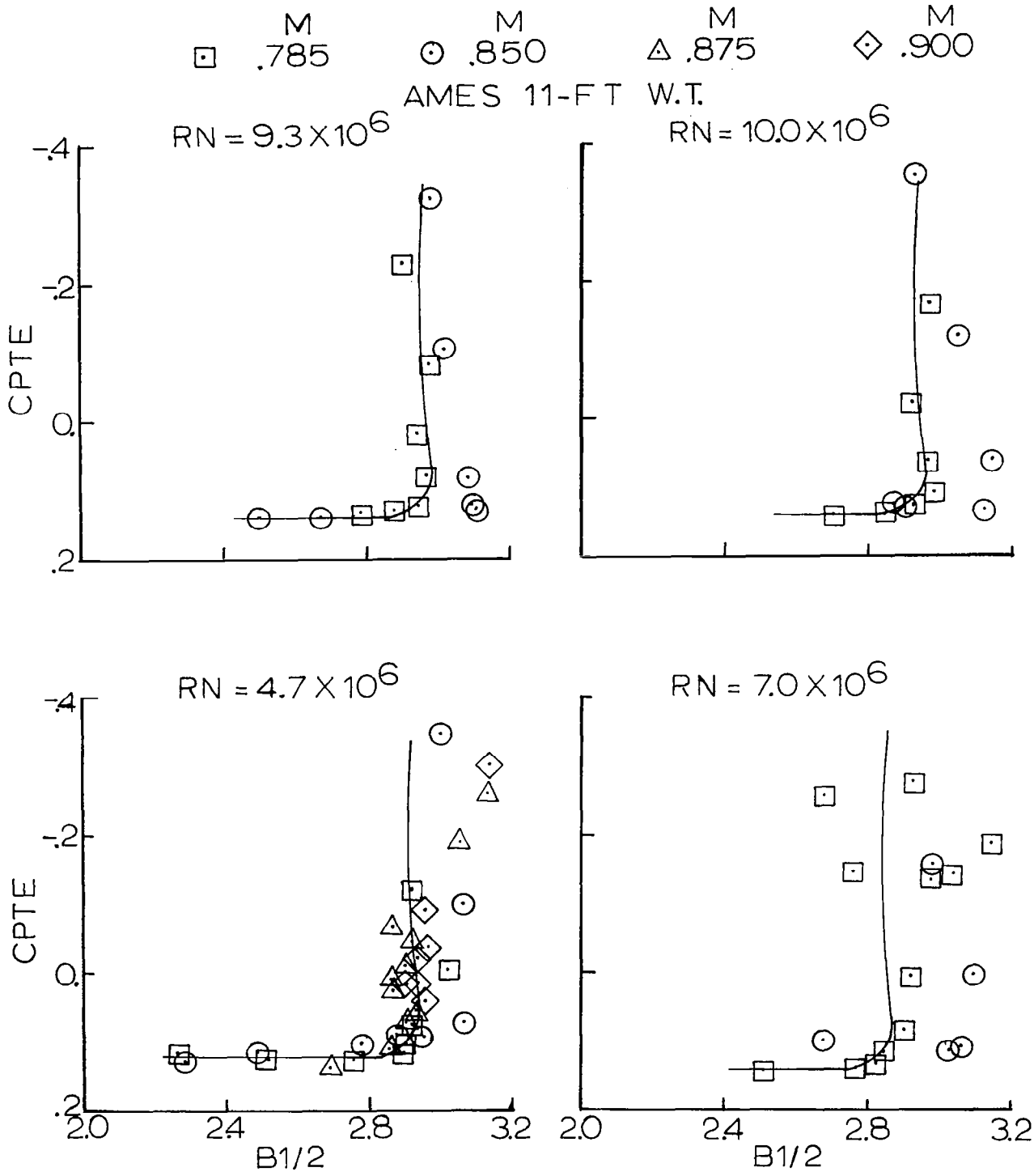

FIGURE 21. - FINAL CORRELATION. RAE MODEL 864, $\mathcal{N}$ = .595, A = 0

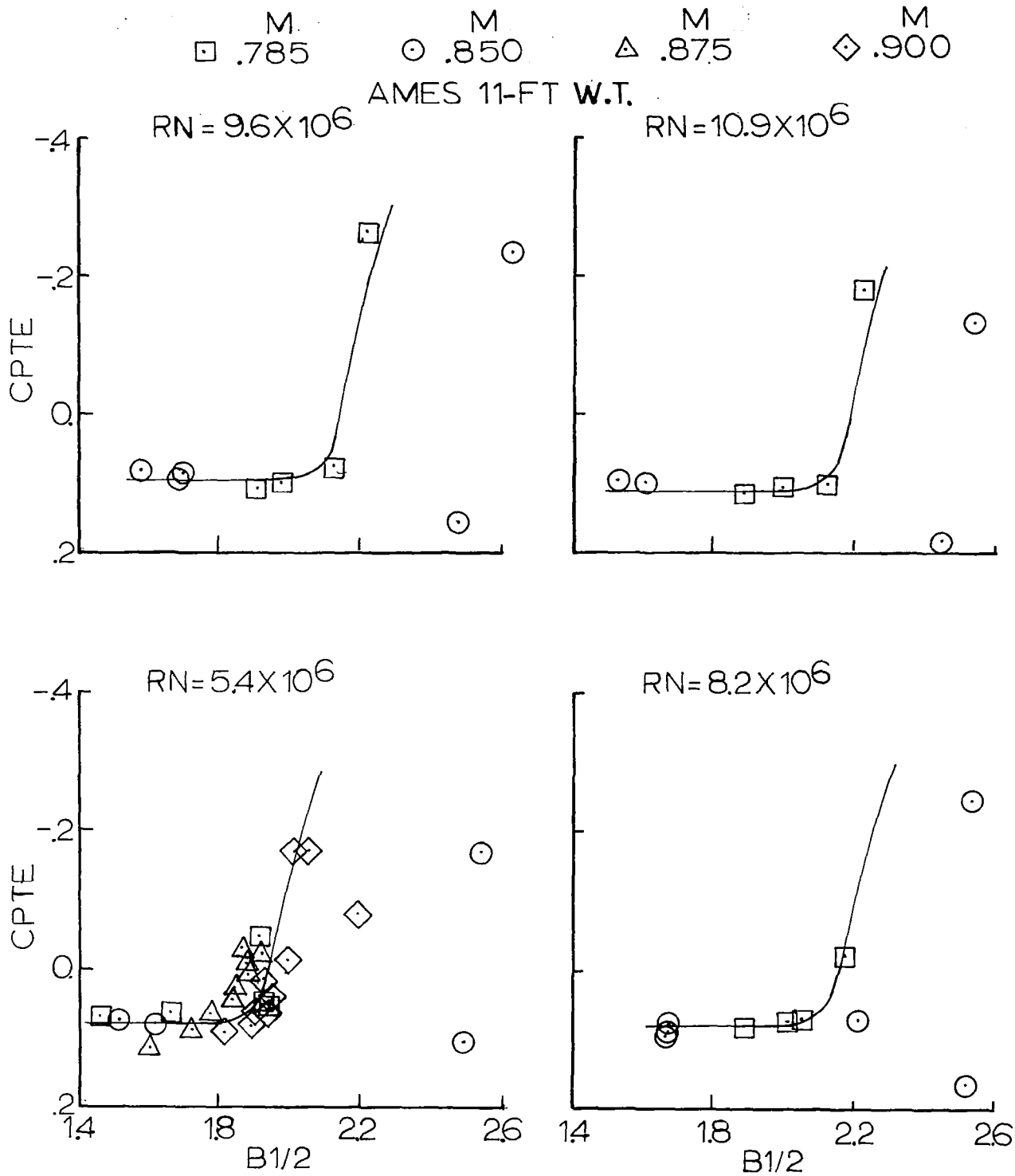

FIGURE 22. - FINAL CORRELATION. RAE MODEL 864, n = .434, A = .700

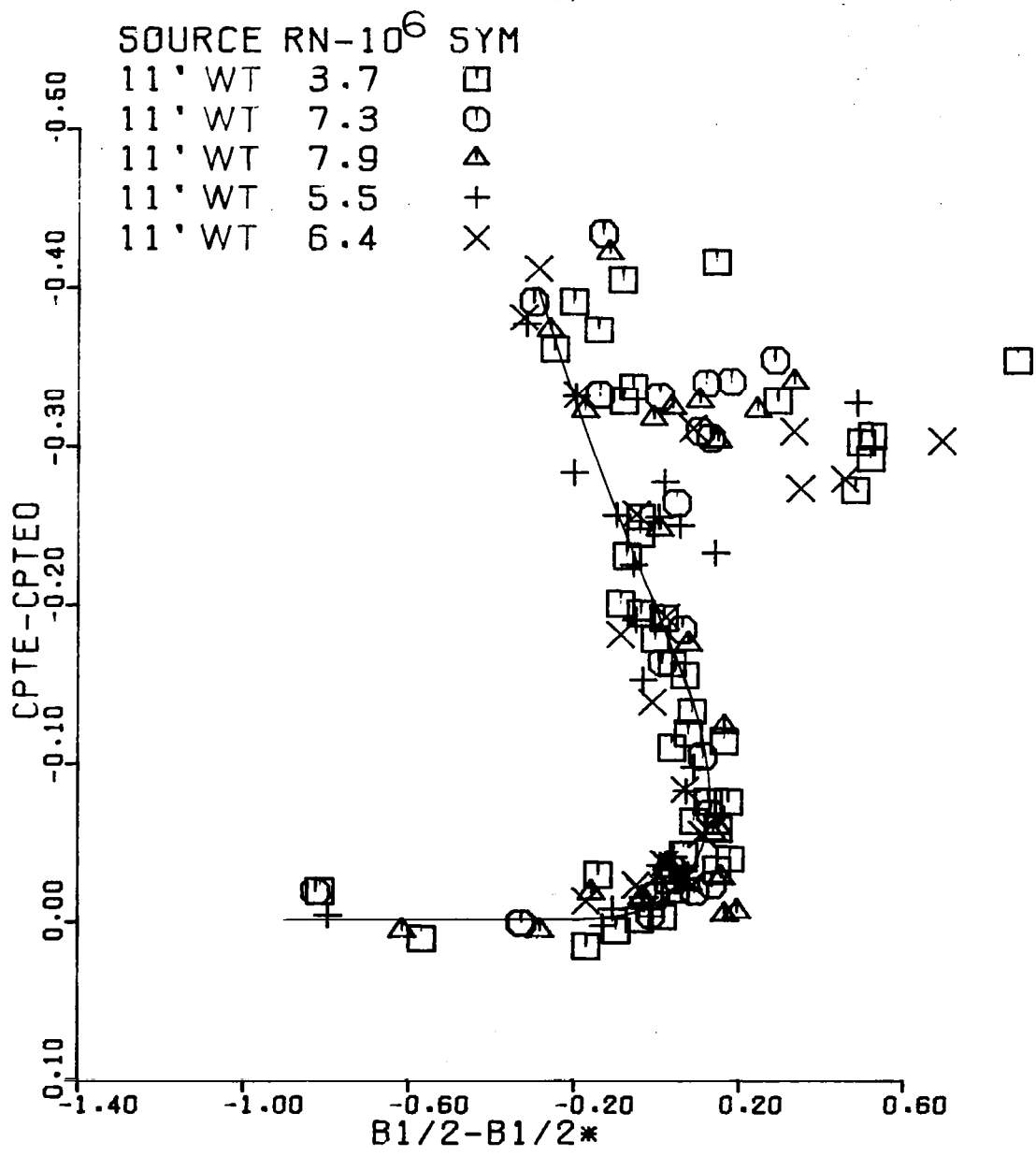

FIGURE 23. - COMPOSITE CORRELATION. RAE MODEL 864, $\mathcal{R}$ = .793

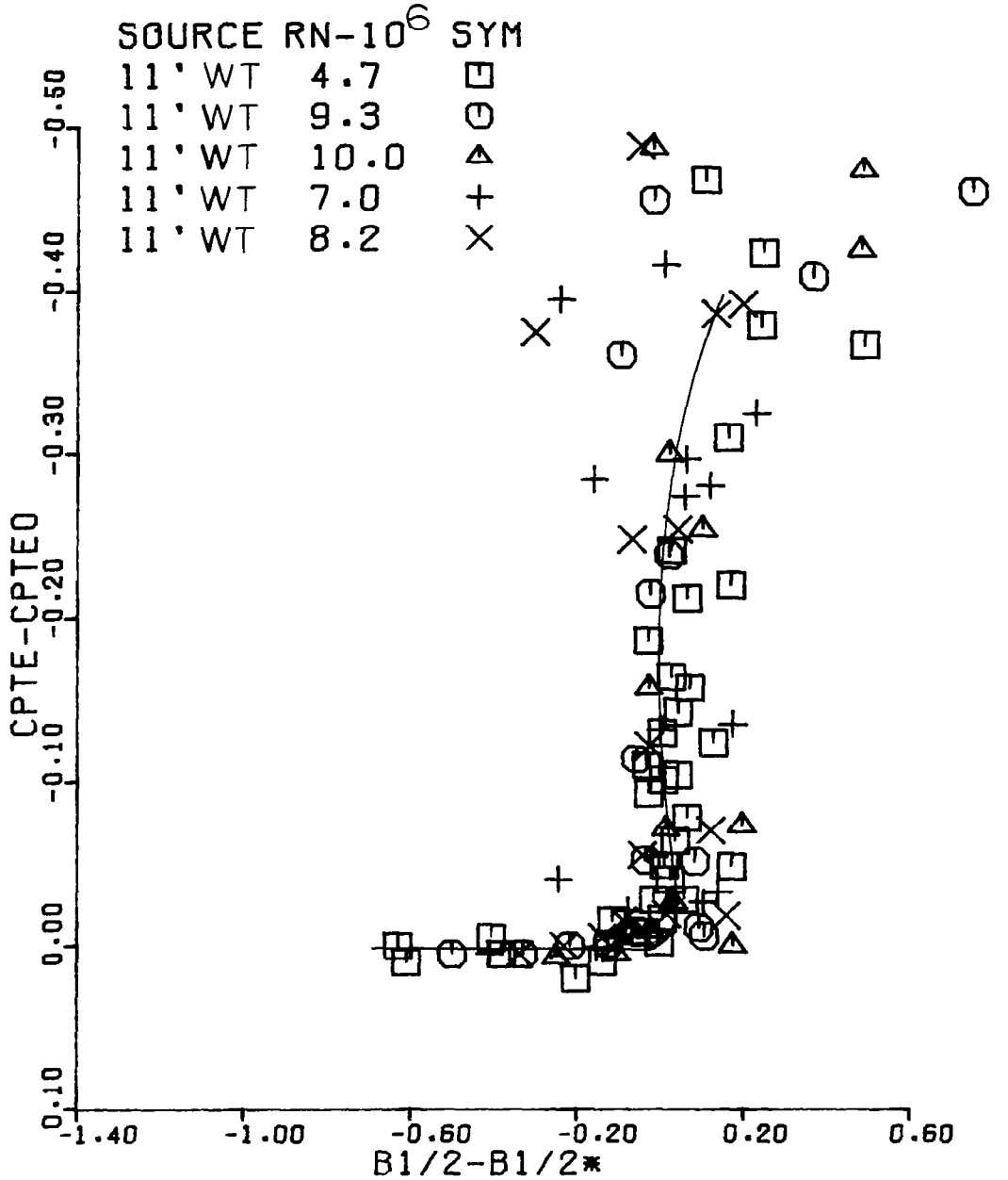

FIGURE 24. - COMPOSITE CORRELATION. RAE MODEL 864, $\mathcal{M}$ = .595

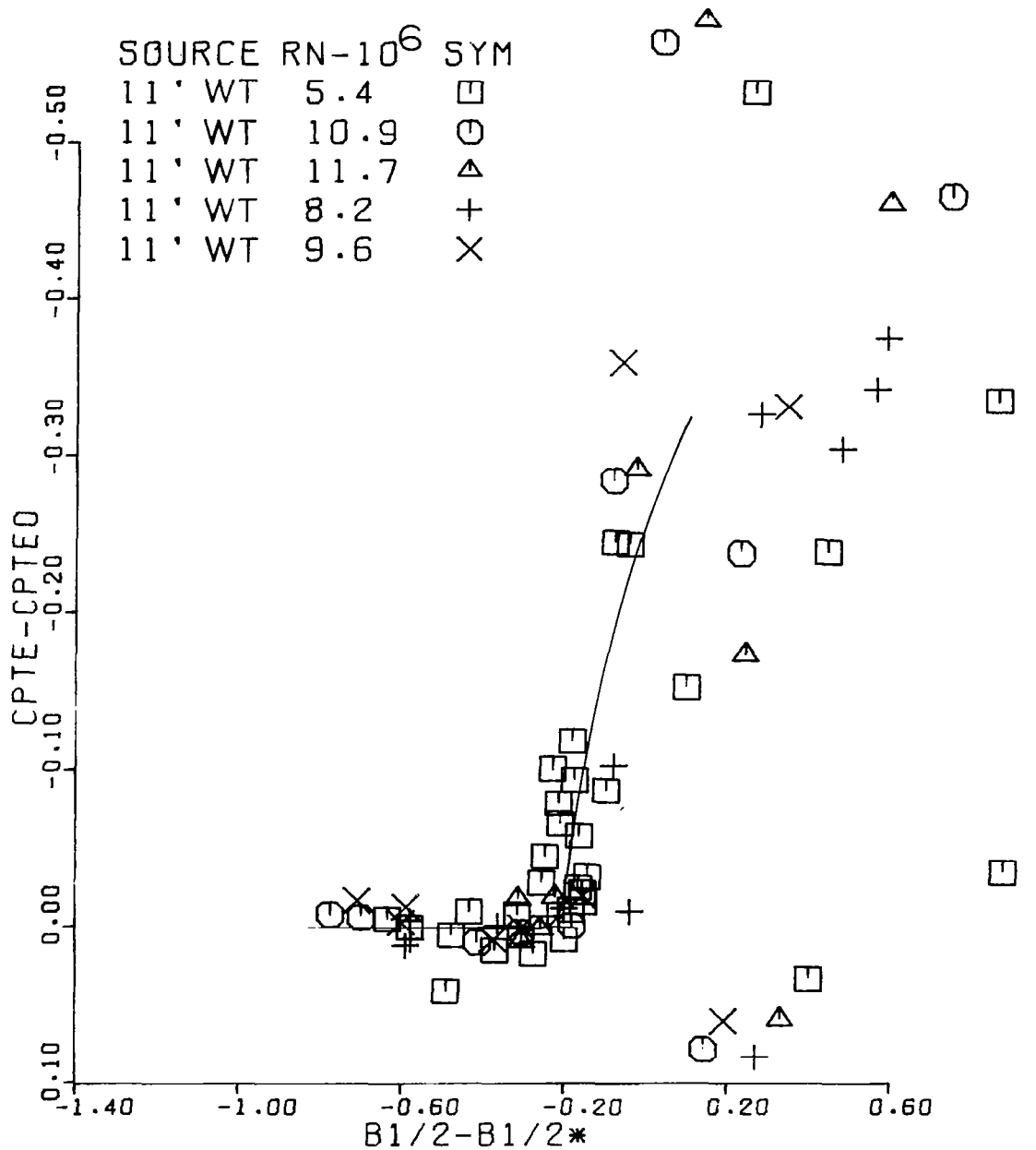

FIGURE 25. - COMPOSITE CORRELATION. RAE MODEL 864, $\mathcal{R}$ = .434

C-141

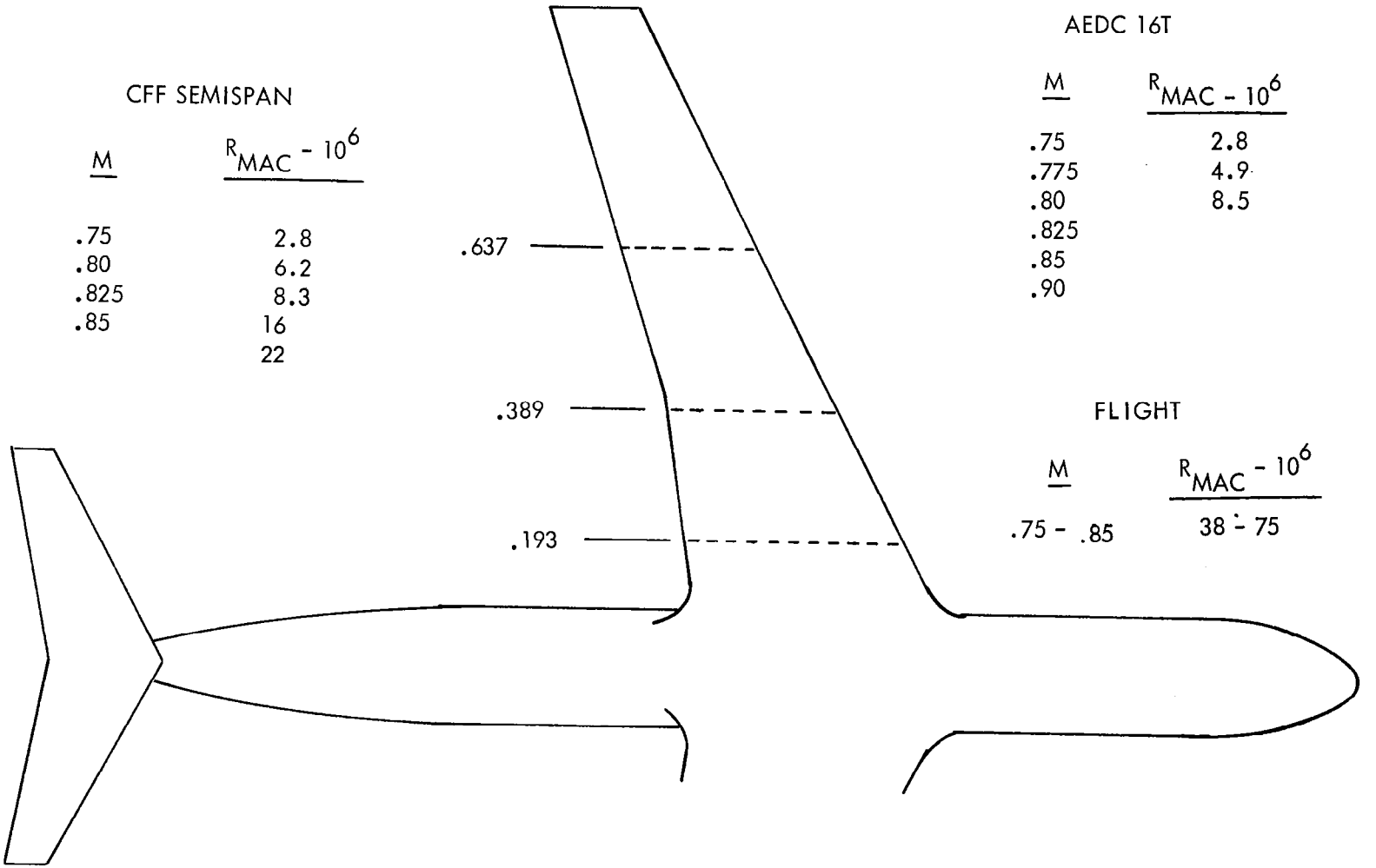

FIGURE 26. - C-141 CONFIGURATION AND DATA.

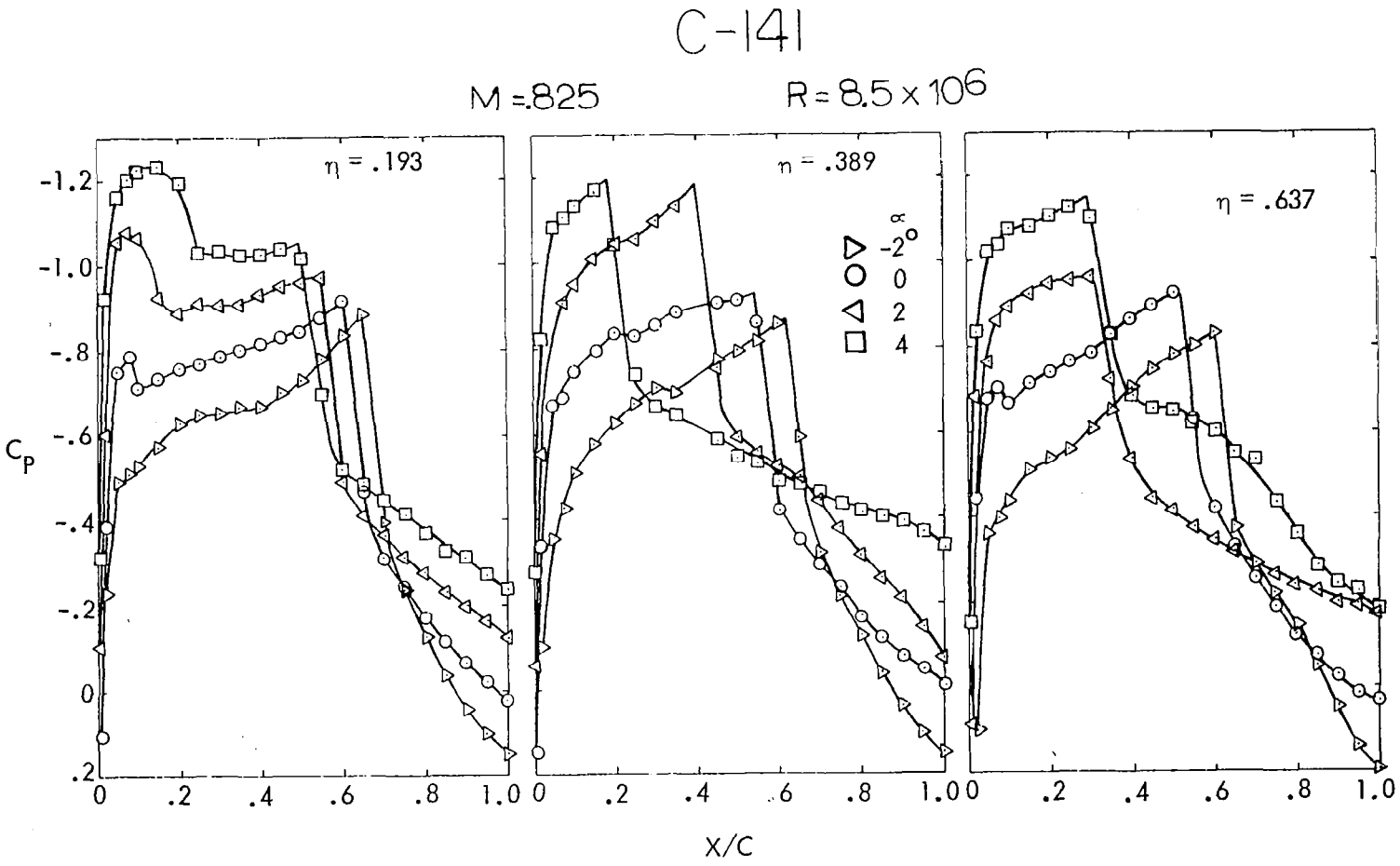

FIGURE 27. - TYPICAL PRESSURE DISTRIBUTIONS, C-141

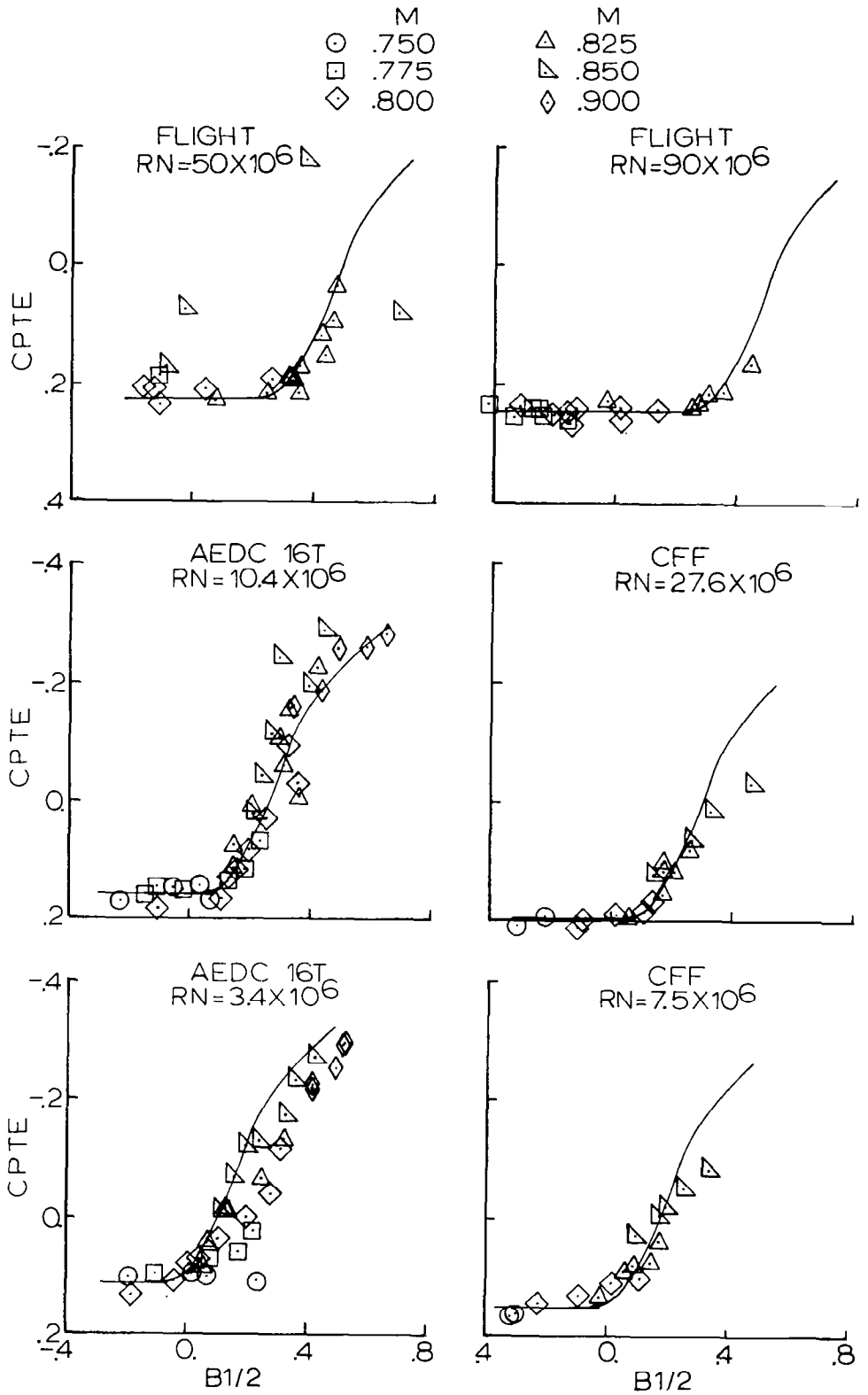

FIGURE 28. - FINAL CORRELATION. C-141, $\mathcal{R}$ = .193, A = 1.50

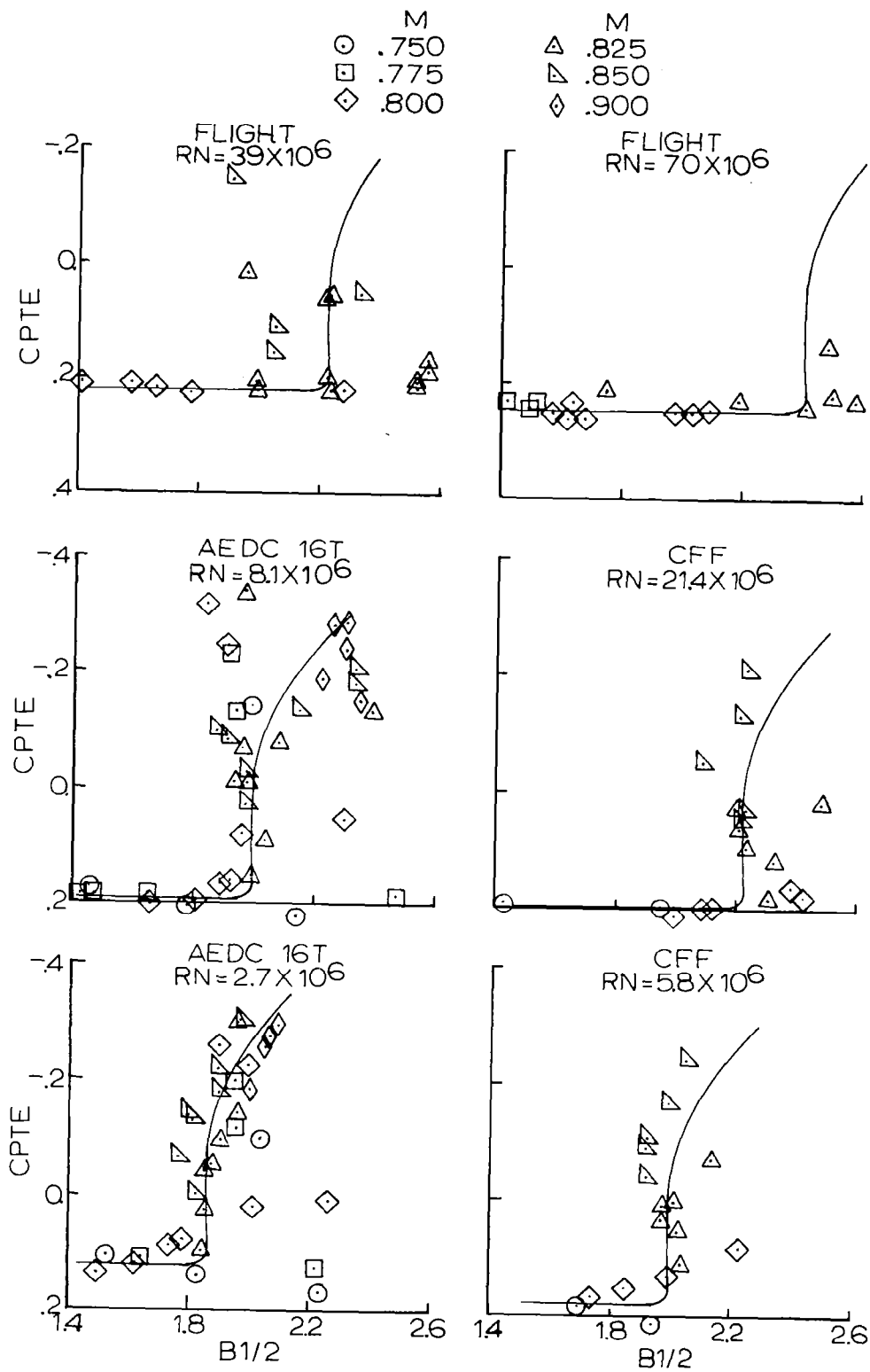

FIGURE 29. - FINAL CORRELATION. C-141, $\mathcal{M}$ = .389, A = .400

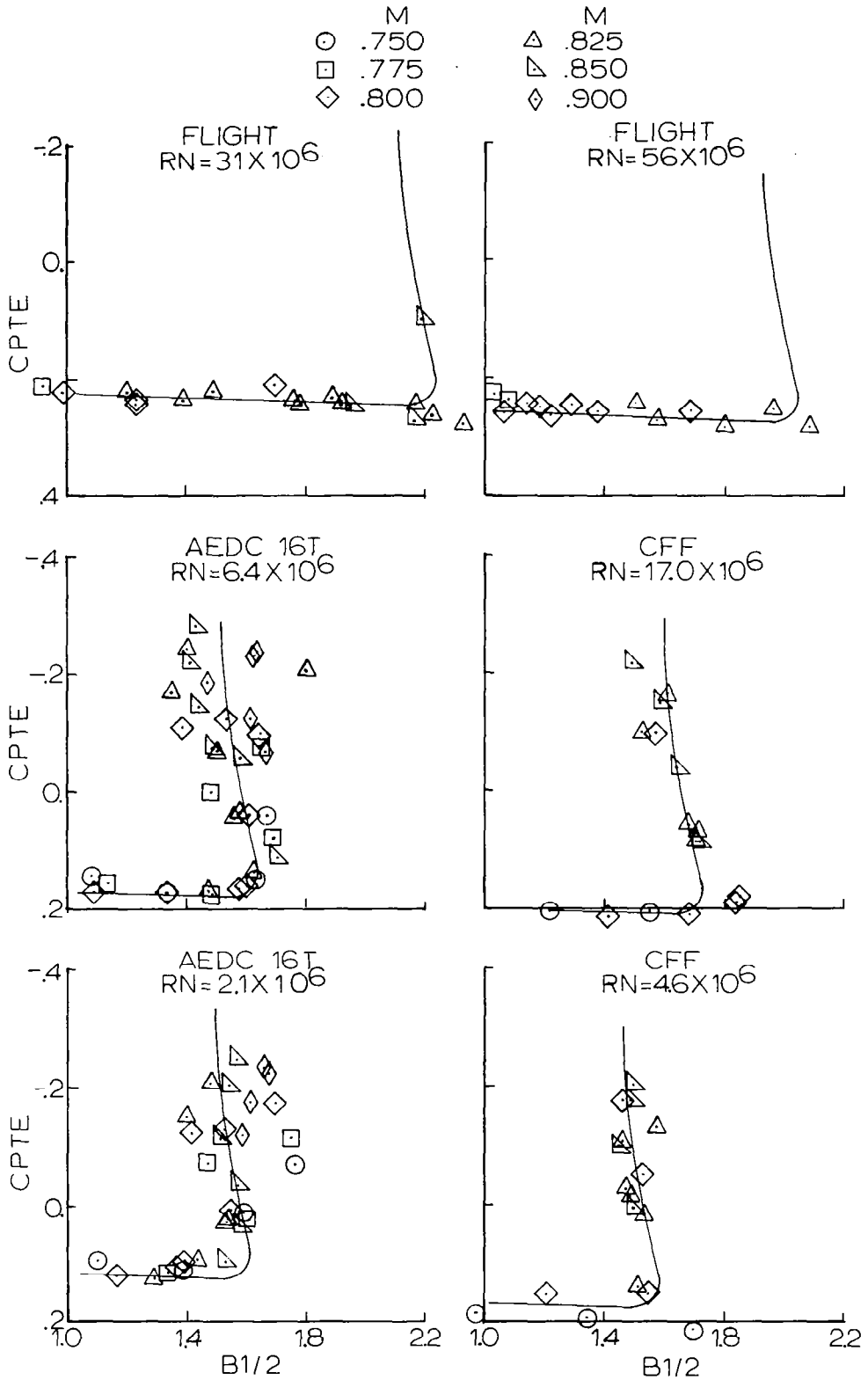

FIGURE 30. - FINAL CORRELATION. C-141, $\mathcal{M}$ = .637, A = .600

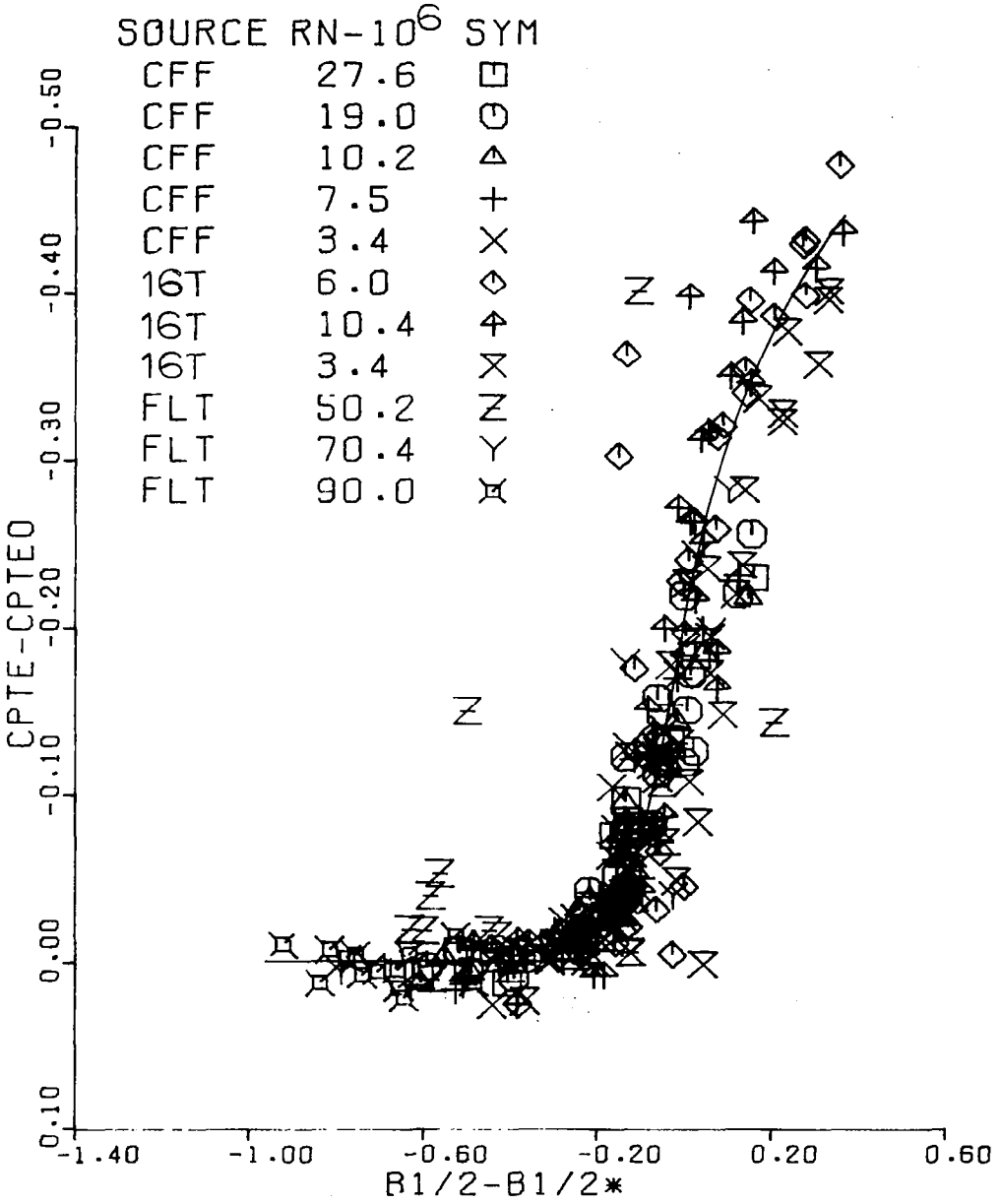

FIGURE 31. - COMPOSITE CORRELATION. C-141, $\mathcal{R}$ = .193

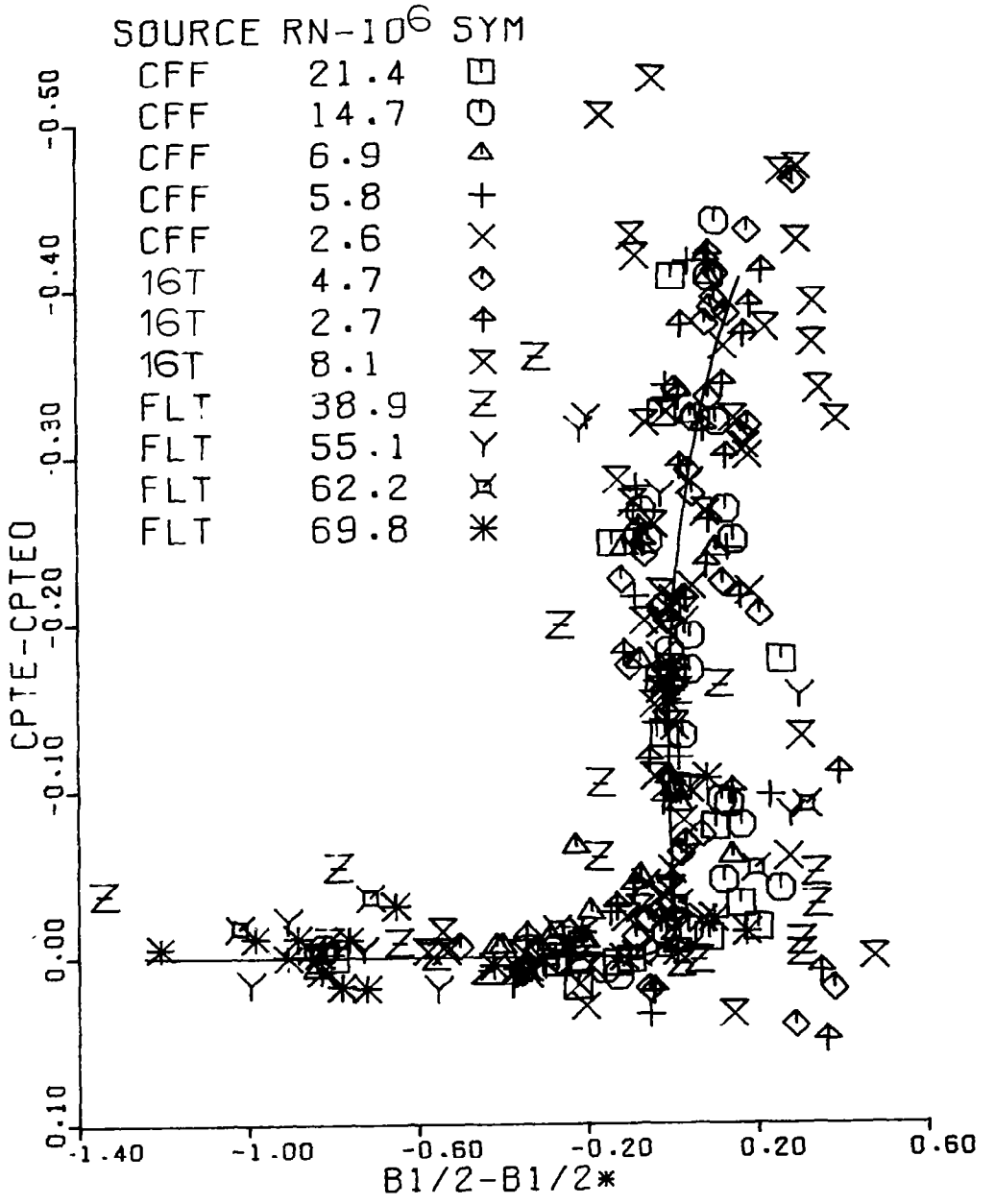

FIGURE 32. - COMPOSITE CORRELATION. C-141, $\mathcal{R}$ = .389

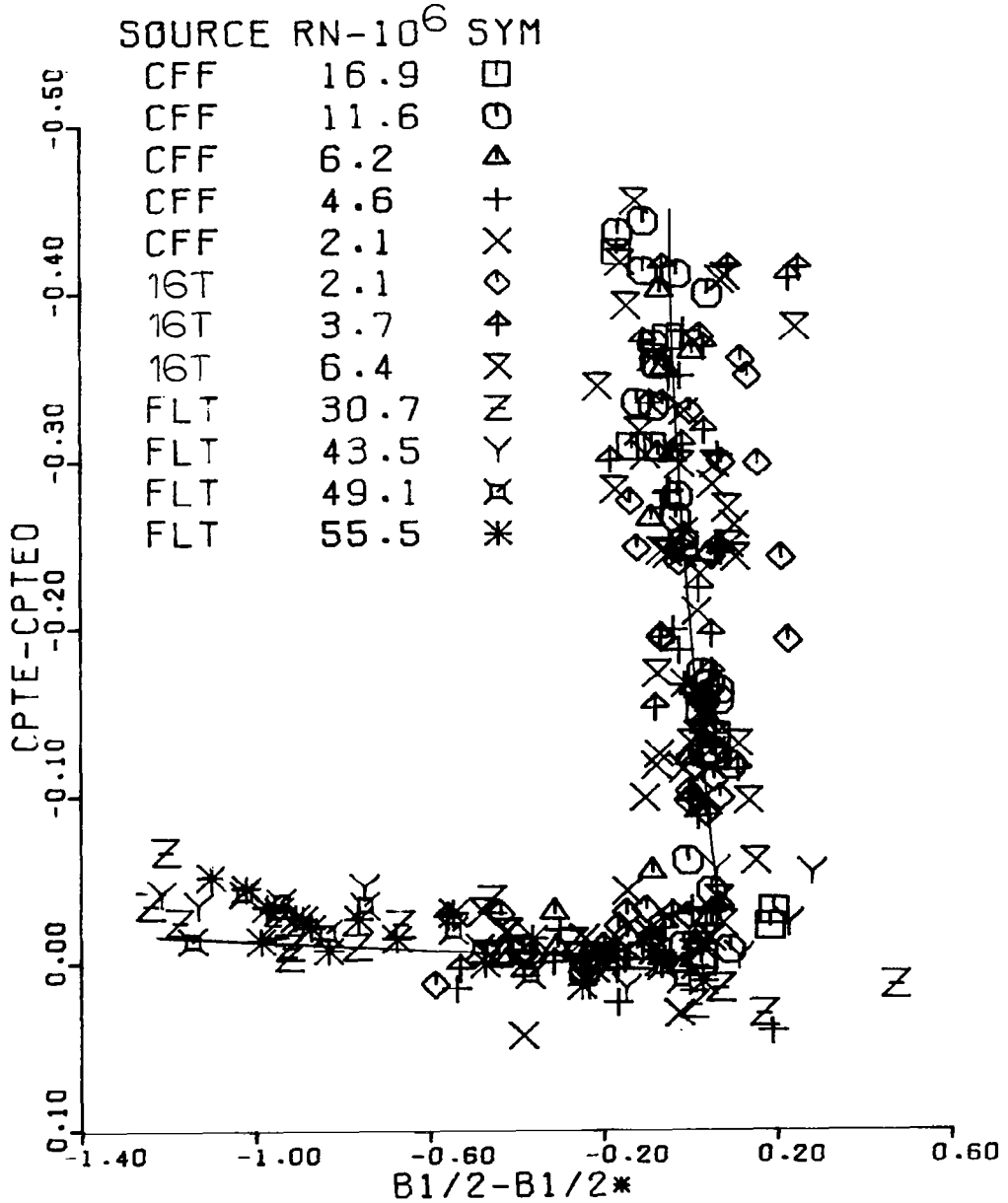

FIGURE 33. - COMPOSITE CORRELATION. C-141, $\mathcal{R}$ = .637

C-5

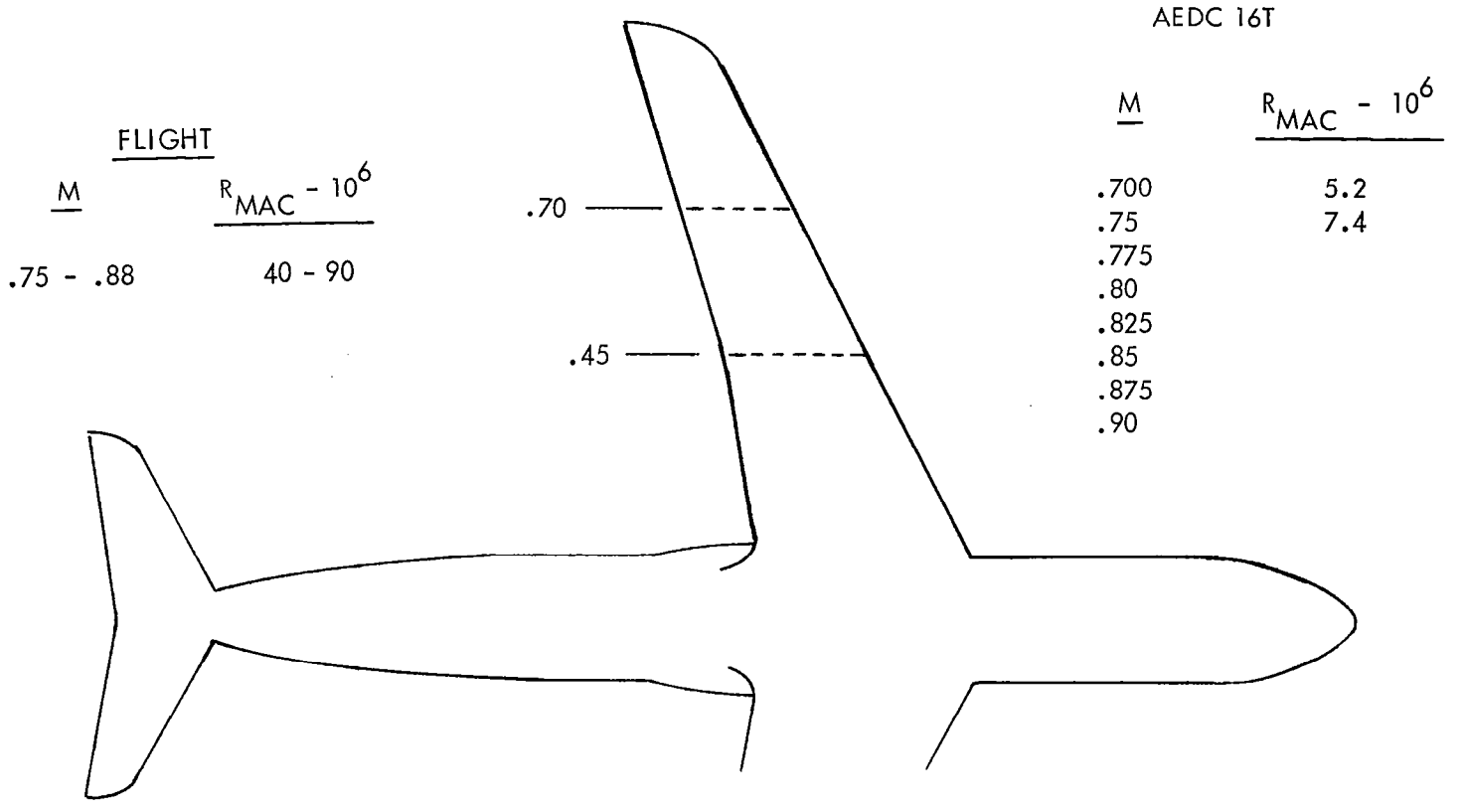

FIGURE 34. - C-5 CONFIGURATION AND DATA.

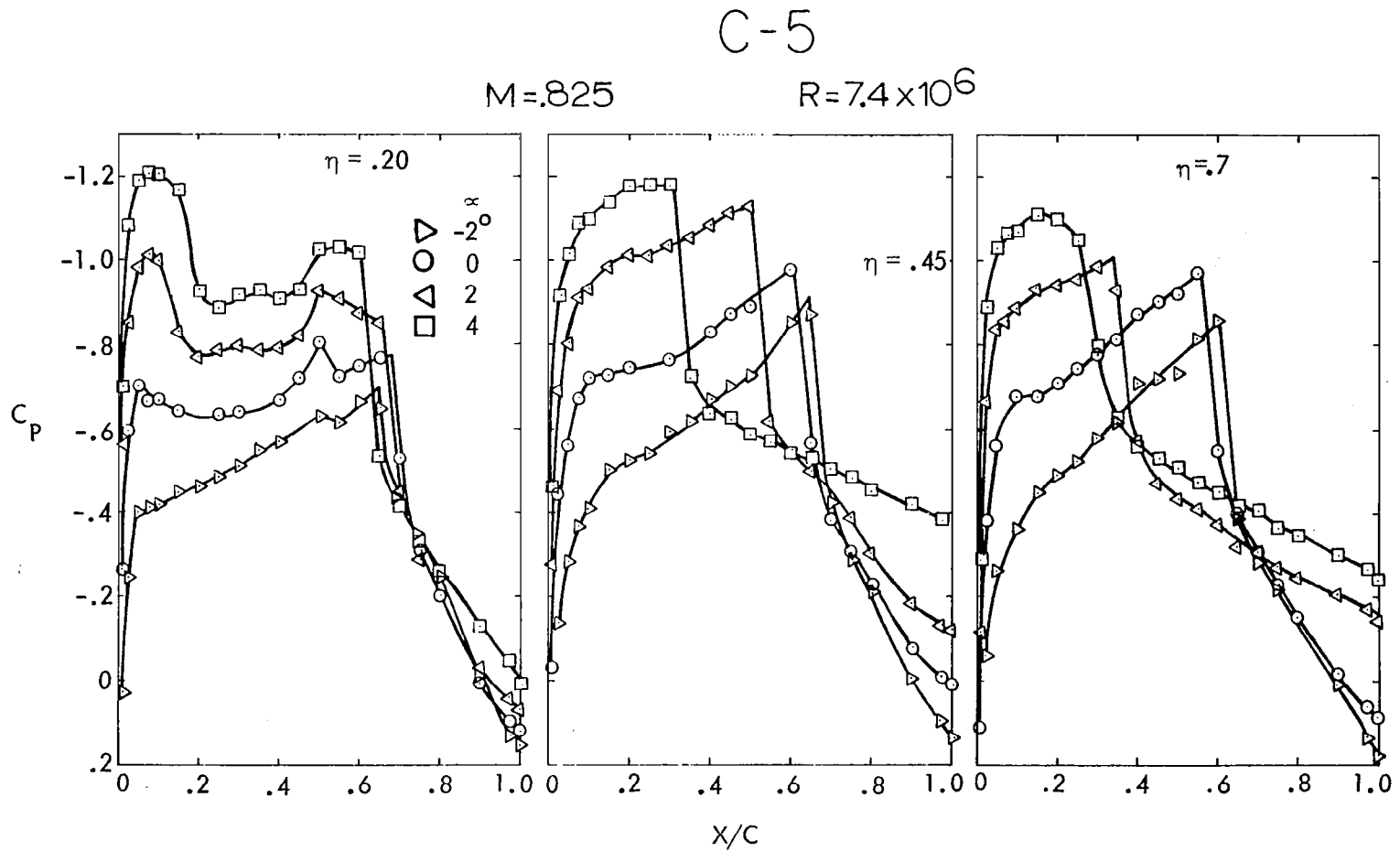

FIGURE 35. - TYPICAL PRESSURE DISTRIBUTIONS. C-5

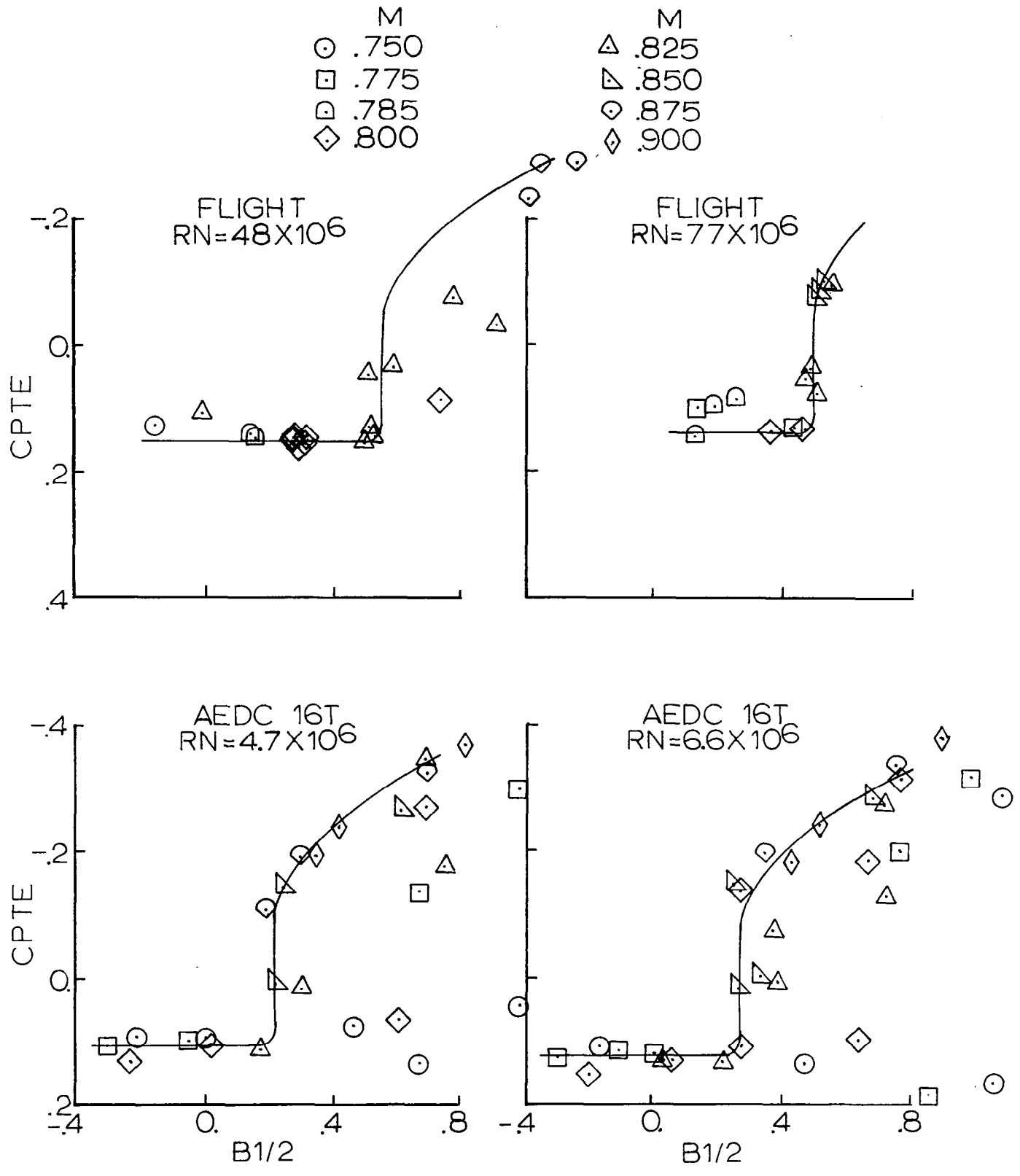

FIGURE 36. - FINAL CORRELATION. C-5, $\mathcal{R}$ = .45, A = 1.50

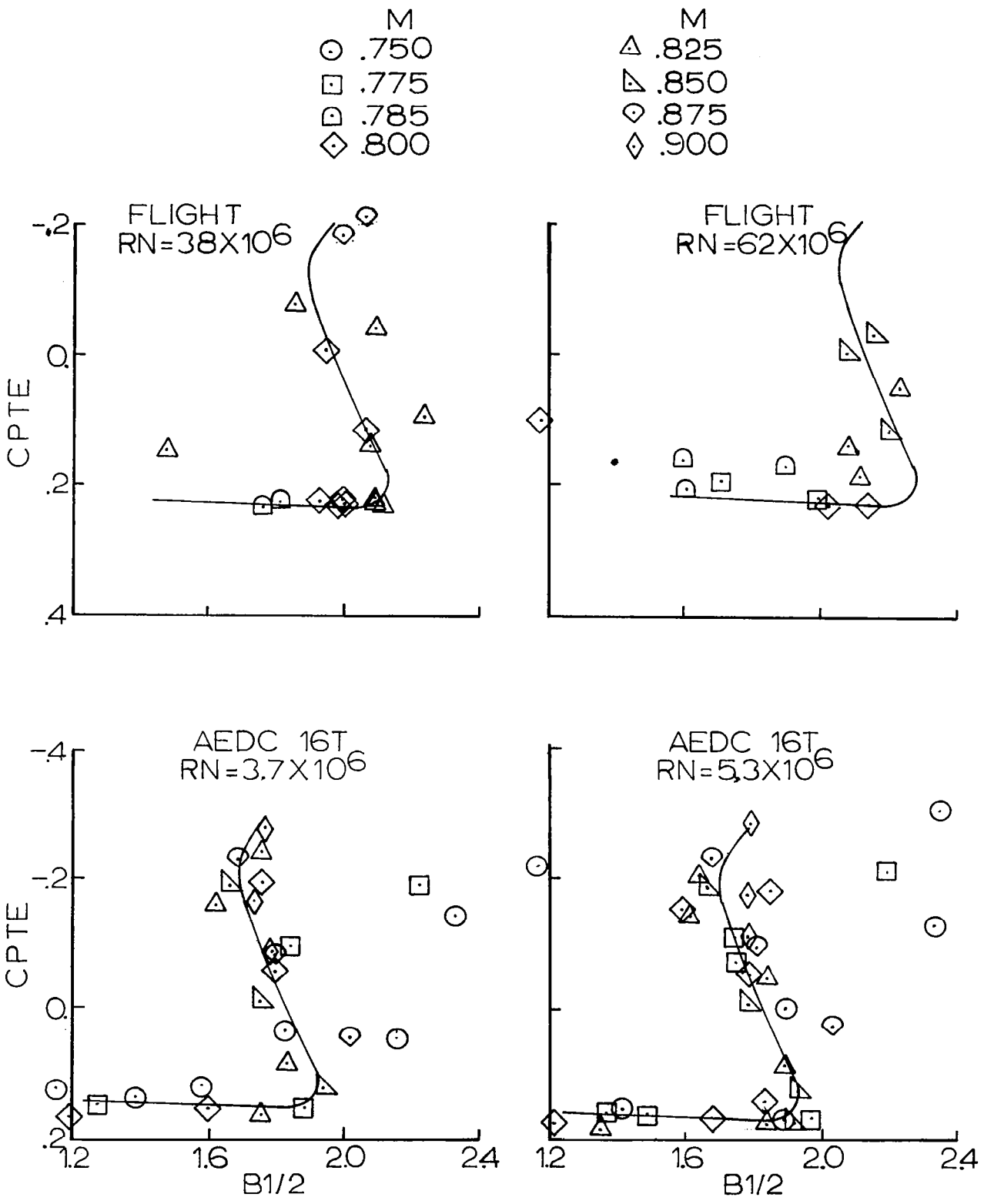

FIGURE 37. - FINAL CORRELATION. C-5, $\mathcal{M}$ = .70, A = .500

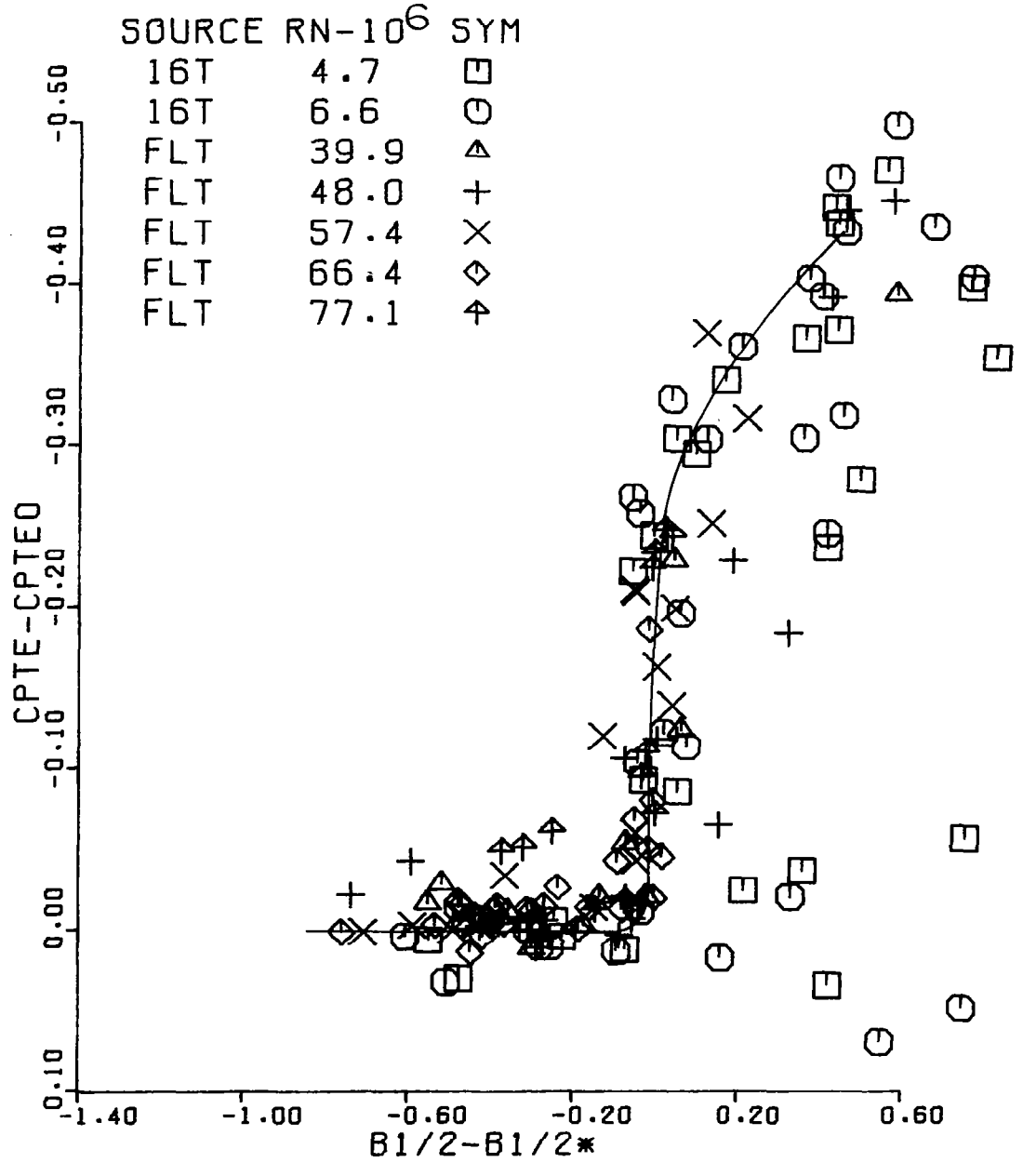

FIGURE 38. - COMPOSITE CORRELATION. C-5, η = .45

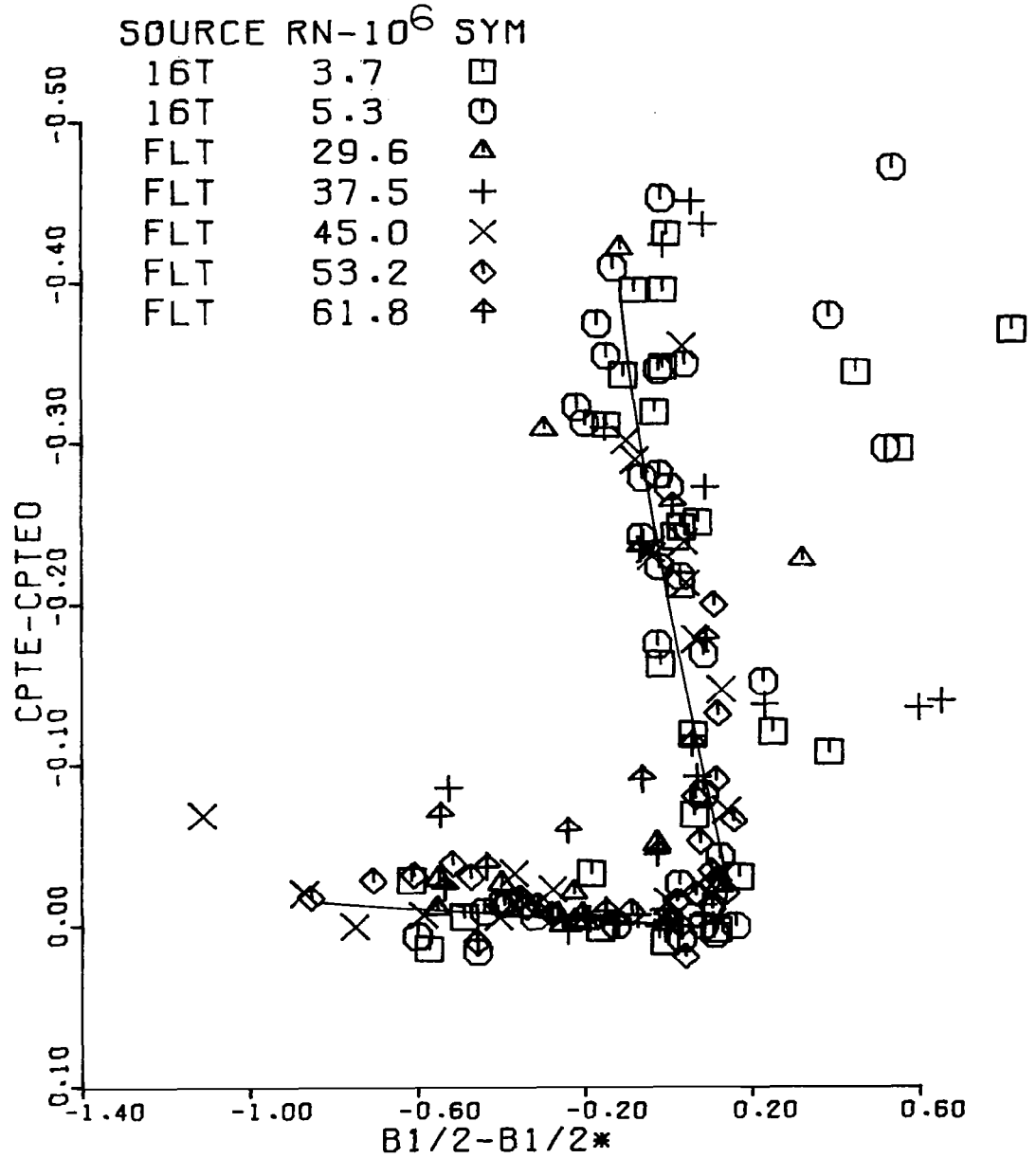

FIGURE 39. - COMPOSITE CORRELATION. C-5, $\mathcal{R}$ = .70

F-8 SCW

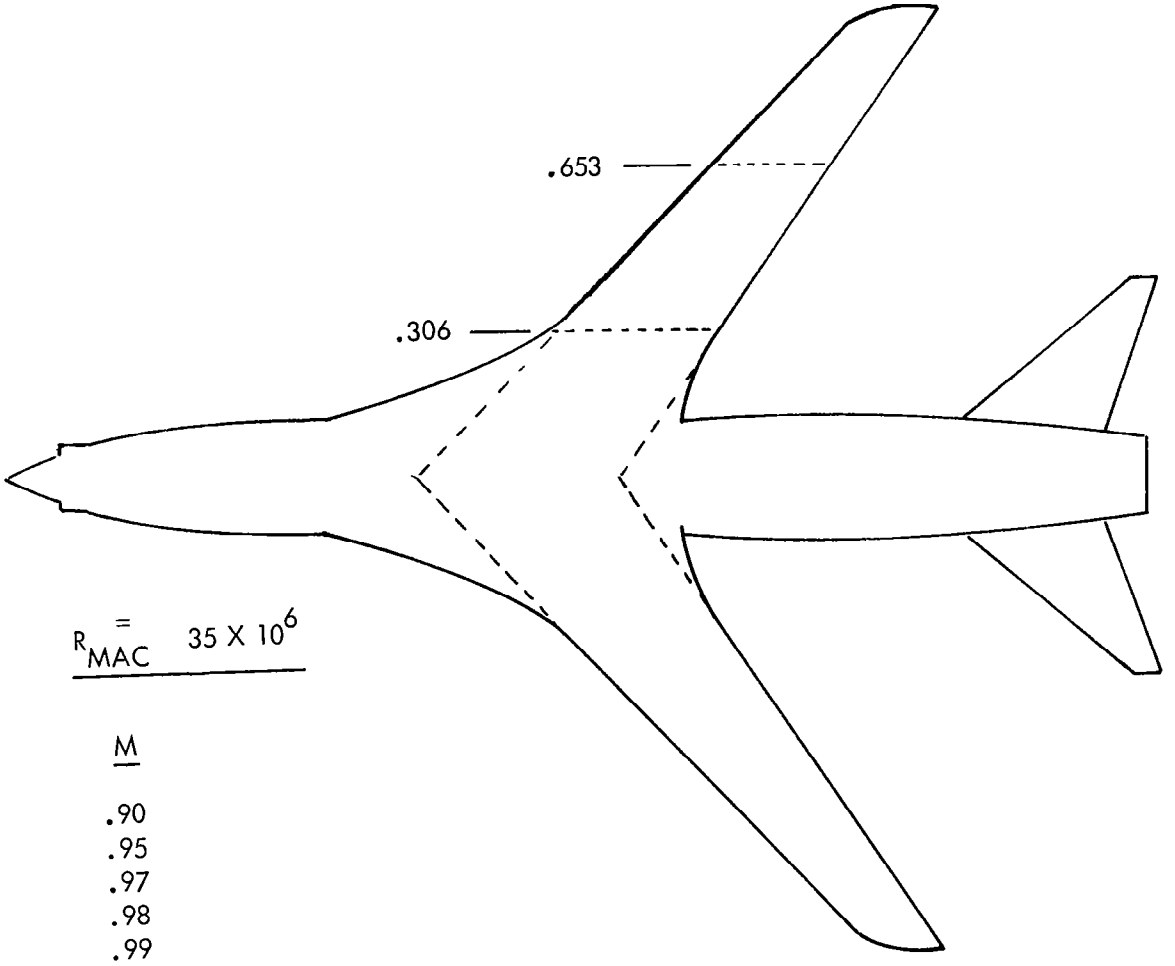

FIGURE 40. - F-8SCW CONFIGURATION AND DATA

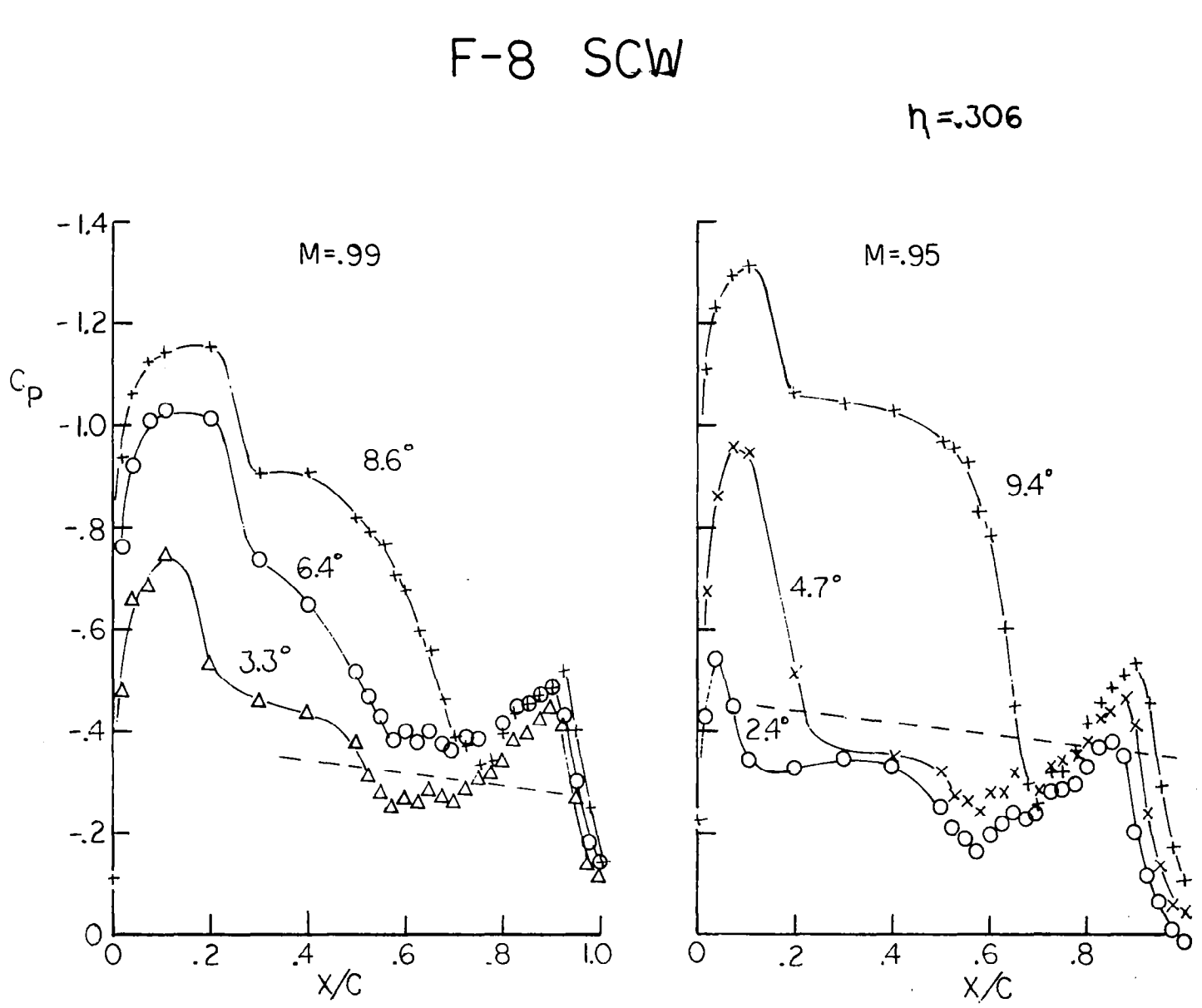

FIGURE 41. - TYPICAL PRESSURE DISTRIBUTIONS, F-8SCW

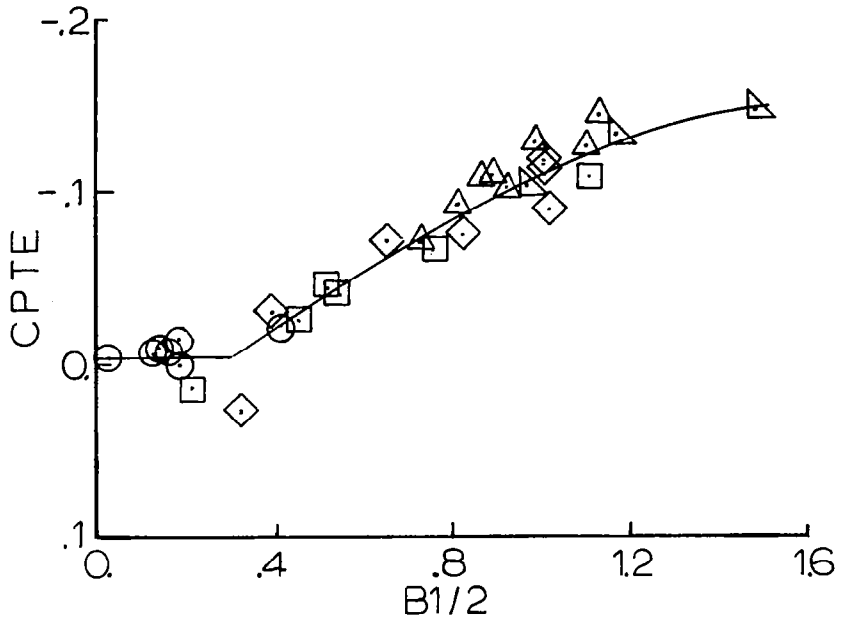

FIGURE 42. - FINAL CORRELATION. F-8 SCW, n = .306, A = 1.20

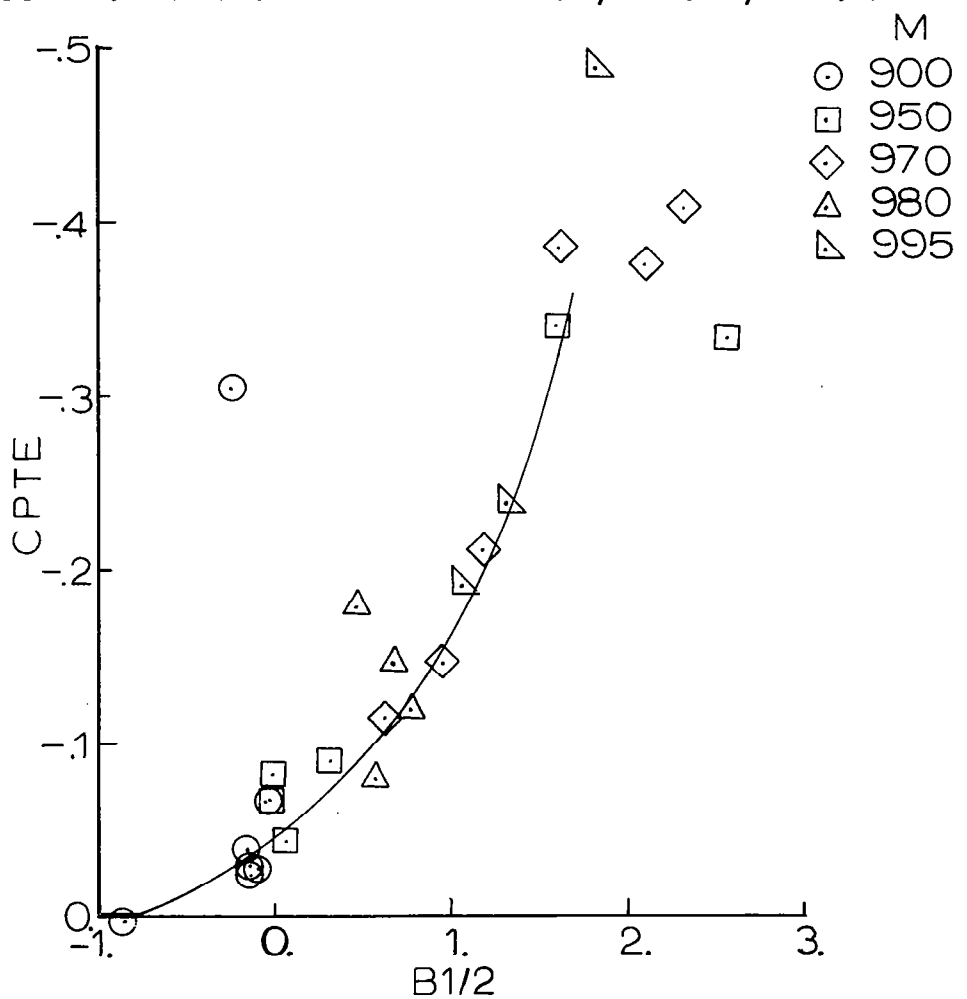

FIGURE 43. - FINAL CORRELATION. F-8 SCW, n = .653, A = 1.40

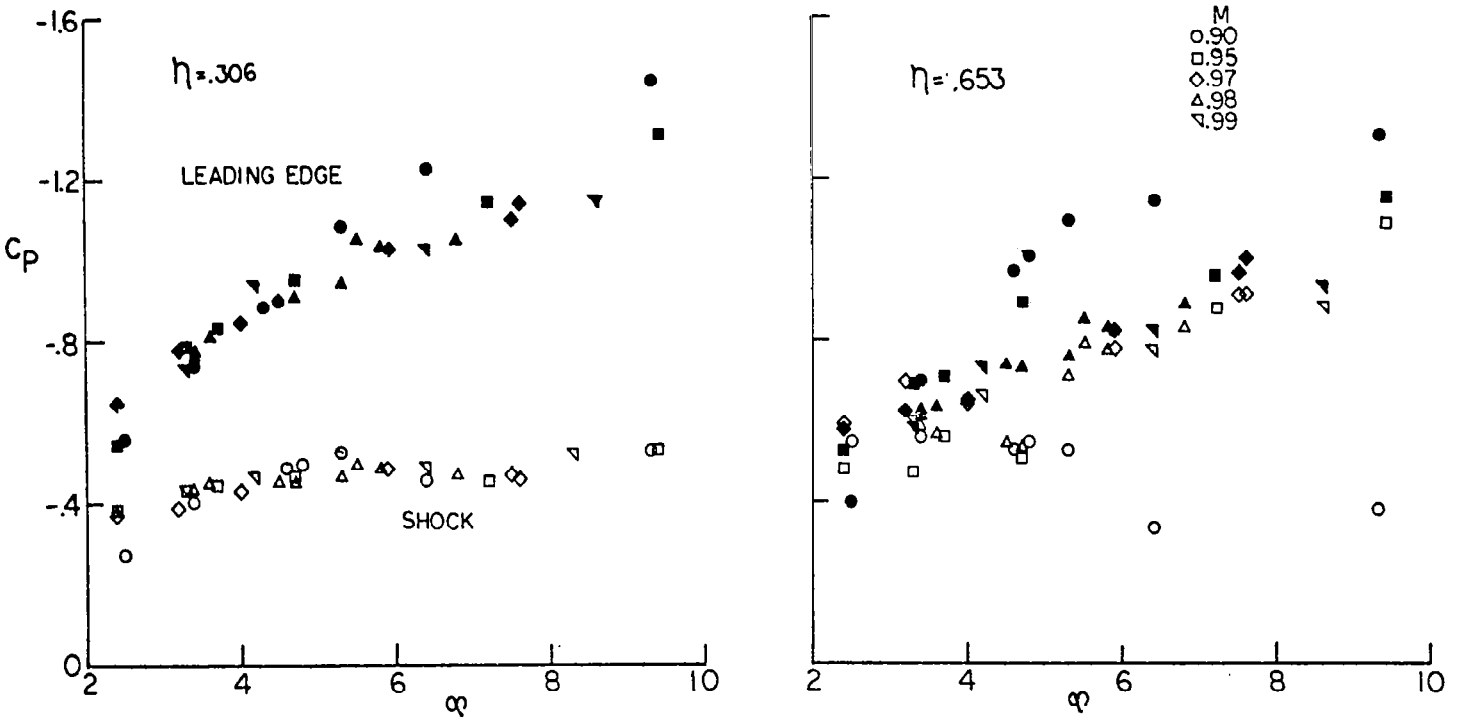

FIGURE 44. - PEAK PRESSURE COEFFICIENTS, F-8SCW.

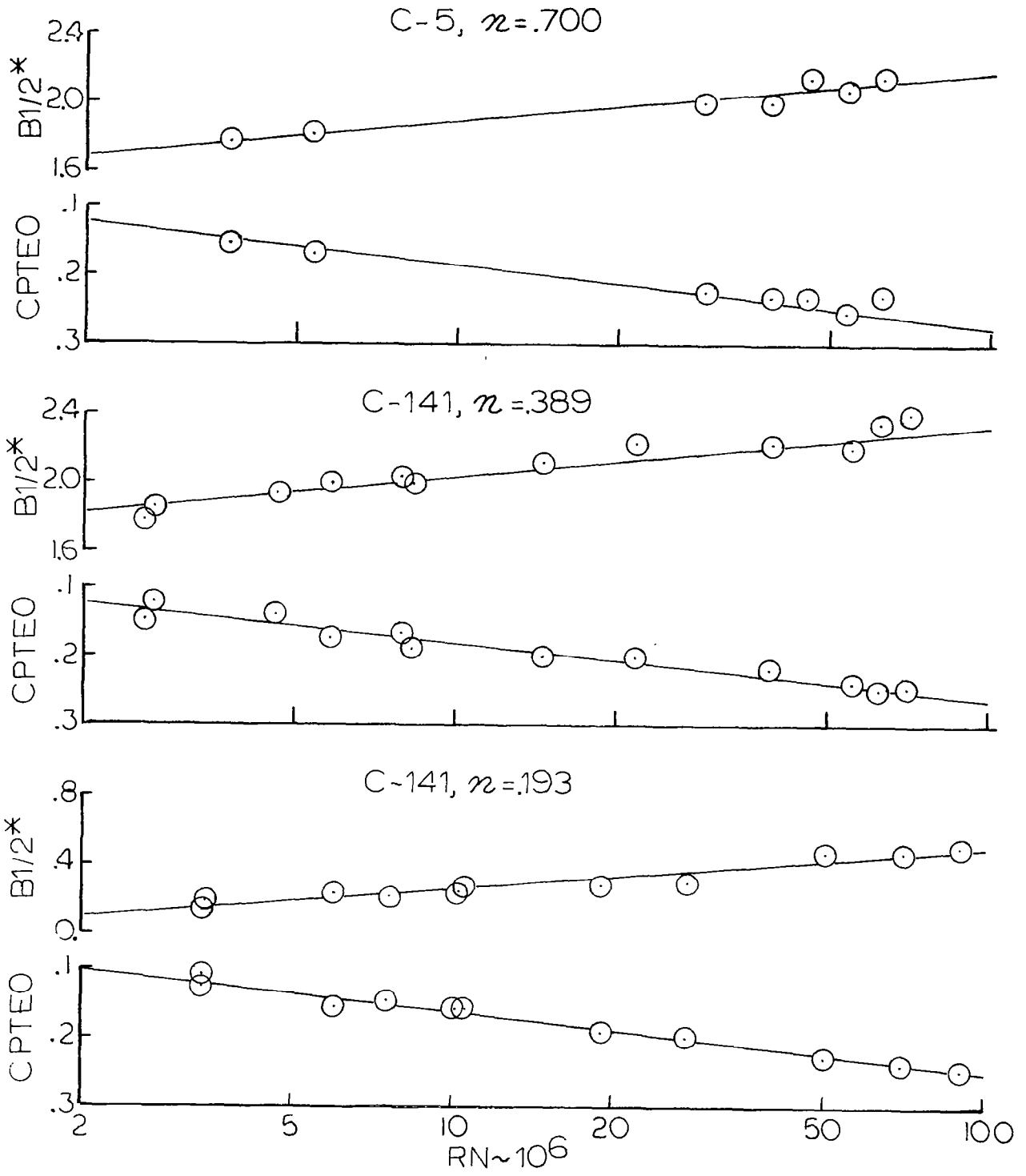

FIGURE 45. - TYPICAL SCALE EFFECTS

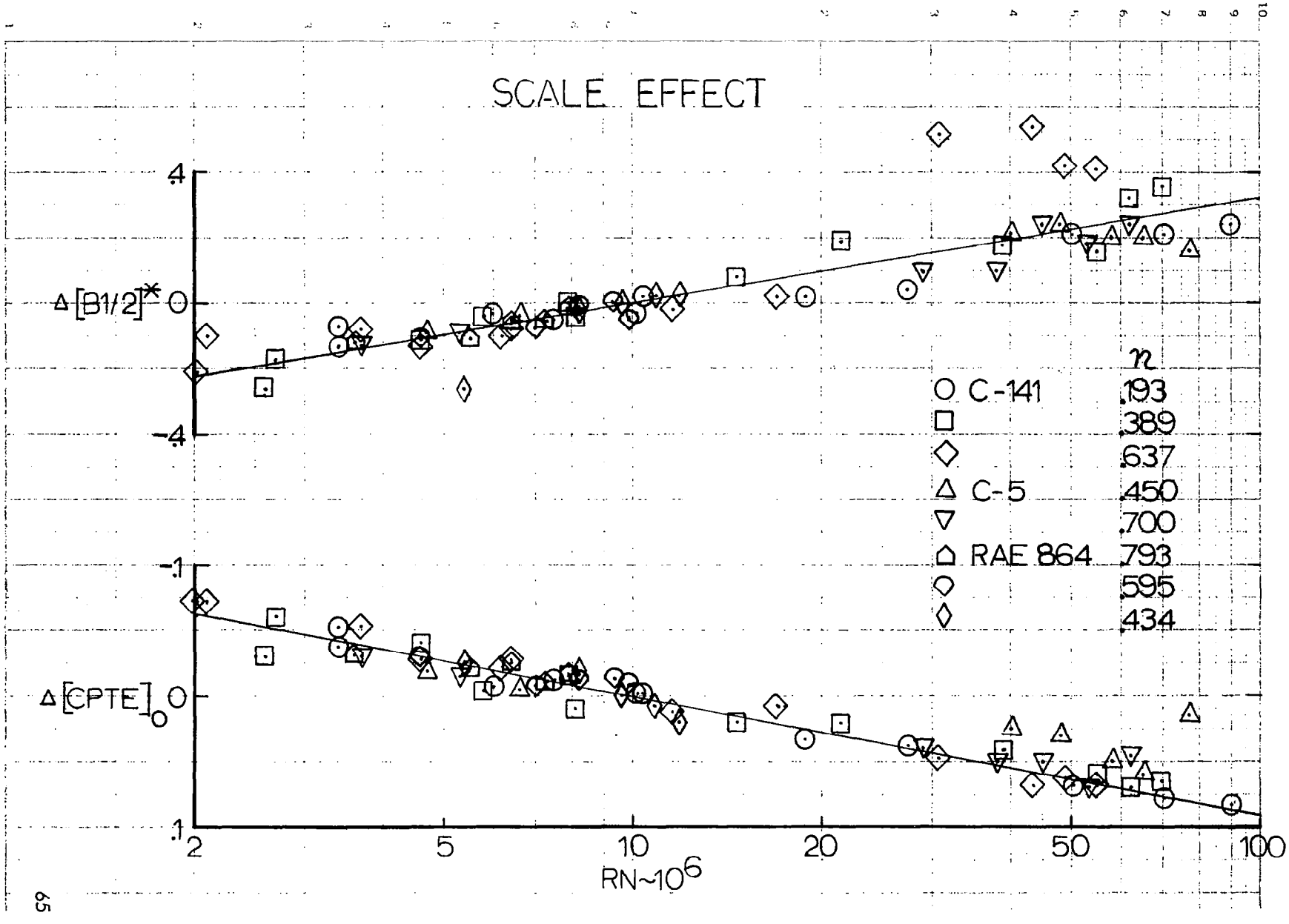

FIGURE 46. - COMPOSITE SCALE EFFECT

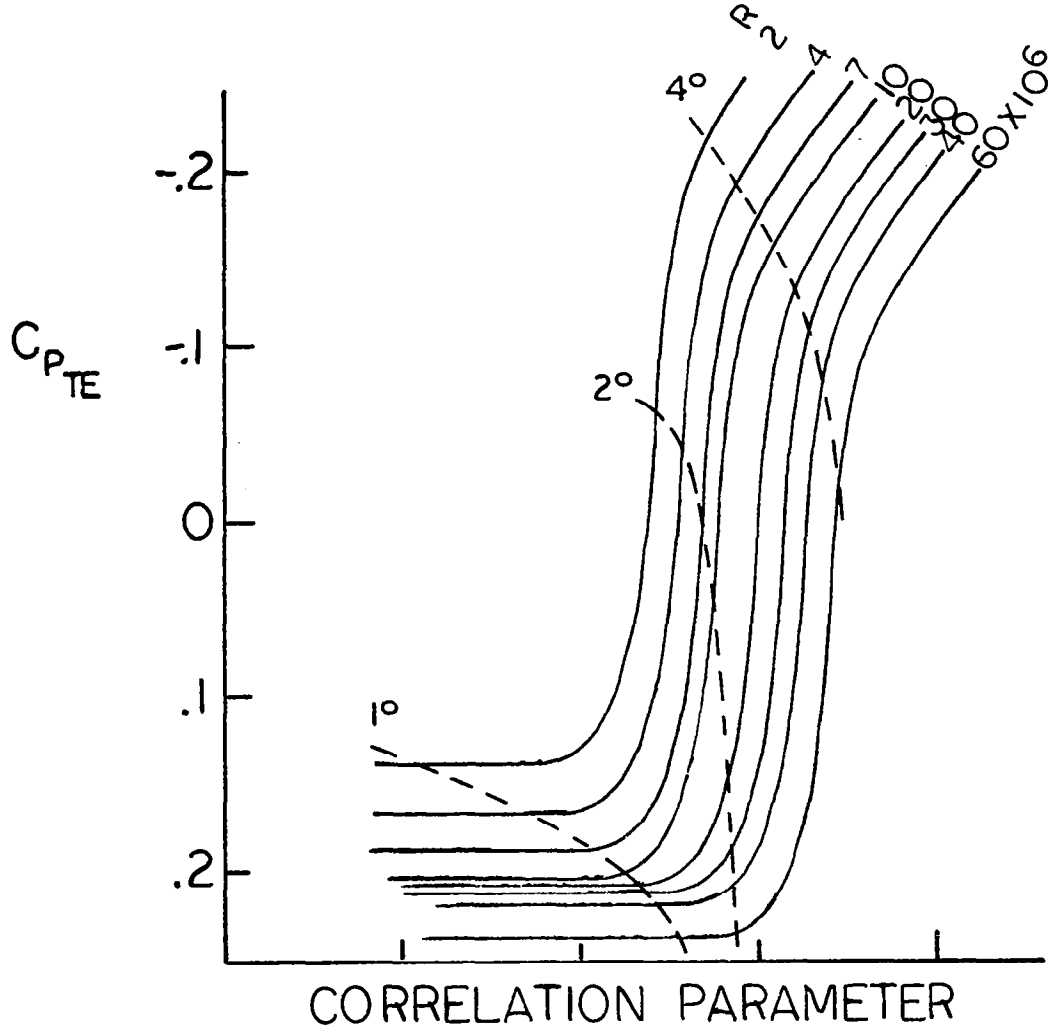

FIGURE 47. - SCALE EFFECT AT CONSTANT ANGLE OF ATTACK

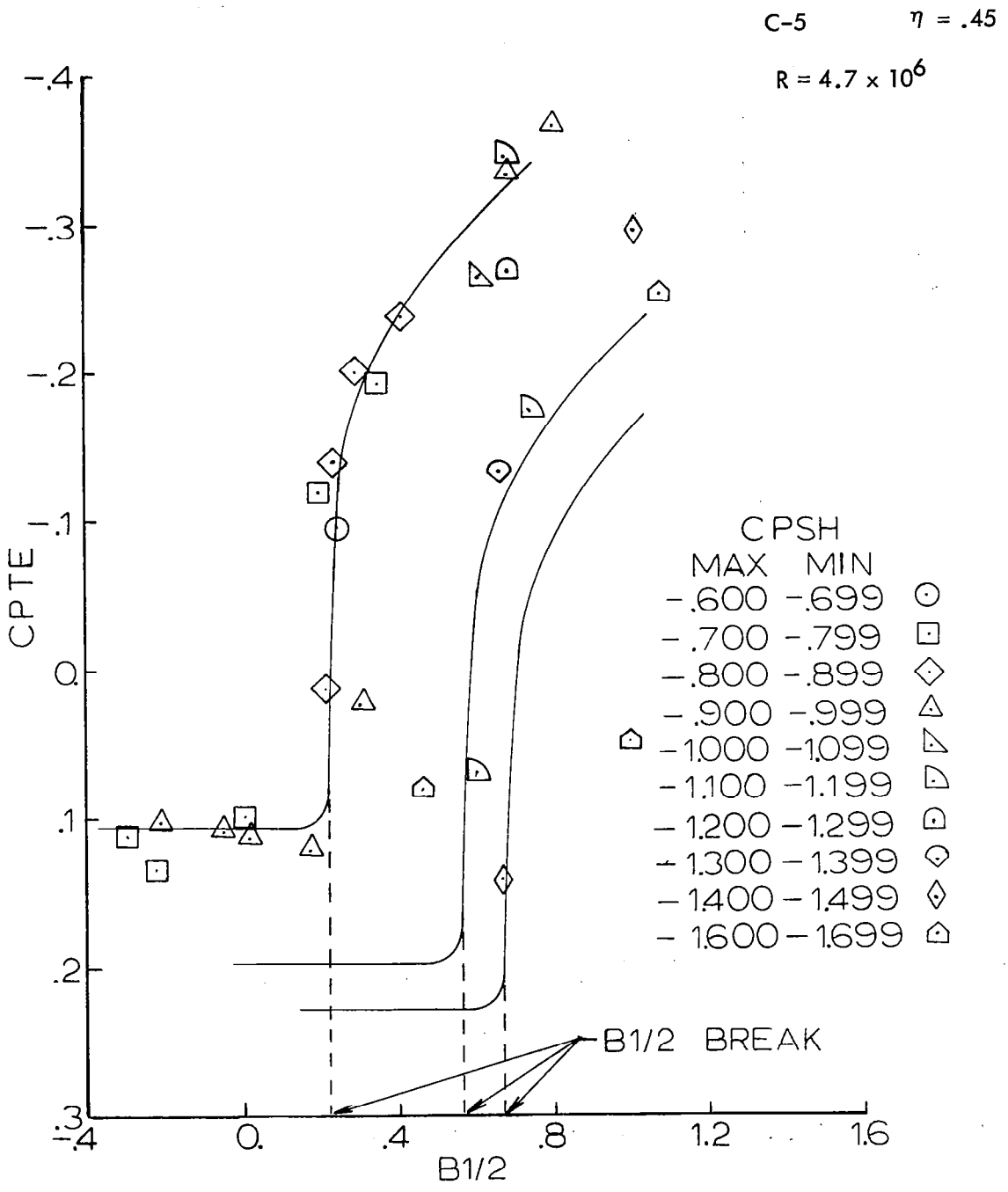

FIGURE 48. - POSSIBLE INFLUENCE OF VERY FAVORABLE VELOCITY GRADIENT

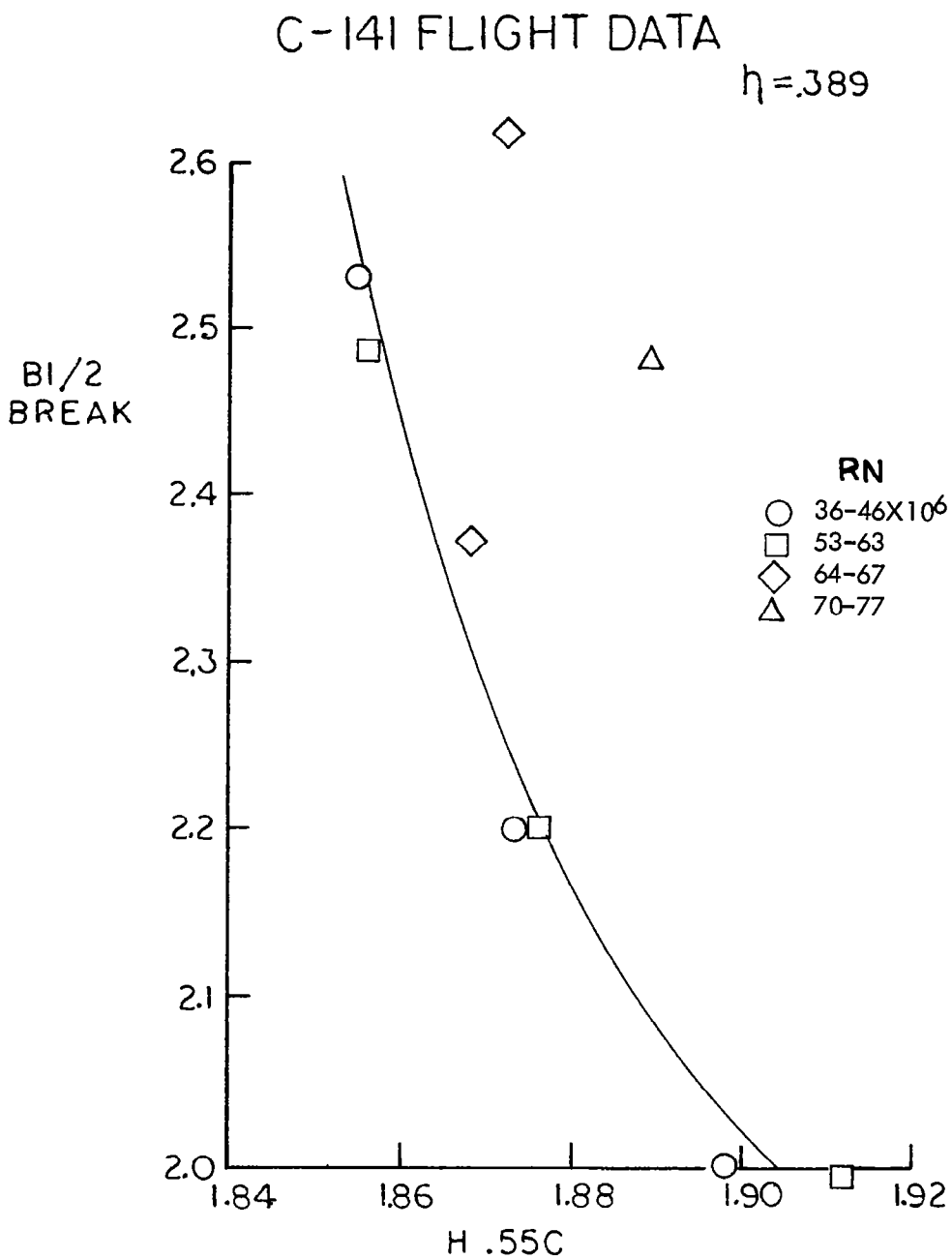

FIGURE 49. - CORRELATION OF B 1/2 FOR INITIAL SEPARATION WITH SHAPE FACTOR H.

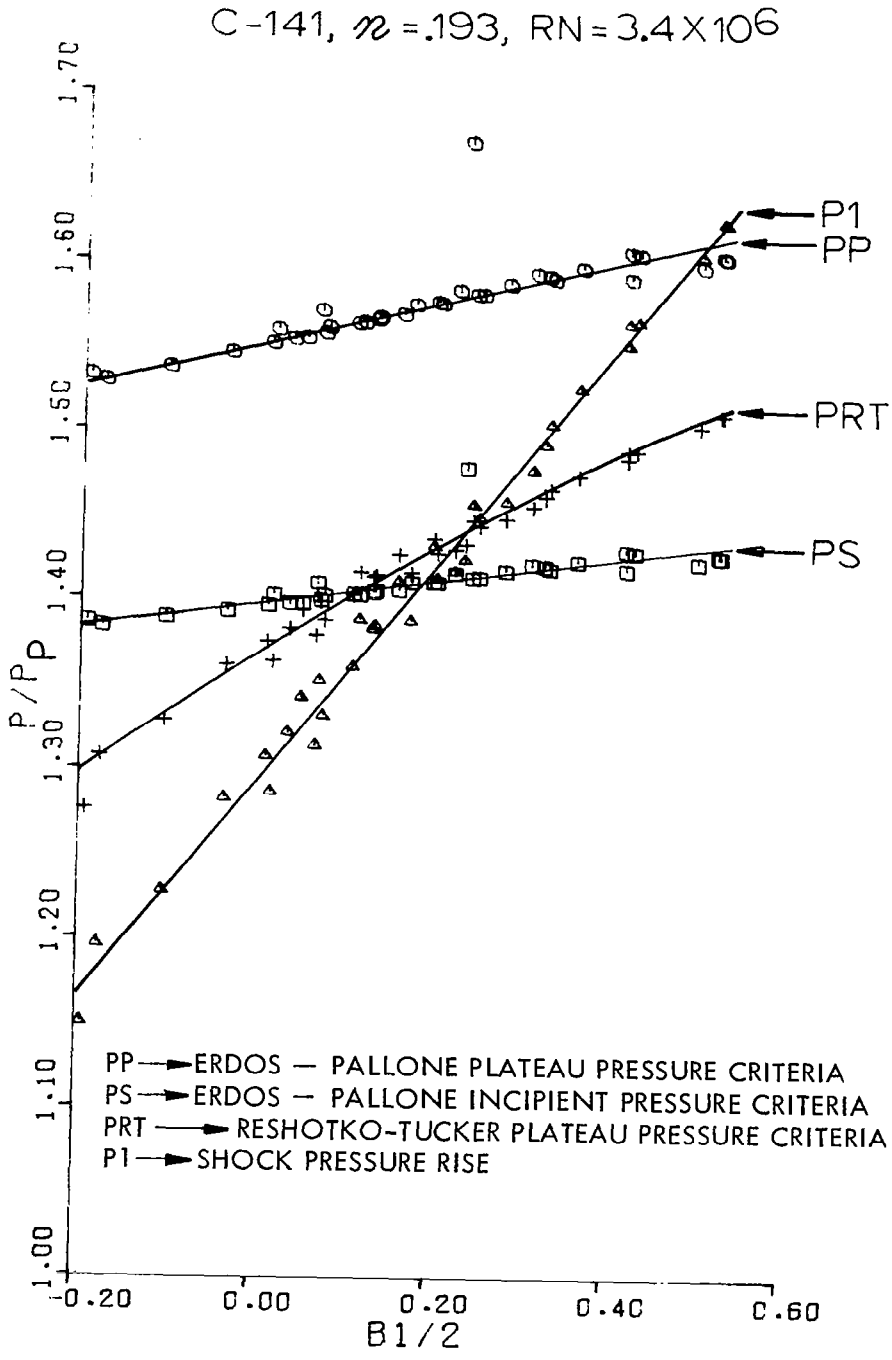

FIGURE 50. - SHOCK PRESSURE RISE FOR SEPARATION

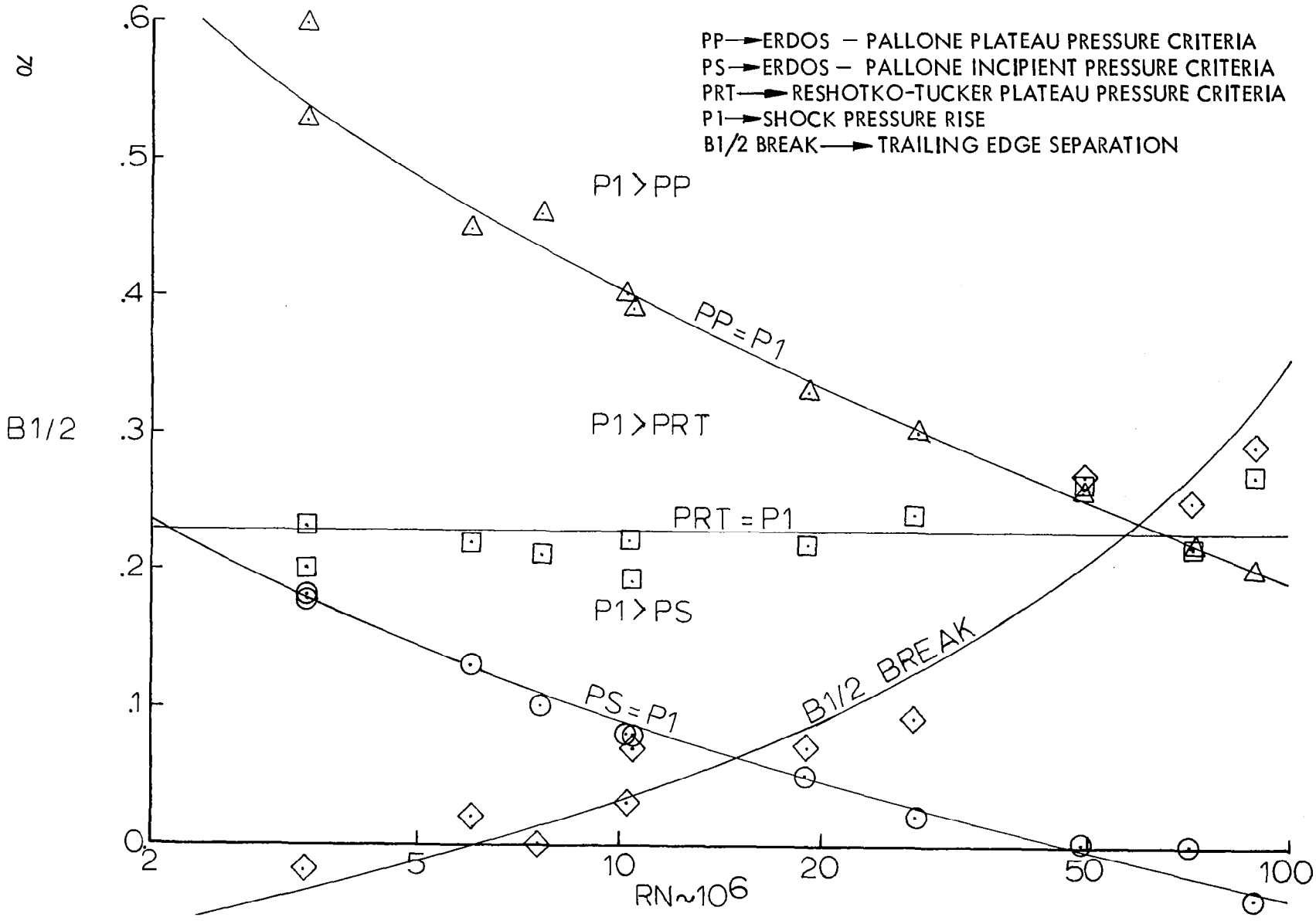

FIGURE 51. - COMPARISON OF B1/2 AT INITIAL SEPARATION AND AT SHOCK SEPARATION PRESSURE RISE

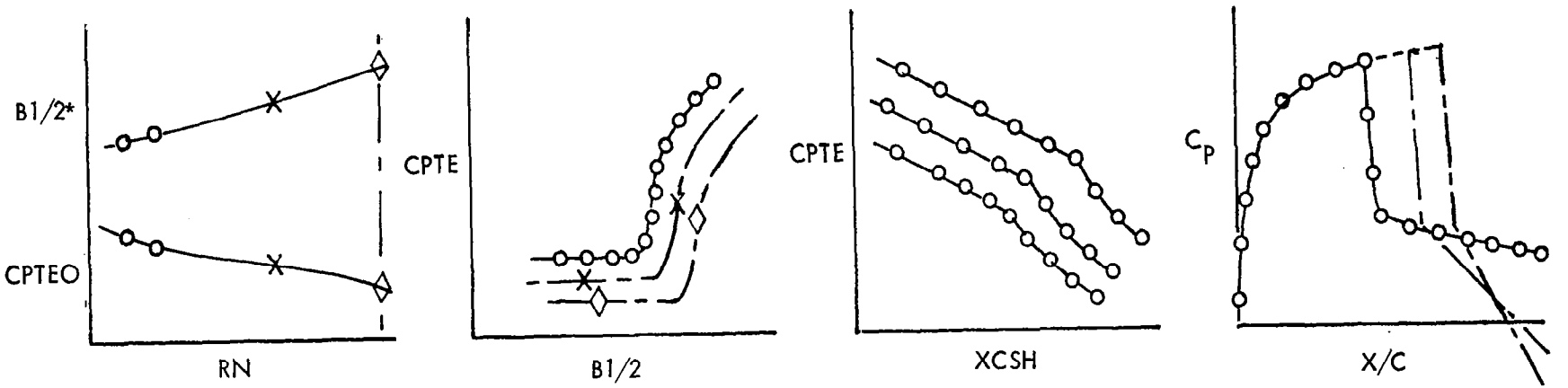

FIGURE 52. - EXTRAPOLATION CONCEPT

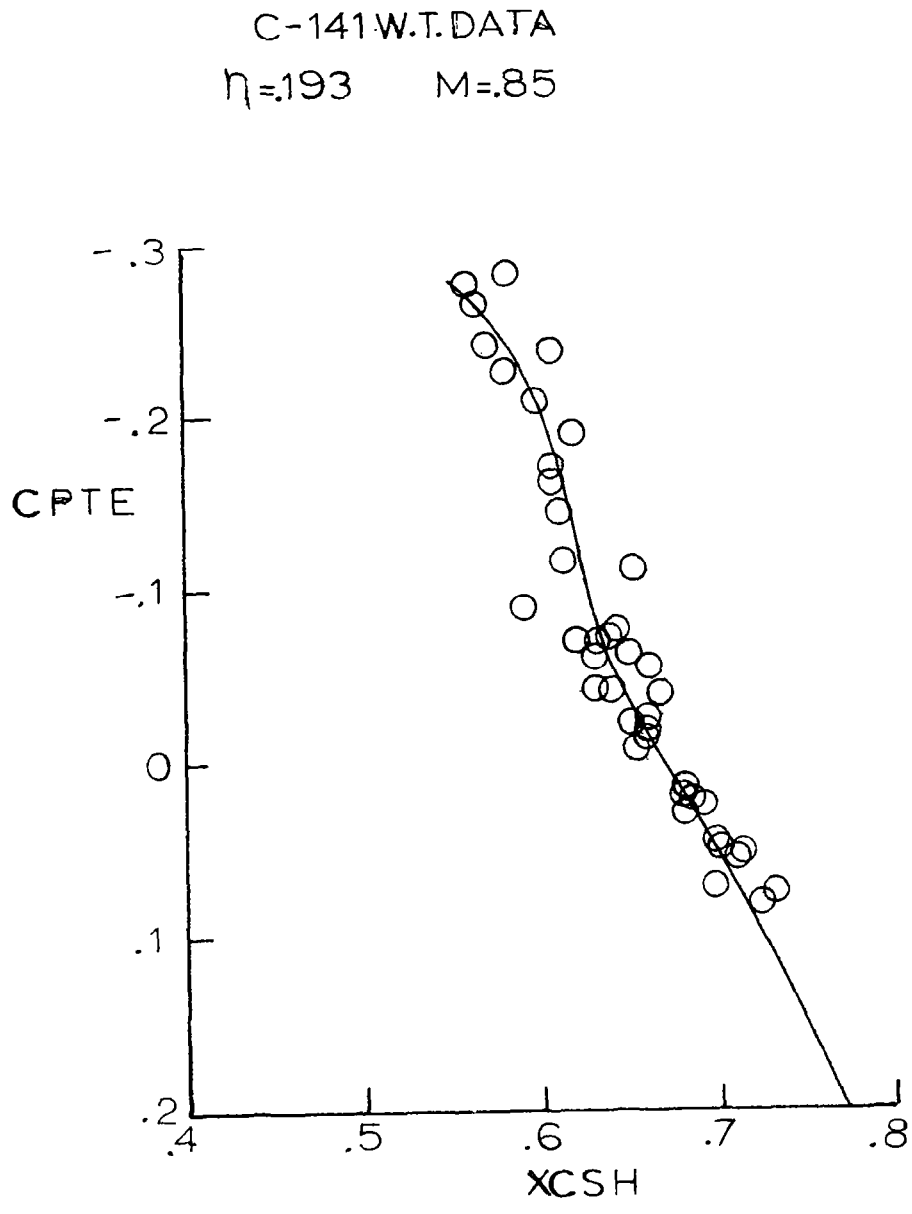

FIGURE 53. - VARIATION OF SHOCK LOCATION WITH TRAILING-EDGE PRESSURE RECOVERY

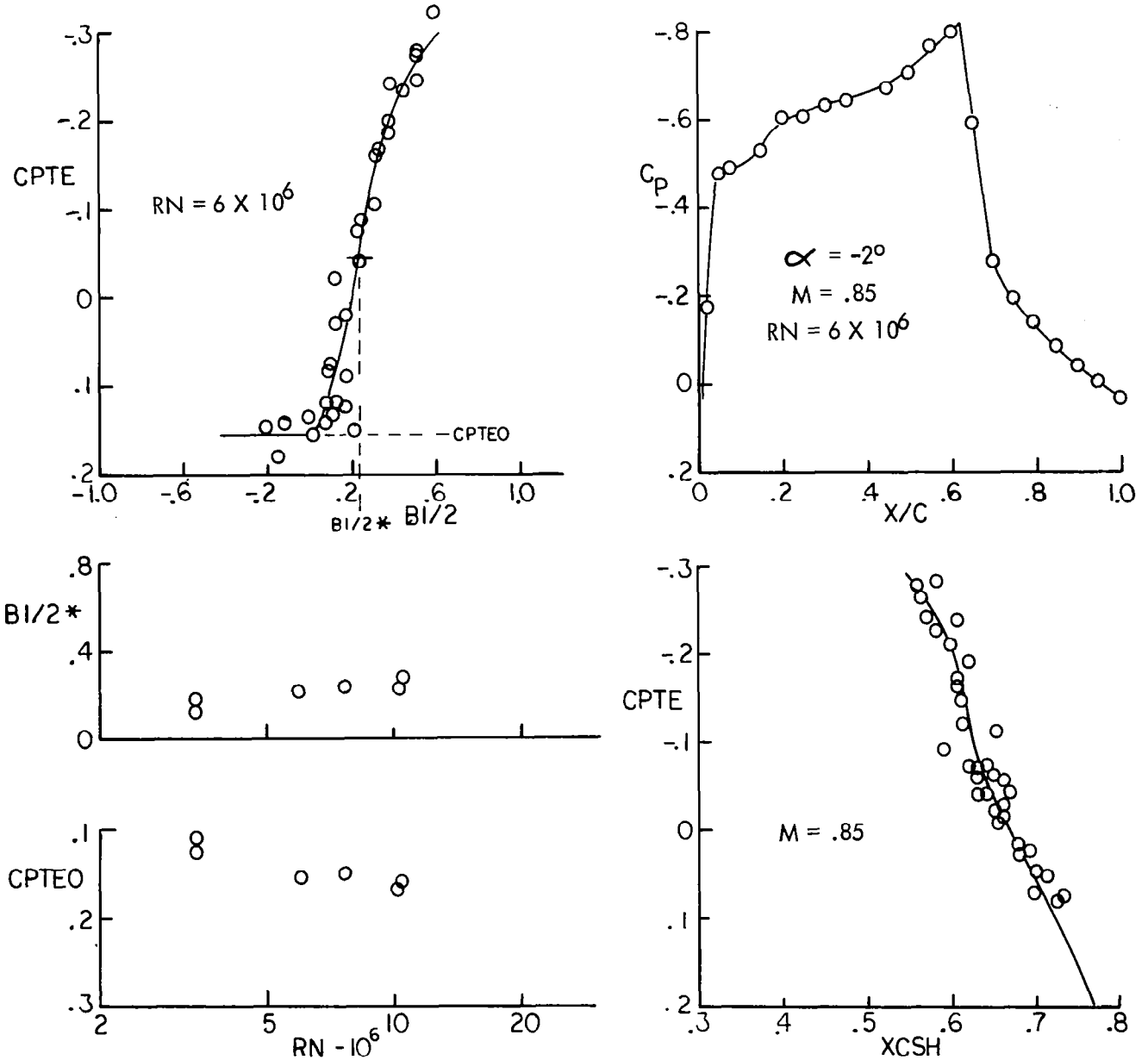

FIGURE 54. - SUMMARY OF TYPICAL LOW REYNOLDS NUMBER DATA. C-141, $\mathcal{M}$ = .193

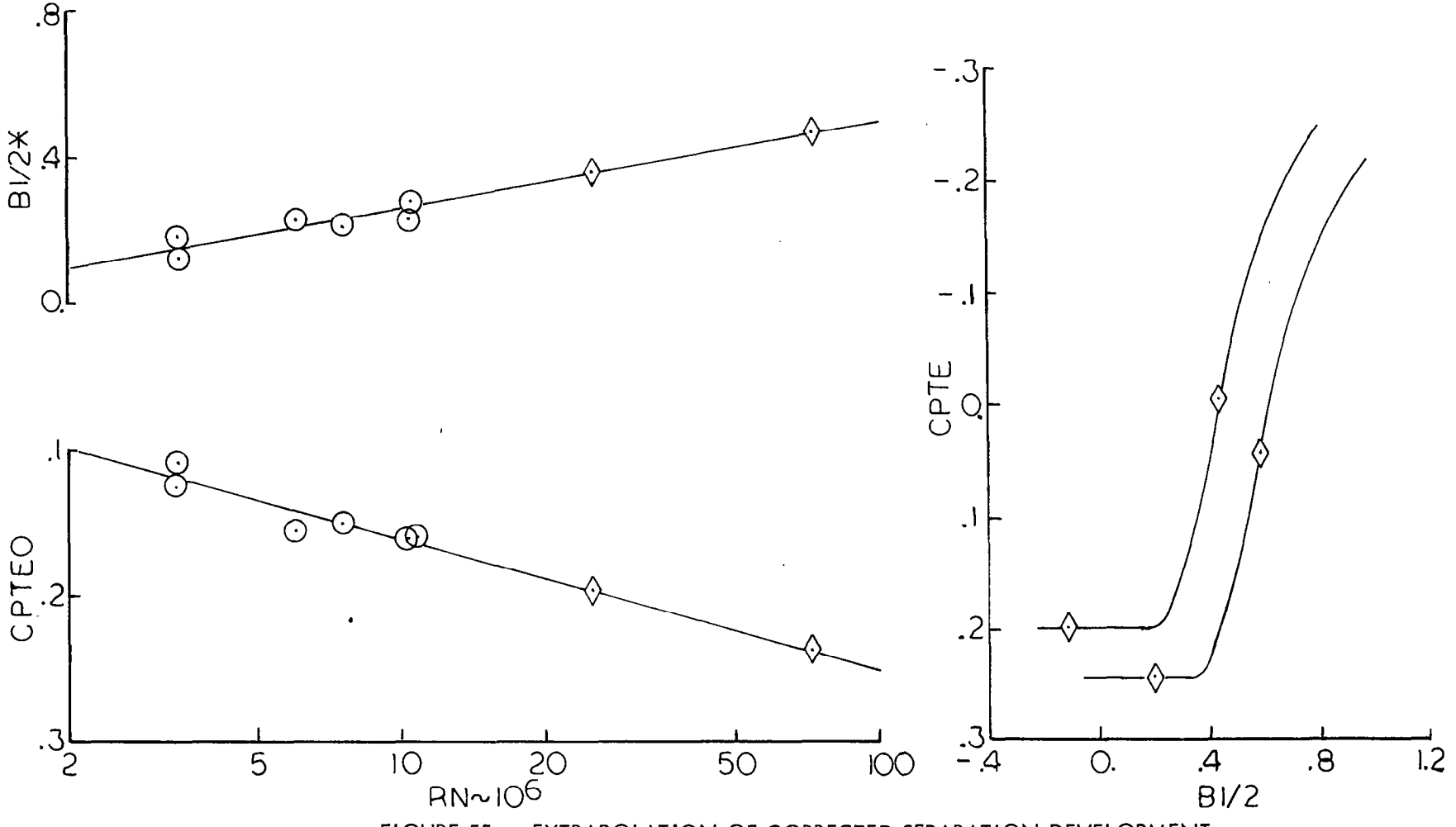

FIGURE 55. - EXTRAPOLATION OF CORRECTED SEPARATION DEVELOPMENT

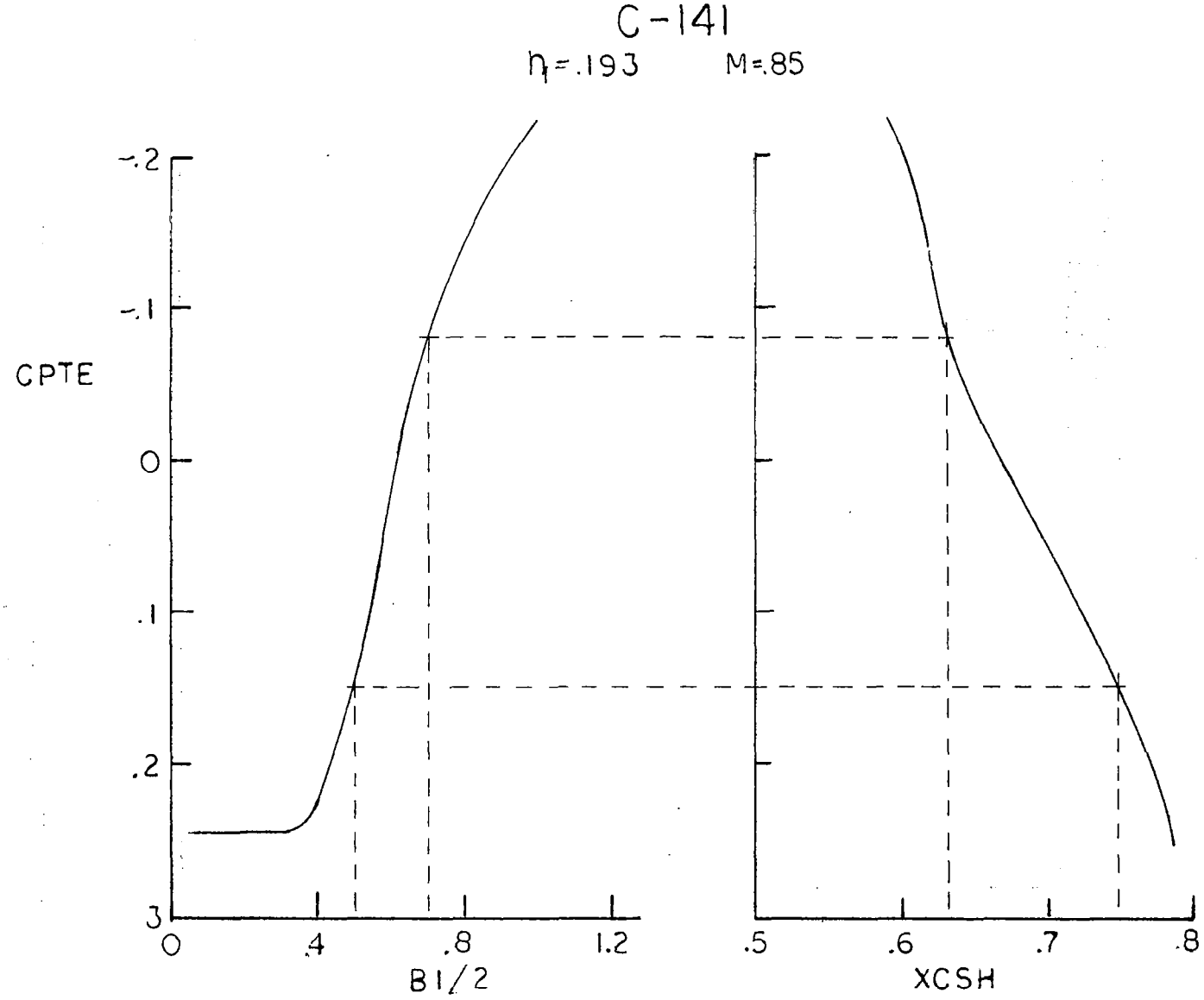

FIGURE 56. - DEVELOPMENT OF SHOCK OCCURANCE LOCUS. RN=72X10^6

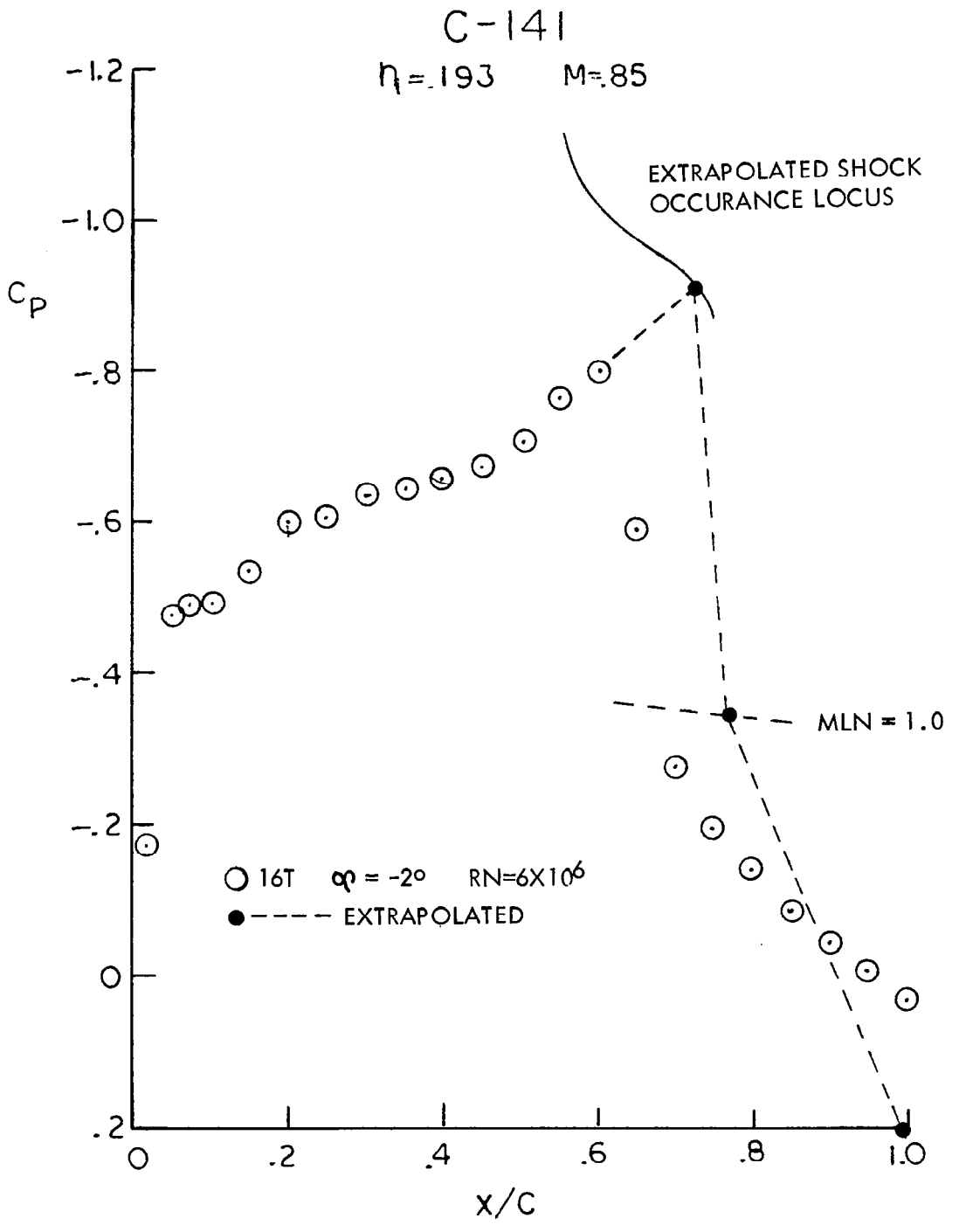

FIGURE 57. - EXTRAPOLATION OF LOW REYNOLDS NUMBER PRESSURE DISTRIBUTION. RN=72X10⁶

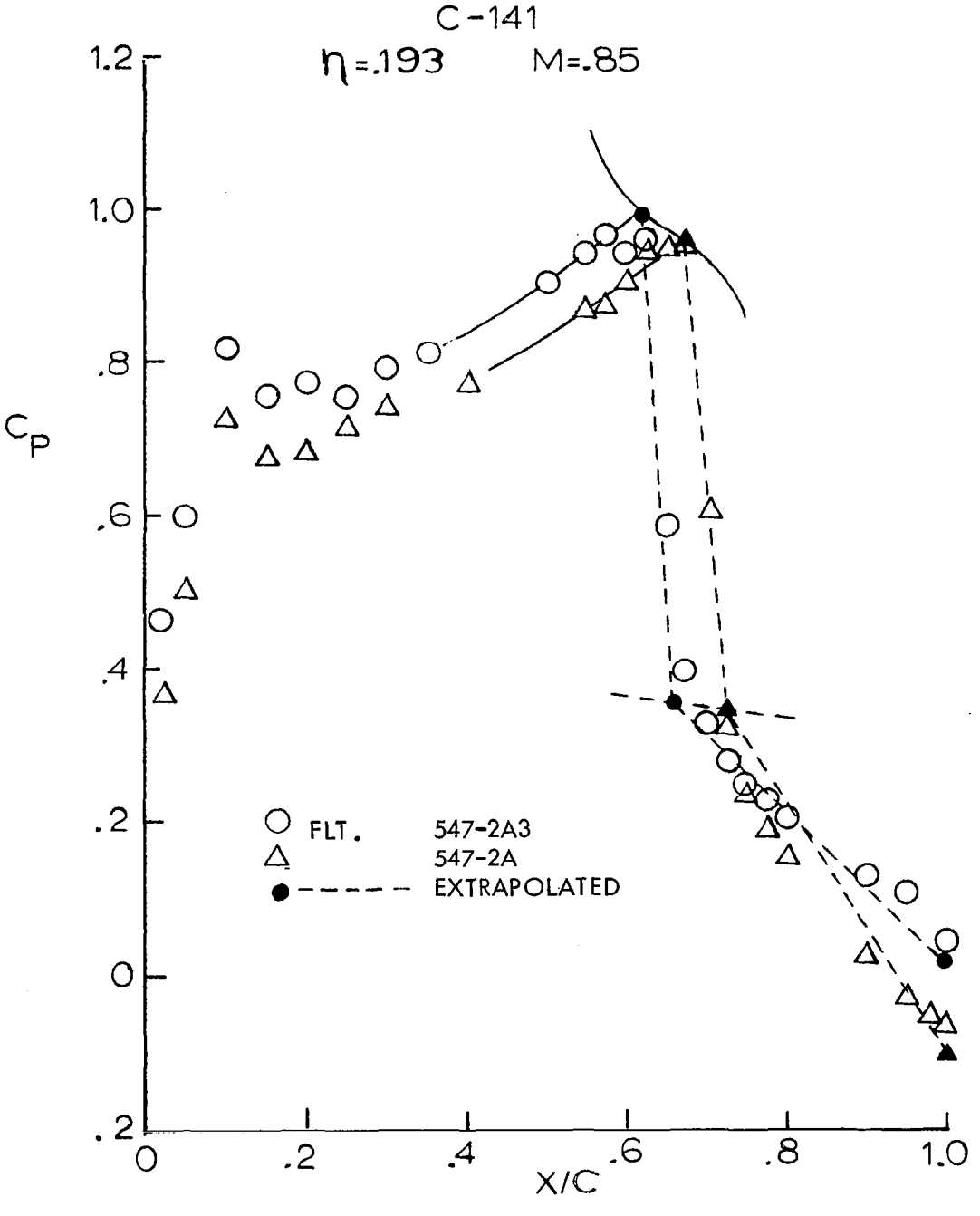

FIGURE 58. - COMPARISON OF FLIGHT DATA WITH EXTRAPOLATION. RN=72X10^6

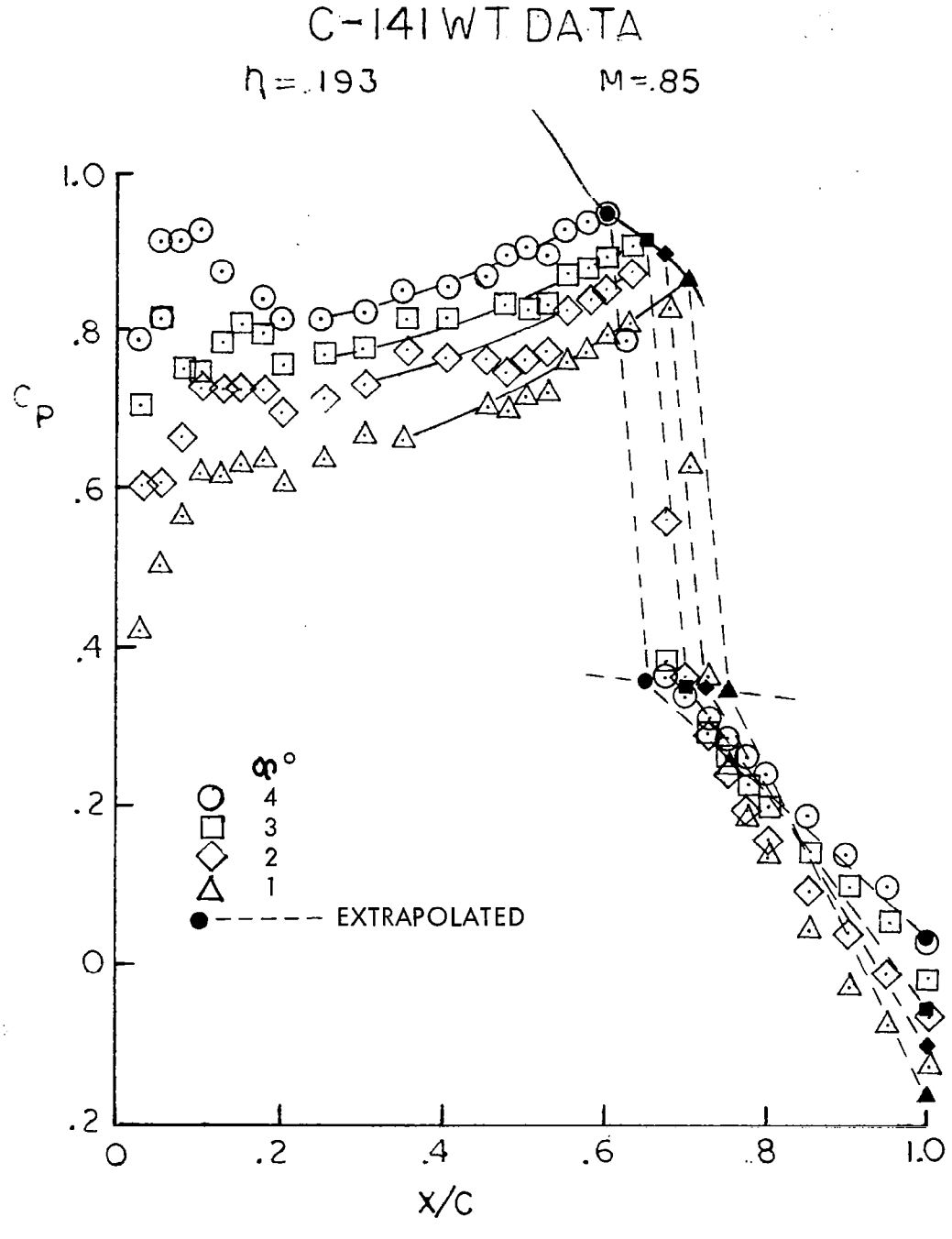

FIGURE 59. - COMPARISON OF HIGH REYNOLDS NUMBER WIND TUNNEL DATA WITH EXTRAPOLATION. RN=25X10^6

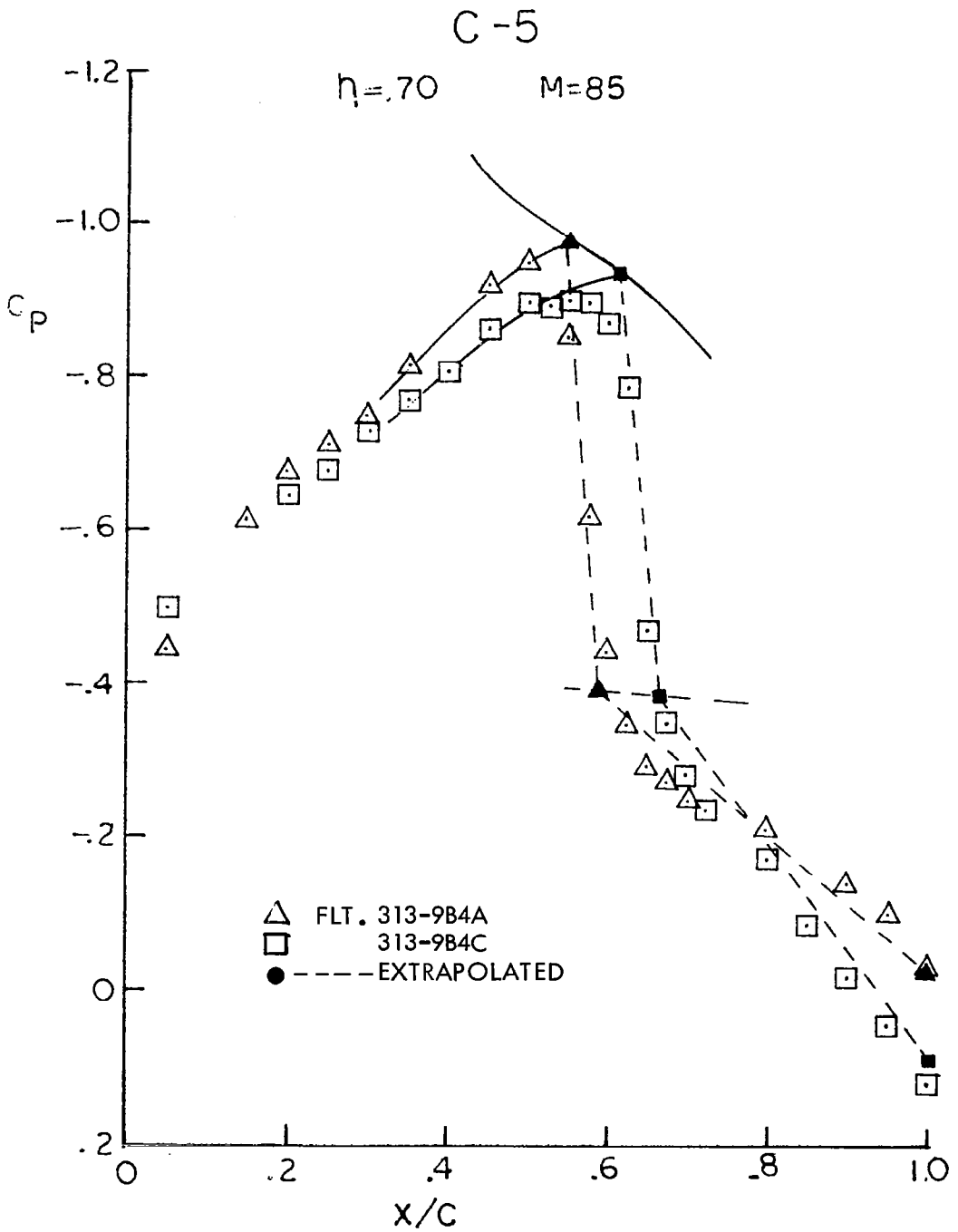

FIGURE 60. - COMPARISON OF FLIGHT DATA WITH EXTRAPOLATION. RN=58X10^6

1. Report No.	2. Government Accession No.	3. Recipient's Catalog No.
NASA CR-3178		

4. Title and Subtitle	5. Report Date
CORRELATION OF DATA RELATED TO SHOCK-INDUCED TRAILING-EDGE SEPARATION AND EXTRAPOLATION TO FLIGHT REYNOLDS NUMBER	September 1979
	6. Performing Organization Code

7. Author(s)	8. Performing Organization Report No.
J. F. Cahill and P. C. Connor	
	10. Work Unit No. 505-06-41
9. Performing Organization Name and Address	11. Contract or Grant No.
Lockheed-Georgia Company Marietta, Georgia	NAS2-9331
	13. Type of Report and Period Covered
12. Sponsoring Agency Name and Address	Contractor Report
National Aeronautics and Space Administration Washington, D. C. 20546	14. Sponsoring Agency Code

15. Supplementary Notes

16. Abstract

Pressure data from a number of previous wind tunnel and flight investigations of high speed transport type wings has been analyzed with the intent of developing a procedure for extrapolating low Reynolds number data to flight conditions. These analyses have produced a correlation of the development of trailing-edge separation resulting from increases in Mach number and/or angle of attack and have shown that scale effects on this correlated separation development and the resulting shock location changes fall into a regular and apparently universal pattern. Further studies appear warranted to refine the correlation through a detailed consideration of boundary layer characteristics, and to evaluate scale effects on supercritical wings.

17. Key Words (Suggested by Author(s))	18. Distribution Statement
TRANSONIC, Wing-Shock Location, Pressure Distribution, Reynolds Number Effects, Extrapolation, Correlation	Unclassified - Unlimited STAR Category - 05

19. Security Classif. (of this report)	20. Security Classif. (of this page)	21. No. of Pages	22. Price*
Unclassified	Unclassified	80	$6.00

*For sale by the National Technical Information Service, Springfield, Virginia 22161

NASA-Langley, 1979